2012-08-27

Investigation of durability and design of direct methanol fuel cells

Kianimanesh, Amir

UNIVERSITY OF CALGARY

Investigation of Durability and Design of Direct Methanol Fuel Cells

by

Amir Kianimanesh

A THESIS
SUBMITTED TO THE FACULTY OF GRADUATE STUDIES
IN PARTIAL FULFILLMENT OF THE REQUIREMENTS FOR THE
DEGREE OF MASTER OF SCIENCE

DEPARTMENT OF MECHANICAL AND MANUFACTURING ENGINEERING
CALGARY, ALBERTA
AUGUST 2012

UNIVERSITY OF CALGARY

FACULTY OF GRADUATE STUDIES

The undersigned certify that they have read, and recommend to the faculty of Graduate studies for acceptance, a thesis entitled "INVESTIGATION OF DURABILITY AND DESIGN OF DIRECT METHANOL FUEL CELLS" submitted by AMIR KIANIMANESH in partial fulfilment of the requirements of the degree of Master of Science.

Supervisor, Dr. Simon Park
Department of Mechanical & Manufacturing Engineering

_____

Co-Supervisor, Dr. Theodor Freiheit
Department of Mechanical & Manufacturing Engineering

_____

Dr. Deyi Xue
Department of Mechanical & Manufacturing Engineering

_____

Dr. Leping Li
Department of Mechanical & Manufacturing Engineering

_____

Dr. Josephine Mary Hill
Department of Chemical & Petroleum Engineering

_____

Date

_____

ABSTRACT

Direct Methanol Fuel Cells (DMFCs) have become a potential alternative for rechargeable batteries in portable electronic devices since they can operate at the higher power density (generated power over the volume of the system) of conventional rechargeable batteries; and have advantages such as a simpler system design (with the potential for low-volume lightweight stacking), eliminating the requirement for fuel reforming, and classification as a zero-emission power system. There are several challenges in DMFCs which need to be overcome before they can become commercially viable energy sources. These challenges are system durability and the design optimization of system components. The durability of the DMFCs has been investigated by considering the effects of operating factors on the degradation of a single-cell DMFC with serpentine flow channels. Degradation in the performance of the DMFC system was observed and modeled over time by a linear regression model considering the cumulative exposure of the operating factors to the fuel cell and the moving average concept in the degradation analysis. In addition, the influence of the flow fields design in the DMFC system with a focus on performance was investigated. Three bipolar/end plates with a single-channel serpentine configuration were fabricated with three different channel widths and experimentally tested the performance. To understand the details of the phenomenon and the fluidic behaviours, a computational fluid dynamics (CFD) model was developed, which showed that the diffusion of fuel to the diffusion layer was higher and the fuel distribution more uniform in the narrower channel. Their performance showed that the cell equipped with the narrowest channel width had an overall higher performance compared to the widest channel width. The results of this study could enhance the performance of DMFC by modeling the polarization and degradation

behaviour of the tested DMFC and provide a better understanding of the degradation phenomenon. Furthermore, the design of the DMFCs can be improved and optimized by studying the geometry of bipolar/end plates and their effect on the performance of cells. This can result in DMFCs with higher overall efficiency that approaches the targets for commercial viability.

ACKNOWLEDGEMENTS

I am heartily grateful to those who made this thesis possible, especially my supervisor, Dr. Simon Park, and my co-supervisor, Dr. Theodor Freiheit, whose encouragements, guidance and support from the initial to the final level provided me with the opportunity to understand the subject and complete this project. My parents deserve special mention for the encouragement and support they offered during my stay in Calgary. I also would like to offer my gratitude to Dr. Deyi Xue for his scientific guidance and support at different stages of this thesis. I appreciate the supervisory committee members who kindly accepted to review this thesis. This project was supported by Canadian School of Energy and Environment (CSEE). I am also very thankful to my colleagues Biao Yu (for the help with CFD simulations), Qinwen Yang , Mehdi Mahmoodi, Majid Mehrpouya, Golam Mostafa, Kaushik Parmar, Chaneel Park, Eldon Graham, in Micro Engineering Dynamics Automation Laboratory (MEDAL) at the University of Calgary who supported me in many aspects during the study.

To my lovely parents,

Parviz and Afagh

Table of Contents

List of Tables

List of Figures

List of Symbols, Abbreviations and Nomenclature

T	Absolute temperature (K)
A_f	Air flow rate (ccm)
R_e	Area-specific resistance ($\Omega \cdot cm^2$)
E_{cell}	Cell potential (V)
V_{cell}	Cell voltage (V)
A	Cross-section area of the channel (m^2)
j	Current density (A cm^{-2})
ρ	Density (kg m^{-3})
D_k	Diffusion coefficient of k-th species (m^2s^{-1})
D_k^{eff}	Effective diffusion coefficient of k-th species (m^2s^{-1})
DL	Diffusion Layer
j_0	Exchange current density (Acm^{-2})
F	Faraday constant (96,485 C/mol)
R	Gas constant (8.314472 J/(mol·K))
I_{Af}	History index for the air flow rate
I_T	History index for the inner temperature of the cell
I_{Cme}	History index for the methanol concentration
I_{Mf}	History index for the methanol flow rate
D	Hydraulic diameter (m)
Y_k	Mass fraction of k-th species
C_{ME}	Methanol concentration (M)
M_f	Methanol flow rate (ccm)
Q_{in}	Methanol solution flow rate (ccm)
μ	Mixture viscosity (kg $m^{-1}s^{-1}$)
$\Delta\overline{g_f}$	Molar Gibbs energy for methanol reaction (–698.5 $kJmol^{-1}$)
S_{mom}	Momentum source term (N m^{-3})
n	Number of electrons transferred for each methanol molecule (6)

K	Permeability (m^{-2})
ε	Porosity of porous media
P	Pressure (Pa)
E_r	Reversible “no-loss” cell voltage (1.21 V)
Re#	Reynolds’ Number
b_{cell}	Tafel slope
α	Transfer coefficient at anode
$\vec{v}$	Velocity vector ($m\ s^{-1}$)

Chapter 1: INTRODUCTION

1.1 Introduction

The pursuit of sustainable alternative energy systems is vital for modern industrialized countries. Among alternative energy sources, direct methanol fuel cell (DMFC) systems have recently emerged as one strategy to replace rechargeable batteries for portable electronic devices, such as cell phones, digital cameras and laptop computers, due to the high energy density of methanol fuels and low power requirements of portable electronic devices [Cheddie *et al*. 2005]. Moreover, DMFC systems can play an important role in off-grid applications, such as medical appliances, remote oil and gas exploration, transponder systems, and military applications.

Fuel cells are highly efficient electrochemical converters that transfer the chemical energy of a fuel and oxygen directly into electricity and heat. The appealing simplicity of the fuel cell, which excludes any further conversion steps of energy, is illustrated in Figure 1.1, together with the conventional electricity production of, for example, gas turbines.

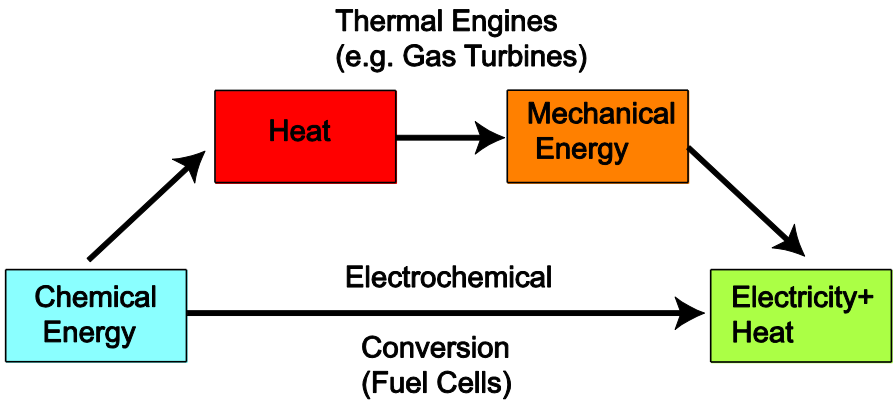

Figure1.1 The Principle of Fuel Cell Technology Compared to Conventional Energy Production

Fuel cells are similar to batteries in electrochemical principle. In contrast to batteries, the fuel cell does not store its fuel within the housing, but can work continuously as long as fuel is supplied, much like a conventional combustion engine. Therefore, the fuel tank in fuel cells has to be refueled from time to time, which is considerably faster than recharging a battery.

One of the main advantages of fuel cells is their potential for producing high-quality electricity with high electrical efficiencies and low emissions [Iwasita *et al.* 1990]. Furthermore, the efficiency of a fuel cell theoretically rises under part load conditions, which is contrary to conventional energy production [Hamnett *et al.* 1992]. Fuel cells are not limited by Carnot's theorem; thus, efficiencies above 70% could theoretically be achieved.

The advantages, power ranges and applications of the different types of fuel cells are summarized in Figure 1.2. In general, there are five different types of fuel cells, including the solid oxide fuel cell (SOFC), molten carbonate fuel cell (MCFC), phosphoric acid fuel cell (PAFC), alkaline fuel cell (AFC) and polymer electrolyte membrane fuel cell (PEMFC).

A brief description of each of these fuel cell types is presented in the following paragraphs [Kordesch and Simader 1996]:

SOFCs (solid oxide fuel cells) have the highest operating temperature among fuel cells, ranging from 600 to 1000°C. The electrolyte consists of a solid, nonporous metal oxide, which is usually yttrium oxide (Y_2O_3) stabilized zirconium oxide (ZrO_2), and is conductive to oxygen ions at these operating temperatures. Due to the high operating temperature, a wide range of carbonaceous fuels can be supplied to SOFCs, and high-grade heat is available. Therefore, SOFCs are mainly considered for stationary applications and to be used by utilities.

DMFC: Direct Methanol Fuel Cell
AFC: Alkaline Fuel Cell
MCFC: Molten Carbonate Fuel Cell
SOFC: Sold Oxide Fuel Cell
PEMFC: Proton Exchange Membrane Fuel Cell
PAFC: Phosphoric Acid Fuel Cell

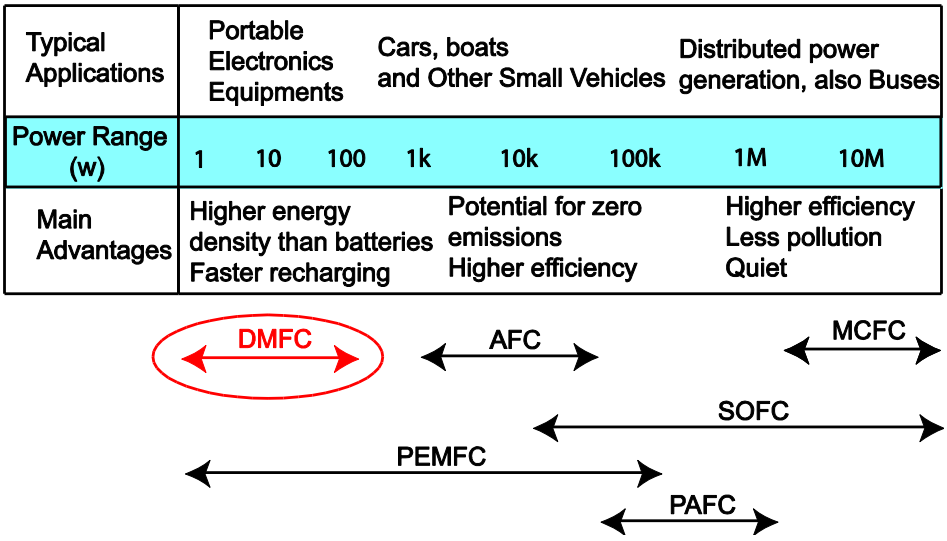

Figure 1.2 Summary of the Application and Range of Power for Different Types of Fuel Cell [Larminie 2003]

Similar to SOFCs, MCFCs (molten carbonate fuel cells) operate at high temperature (600-700°C). Consequently, the electrode kinetics is fast, and noble metals are not needed. The electrolyte is usually a combination of alkali carbonates, which is immobilized in a ceramic matrix of lithium aluminate ($LiAlO_2$). The melting point of the electrolyte is at around 480°C; thus, a highly conductive molten salt with carbonate ions as charge carriers is formed at the operating temperature. High-grade heat is available, which make MCFCs suitable for stationary applications and use by utilities.

The electrolyte of PAFCs (phosphoric acid fuel cells) consists of concentrated phosphoric acid, which is typically held at an operating temperature of 195°C. This operating temperature allows for, on the one hand, compensation of the relatively poor ionic conduction of

phosphoric acid at low temperatures and, on the other hand, tolerance of impurities in the hydrogen gas.

The AFC (alkaline fuel cell) features high specific power and energy density when used as a hydrogen/oxygen fuel cell. In addition, less cost-intensive catalysts, such as silver (Ag) based catalysts, can be used. However, the electrolyte is concentrated potassium hydroxide (KOH), which does not reject carbon dioxide (CO_2). Therefore, the choices of fuels and oxidants are limited to those that do not contain CO_2 and from which CO_2 cannot be produced. Therefore, the AFC is usually operated on H_2/O_2, which, in principle, restricts its range of possible applications to the aerospace industry.

The PEMFC (polymer electrolyte membrane / proton exchange membrane fuel cell) consists of a proton-conducting membrane that requires enough humidity to achieve adequate conductivity. Therefore, the operating temperature is usually limited to less than 120°C. Due the relatively low operating temperature, noble metal electrocatalysts are required, and the carbon monoxide (CO) tolerance of the PEMFC is limited to low levels (i.e. < 100 ppm) [Gubler 2001]. The DMFC (direct methanol fuel cell) is usually based on the PEMFC, i.e., in principle, the cell assembly is the same. The DMFC directly converts methanol and oxygen to electricity.

Fuel cells have many advantages, making them an alternative option for an electric power source. These advantages, which are common for almost every type of fuel cell, include [Larminie *et al*. 2003]:

- *Efficiency*: Fuel cells are generally more efficient than combustion engines, both piston and turbine based.

- *Simplicity*: The essentials of a fuel cell are very simple, with few, if any, moving parts, making them easy to manufacture.
- *Environmental Friendly*: When pure hydrogen is used directly as a fuel in fuel cells, only water is generated, and no other pollutants are emitted. In the DMFC type, although it produces CO_2, the amount generated is significantly lower than combustion engines, due to higher overall efficiency.
- *Quietness*: Fuel cells are very quiet, which is very important in both portable power applications and for local power generation, especially for military applications.

As shown in Figure 1.2, DMFCs are used for portable devices, since methanol provides higher energy density than conventional rechargeable batteries; for example, lithium batteries deliver 45 W/cm^3, while DMFCs deliver 280 W/cm^3 [Dillion *et al*. 2004]. Although there are several different types of fuel cells, the DMFC offers the most potential as a promising alternative for portable power applications, due to its low operating temperature, environmentally friendliness, and the portability and inexpensiveness of its fuel. Therefore, considerable research effort is being focused on miniaturizing and improving the efficiency of DMFCs.

Recently, a number of companies, including Toshiba, Hitachi, Fujitsu, Samsung, and Sanyo, have all developed prototype laptops, cellular phones and personal digital assistants that are powered by DMFCs [Paulson 2003]. Unlike hydrogen-based fuel cells that require catalytic reforming for the fuel before its use in the system, reforming is not required in DMFCs, as methanol is fed directly to the fuel cell. In addition, methanol does not have the problems of hydrogen production or storage. Methanol is a readily available and low-cost liquid fuel that has an energy density not very different from gasoline. Therefore, with the use of methanol directly

in fuel cells, the resulting weight of any portable fuel cell system can be reduced [Larminie *et al*. 2003]. DMFCs can also be adapted to different power-life demands of devices by changing fuel cartridge size.

DMFCs are capable of converting the chemical energy in methanol into electrical energy through a reduction/oxidation reaction between methanol and oxygen. The overall chemical equation for the reaction is described in Equation (1.1) [Appleby *et al*. 1989]. Also, Equations (1.2) and (1.3) show the half reactions occurring in the anode and cathode sides, respectively.

$$CH_3OH + 1.5\ O_2 \rightarrow 2\ H_2O + CO_2 \quad (1.1)$$

$$CH_3OH + H_2O \leftrightarrow CO_2 + 6H^+ + 6e^- \quad (1.2)$$

$$1.5\ O_2 + 6H^+ + 6e^- \leftrightarrow 3H_2O \quad (1.3)$$

The main components of a DMFC are the membrane electrode assembly (MEA), (gas) diffusion layers, and bipolar/end plates. An MEA is composed of a polymer electrolyte membrane, electrode catalyst layers and support layers. Carbon backing material, also called the diffusion layers, provides mechanical structure for the electrode and carries reactants towards the catalyst and reaction products away from the electrode [Park *et al.* 2008]. The graphite bipolar/end plates have a series of flow channels used to distribute the fuel to the diffusion layer, and they also provide heat removal from the active areas and a current path for the circuit. The detailed explanations of each of the components and their roles are discussed in Chapter 2.

Figure 1.3 illustrates the mechanism of a working DMFC system. When the cell is operating, the methanol solution enters the system and then breaks down to hydrogen (H^+) ions

and electrons. The ions travel though the MEA, and the electrons travel outside the system through the electric load. On the cathode side, the electrons and H^+ ions react with the oxygen in the air and produce water. The number of methanol molecules provided in the solution is usually more than the methanol consumed in the system, and the unused methanol comes out of the system and is sometimes recycled to the system. In Figure 1.3, reactants enter and exit the cell at one side; while the locations of the inlet of reactants and the outlet of the by-products can vary depending on the design of the cell, for example in our DMFC the inlets of the methanol solution and air are at the same side and outlets are at the other side which is shown in Chapter 3.

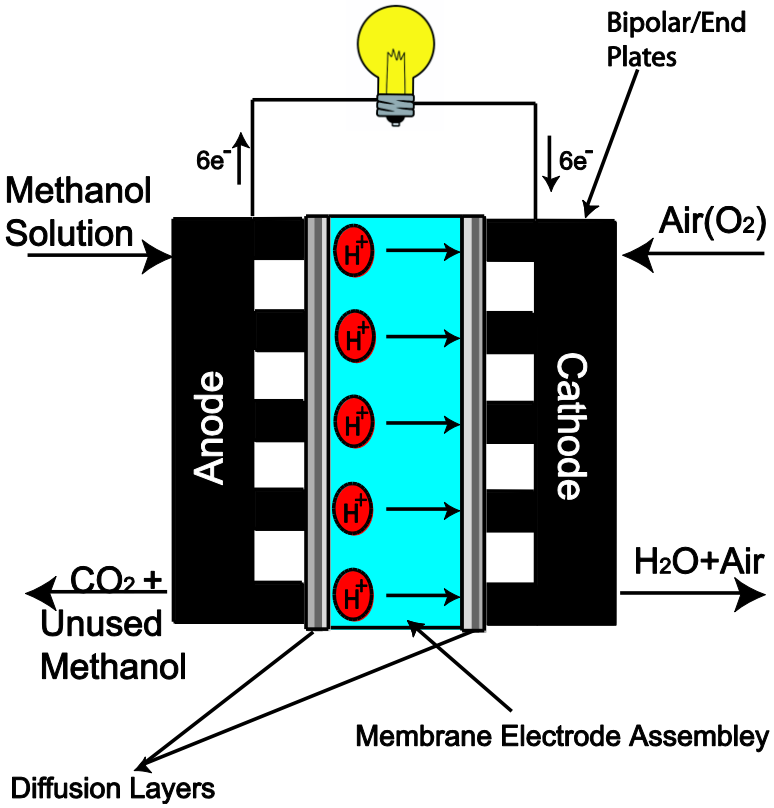

Figure 1.3 Schematic of a Working DMFC

1.2 Motivation

Although DMFCs are becoming more and more popular as a portable power alternative, they have not been widely commercialized. Investigations of DMFC as a potential alternative

source of electrical power in the past decades have mainly been focused on the catalysts [Choi *et al.* 2006, Han *et al.* 2006], methanol crossover [Munichandraiah *et al.* 2003, Gurau *et al.* 2002, Jiang *et al.* 2008], carbon support [Xu *et al.* 2006, Figueiredo *et al.* 2006], Nafion modification [Tian *et al.* 2007], and the optimization of gas electrode layer [Zhang *et al.* 2007]. Significant advances have been made in the development of DMFCs; however, at present, their performance and durability cannot meet the demands of the market.

Besides, the costs of DMFCs are still relatively high, due to expensive noble metals, such as platinum (Pt) and ruthenium (Ru) used as catalysts in the cathodes and anodes. Pt resources are limited, and Ru resources are very rare, thereby restricting the commercialization of DMFC. Hence, it is worth enhancing the efficiency of DMFCs, prolonging the life of catalysts and/or lowering the cost by using new techniques.

Extending the life of the system requires an understanding of the mechanisms that cause the system to degrade and the subsequent resolution or deceleration of these mechanisms to lengthen the life of the DMFC system. On the other hand, optimization of the design of the system significantly affects the efficiency of the system. Therefore, as sources of electrical power generation, DMFCs should be both reliable and efficient, in order to be commercialized. In this study, two main factors in DMFC systems are investigated: the durability as a factor of reliability in time, and the design of a DMFC system for enhancing its efficiency.

The performance degradation rates of DMFCs, are typically in the range of 10–25μVh^{-1}, which are generally higher than those of hydrogen PEMFCs [Knights *et al.* 2004]. The commercialization of DMFC demands a stable operation for at least thousands of hours; for example, fuel cell vehicles and residential power generators usually require between 5000 and 40,000 hours, which is not easy to achieve [Ahn *et al.* 2002].

Most of the fundamental mechanisms determining the life of DMFCs are poorly understood, such as changes in the hydrophobic/hydrophilic properties in the catalyst layers and diffusion layers and MEA failure mechanisms, including the growth and corrosion of catalyst particles, poisoning of electrocatalysts by accumulated intermediates or impurities, and the aging of polymer electrolyte membrane (PEM) [Washington *et al.* 2000, Chen *et al.* 2006]. In addition to an understanding of the reasons for DMFC degradation, knowledge of the degree of the degradation over a certain operating time and conditions can help predict the voltage-current (V-I) characterization of the DMFC at a specific operating hour. Predicting the value of performance loss of the DMFC over time can provide an estimate of its service life and also the power generation capacity of the system.

As mentioned earlier, past DMFC development efforts have been concentrated on modifying and searching for alternatives to existing membranes, evaluating and optimizing anode catalysts, in addition to studying the effect of the cathode on cell performance. Relatively few studies have been reported on the DMFCs' flow field. A uniform fuel distribution to the MEA surface is vital for the optimal operation of a DMFC. The overall efficiency of fuel cells is greatly influenced by the performance of the bipolar plates in their stack [Besmann *et al.*, (2000)], which is another focus of this study.

1.3 Objectives

The durability and design of DMFCs are significant factors impacting their commercialization. The durability of the DMFC over time is one of the factors affecting the reliability of the system as a power generation system. The design of the DMFC system influences the performance and overall efficiency of the system. The durability study in this thesis mainly deals with degradation modeling and the causes of the performance loss in the

system. The design investigation in this thesis focuses on the bipolar/end plates design and optimization. The following research questions are addressed:

- How can the performance of a DMFC system be measured and modeled?
- Which operating parameters are significant in affecting the performance of DMFCs?
- Is the degradation in DMFC systems significant?
- How can the degree of the degradation in the DMFC system be modeled?
- What are the reasons for the degradation in the DMFC?
- Which component in a DMFC system most affects the efficiency of the system?
- What is the optimal design for the geometry of the end plates in the DMFC system, considering the overall generated power?

This thesis has two main objectives:

a) Investigation of the durability of DMFCs and modeling of the performance degradation of the DMFCs, and
b) Investigation and optimization of the design of DMFC systems.

The durability study primarily investigated the degradation behaviour in DMFC performance over time, considering the effects of fuel cell operating parameters and their interactions on the overall performance of a DMFC. A series of experiments on a single-cell DMFC system were required to observe the effects on cell performance of the interactions between the four operational parameters of temperature, methanol concentration, and methanol and air flow rates.

To best evaluate the degradation in the performance of the cell over its operating time, a model should estimate the performance change as a function of the operating conditions and time of the cell. The aims in this model were the prediction of the V-I curve of the system, considering data that compensated for changes over time, and the determination of the polarization behaviour of the system from operational factors independent of degradation.

The four operational parameters - temperature, methanol concentration, air flow rate, and methanol flow rate - were empirically fit to the polarization curves based on time-compensated experimental data. Some of the experimental data that was not used in the fit was used to validate how well the model predicts the polarization curve. The uncompensated data in the polarization model was used to confirm the model's capability in predicting the V-I curve of the cell, independent of degradation (time-compensated data), thereby allowing the study of the degradation behaviour.

The second objective was the investigation and optimization of the design of DMFC systems, particularly the bipolar/end plate channel width geometry. The effect of the channel width of the bipolar/end plates on the performance of the DMFC was investigated through a series of experiments on each of three geometric configurations. In these experiments, each geometry was used for both the anode and the cathode. The performance curve for that geometry was measured to observe the effect of the geometry.

The change in performance due to geometry was mainly due to differences in the flow characteristics of the fluid inside the bipolar/end plate channels. In order to elucidate the performance differences between the different widths, a single-phase computational fluid dynamics (CFD) model for the flow in the channel was developed. The comparison between the

flow simulations for the three bipolar/end plates geometries was then used to investigate the reasons for performance differences in the system.

The objectives, therefore, targeted investigations into the durability of the DMFC system and the design of the bipolar/end plates used in the system. In the durability study, degradation mechanisms of the DMFC were investigated, which helped to understand the causes of performance degradation and possible solutions The design of flow fields in bipolar/end plates was studied to improve the efficiency of the system and achieve higher performance in DMFCs. Achievement of these two main research objectives may provide a better understanding of DMFC systems and facilitate their commercialization.

1.4 Organization of Thesis

This thesis consists of six chapters. Chapter 2 consists of an overview of the previous research on DMFC durability and design. Several studies are reviewed, investigating and modeling the degradation of DMFC system performance and its causes. Previous literatures regarding the design of the bipolar plates and its effect on the performance are also reviewed in this chapter.

Chapter 3 outlines the experimental procedure and setup. The experimental setup is presented in this chapter. The design of the experiments and experimental results on the modeling and durability tests are presented. Finally, the manufactured bipolar plates are explained, and the experimental results for different designs are discussed.

Chapter 4 focuses on the study of the degradation of the tested DMFC system. First, a semi-empirical polarization model is discussed, including time compensation of the experimental data, the calculations in the model, and the validation of the model. A degradation model, containing the concept of moving average and step-wise linear regression used in the model

calculations, is described; and, the results and discussions of the model are explained. This chapter also reviews the possible reasons for DMFC degradation.

Chapter 5 studies the design of the flow field for the tested DMFC system. The flow field design is discussed, and the experimental results for different designs are presented. In addition, the results from different designs are modeled and compared. Finally, a CFD simulation that was developed to investigate the reasons for performance differences in the designs is presented.

The last chapter provides a summary of the research. The novel scientific contributions of this thesis are summarized. This chapter contains the methodologies developed in this research, the limitations and assumptions, along with proposed future work for researchers in related fields of study.

Chapter 2: LITERATURE REVIEW

Compared to the other types of fuel cells, the direct methanol fuel cell (DMFC) is currently still at an "infant stage" [Lamy *et al.* 2001] because of its high cost and relatively low power density (100 to 200 $mW.cm^{-2}$) compared to hydrogen-type fuel cells. At the present time, the cost of a DMFC system is mainly determined by its high catalyst loadings, which consist predominantly of expensive metals (such as platinum and ruthenium), and the use of DuPont's Nafion® membranes [Wasmus *et al.* 1999, McNicole *et al.* 1999].

This chapter intends to identify the challenges that are combined with the commercialization of DMFCs and give an overview of the different research that has been undertaken to tackle those challenges. The main components and operating conditions of the DMFC are explained first in this chapter. The previous studies are summarized regarding the durability and degradation of DMFCs, and also the state of the art research about the geometry of flow fields. Moreover, the research conducted regarding the performance modeling, degradation, and geometry of the bipolar/end plates is also examined.

2.1 Main Components and Operating Conditions of DMFC

The main components of a Direct Methanol Fuel Cell (DMFC) are the membrane electrode assembly (MEA), (gas) diffusion layers, and bipolar/end plates. An MEA is composed of the polymer electrolyte membrane, the electrode catalyst layers and the support layers. Carbon backing material, also called the diffusion layers, provides mechanical structure for the electrode and carries reactants towards the catalyst and reaction products away from the electrode [Park *et al.* 2008]. The graphite bipolar/end plates have a series of flow channels used to distribute the

fuel to the diffusion layer, and they also provide heat removal from the active areas and a current path for the circuit. The detailed explanation of each of the components and their role is discussed as following.

Membrane Electrode Assembly: A typical MEA used in DMFCs consists of three layers; an anode catalyst layer, a cathode catalyst layer, and a Proton Exchange Membrane (PEM) (also referred as Polymer Electrolyte Membrane). The anode and cathode catalyst layers are areas of the cell where the chemical reactions occur. Catalyst layers in PEMFCs (hydrogen feed fuel cell) usually consist of platinum supported on carbon black. However, in DMFCs, ruthenium is also used at the anode side of the cell. The catalyst layer is a very expensive part of the membrane electrode assembly due to high platinum content. Efforts have been made to replace platinum-based catalysts with nickel-based catalysts in order to reduce costs, but the nickel-based catalysts are not as effective at catalyzing the fuel cell reactions. There are also other factors that affect the catalyst layer effectiveness such as, particle size, catalyst layer thickness, and porosity.

The catalyst layers have to be held by a supporting layer. The catalyst layers are applied to the Proton Exchange Membrane (PEM) directly. The PEM should be an ionic conductive material which can pass through the protons but is impermeable to electrons. In addition, it should separate the reactants at the anode and cathode side. The most commonly used PEM is Nafion® which is ionically conductive polymer patented by DuPont Chemical Company. Nafion® is a polymer similar to PTFE (Teflon) with sulfonic acid side chains. The capacity of Nafion® to conduct ions strongly depends on its level of hydration. However, one main disadvantage of Nafion® to be used in DMFCs is that it is also permeable to methanol. This causes methanol permeating from the anode to the cathode through the PEM membrane which is known as methanol crossover. As a solution, increasing the thickness of the Nafion® membrane

has been shown to lessen the degree of methanol crossover, but it also increases the cost of the MEA.

Diffusion Layers: The diffusion layers disperse the fuel coming from the flow channels through the area of the catalyst layer, and providing a conductive path through which electrical current can pass. Diffusion layers are typically made of processed carbon cloth or paper which are porous, and also electrically conductive. Several different kinds of diffusion layers are fabricated which are designed for different applications.

Bipolar/end Plates: Bipolar/end plates, also known as current collectors, have two main roles in DMFC operation. The first is to provide the flow of the methanol fuel and air (oxygen) from the sources to the diffusion layer of the cell. The second duty is to transfer the current generated in the catalyst layers to the electronic load connected to the cell. Bipolar/end plates are typically made of conductive materials such as graphite or stainless steel. Flow channels are usually machined on the plates, and there are different flow channel configurations each designed to achieve a different goal.

The assembled functioning DMFC system is shown in Figure 1.3. The methanol solution goes into bipolar/end plates and the channels distribute the fuel to the diffusion layers. The methanol solution then breaks down to H^+ ions and electrons at the catalyst layer. The ions travel though the MEA and the electrons travel outside the system through the electric load. The electrons and the H^+ ions react with the oxygen in the air and produce water on the cathode side.

DMFCs' performance depends on different operating conditions. Several researchers have also studied the influence of operational conditions on fuel cell behaviour such as temperature, methanol concentration, and air and methanol flow rates, e.g., Song *et al.* [2004] showed that as temperature increases, faster methanol oxidation and oxygen reduction kinetics

reduces the charge-transfer resistance of the fuel cell impedance. The effects of methanol and air flow rates, which are seldom included in the existing models, have also been examined empirically. Yang *et al.* [2010] showed that as the air flow rate is increased, the fuel cell impedance arc decreases because faster reactions occur at both the anode and cathode. The air flow rate critically affects the cell performance because of the limited reaction rate at the cathode and the slower proton-transfer process. Ge and Liu [2006] explored methanol flow rate and found that at low methanol flow rates, the methanol concentration is too low in the catalyst layer due to mass transfer resistance, especially downstream. When the flow rate is high enough, a further increase in the flow rate has no significant effect on the methanol concentration in the channel and the catalyst layer, thus has no significant effect on the cell current density. These studies indicate that air and methanol flow rates, methanol concentration, and cell temperature all have a significant effect on the DMFC performance.

Despite progress in this research area, the effect of operating parameters on performance on the degradation phenomenon that occurs in the DMFC system has been rarely studied which is the main focus of this thesis. In this thesis, the four parameters of temperature, methanol concentration, methanol and air flow rate are varied instead of just varying one or two of these parameters. By considering all of the operating parameters and having a proper design of experiments, the interaction between the changes in the parameters can be observed from the measured performance in different operating conditions. The interaction between these four operating conditions has not been researched previously.

2.2 DMFC Performance Modeling

To design and control DMFC systems that can be used in different applications, a good understanding and accurate modeling of DMFC behaviour is necessary. From an engineering

application point of view, fuel cell behaviour is usually described by performance measures such as output voltage and current density, which are mainly influenced by design and operating parameters. Typical design parameters include the type of proton exchange membrane, the catalyst and its preparation, the electrode structure, and the geometric shapes of the fuel cell components. As mentioned in Section 2.1, typical operating parameters include temperature, methanol concentration, flow rates of methanol and air, and pressures of methanol and air.

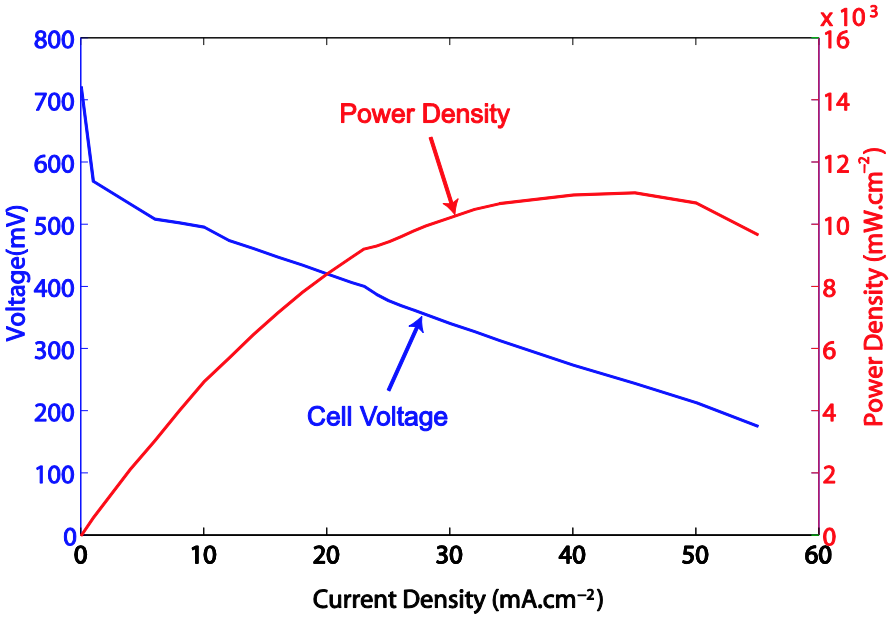

Figure 2.1 Performance Curves of the DMFC System

The fuel cell performance is usually described by the relationship between current density, j (Acm^{-2}), and output cell voltage, V_{cell} (V), as shown in Figure 2.1. Sometimes, the power density curve is also reported for the performance measure of DMFCs. Many studies have investigated the modeling of DMFC behaviour to approximate the relationship between DMFC performance and its operating parameters, including mass transportation processes [Scott *et al.* 1999], the kinetics of the methanol electrochemical oxidation reactions, diffusion, and crossover

[Dohl and Wippermann 2004], and empirical and semi-empirical models of performance [Dohl and Wippermann 2004,Wang *et al.* 2008]. In this research area, Scott *et al.* [1999] developed a model to describe the methanol transport process that can be used to predict the effective methanol concentration at the catalyst surface and polarization at the anode. They used this model, together with an empirical model of the open circuit voltage and a cathode overpotential model, to predict the voltage and current density of the DMFC.

Kulikovsky [2003] introduced an analytical model for the anode side of a DMFC, taking into account the non-Tafel kinetics of electrochemical reaction of methanol oxidation, diffusion, and transport of methanol through the backing layer and methanol crossover. Argyropoulos *et al.* [2003] and Scott *et al.* [2006] developed semi-empirical models considering the influence of methanol concentration and temperature on DMFC performance. Through DMFC experiments, Dohle and Wippermann [2006] investigated the influence of operating conditions on the anode, the cathode, and methanol permeation to determine the parameters for a DMFC model. Ge and Liu [2006] developed a three-dimensional single phase (i.e., liquid phase at anode and gas phase at cathode), multi-component mathematical model of a DMFC. The result calculated using this model was also compared with the experimental data in their research. Casalegno and Marchesi [2008] investigated the influence of two-phase flow on anode performance by combining experimental and modeling approaches. Wang *et al.* [2008] developed a semi-empirical model to derive a nonlinear equivalent circuit from a special group of impedance fuel cell models.

Wang *et al.* [2008] developed a DMFC performance model based on adaptive-network-based fuzzy inference with methanol concentration, temperature, and current as inputs and cell voltage as output. Yan and Jen [2008] developed a two-phase flow model to evaluate the effect of various operating parameters such as temperature and methanol concentration on DMFC

performance. Celik and Mat [2010] studied the concentration of methanol through experiments and numerical methods. Zenith and Krewer [2010] developed a dynamic model for a portable DMFC system.

Despite the progress in modeling DMFC behaviour, these models focus on two key operating parameters: temperature and methanol concentration. Although the impact of methanol flow rate and air flow rate has been studied by researchers, a systematic approach to model the relationships between all important operating parameters and the DMFC performance measures is still required.

In this study, a semi-empirical model has been developed to describe the relationships between all major operating parameters and performance measures by integrating theoretical and approximation models for a single stack DMFC. Four operating parameters, including temperature, methanol concentration, and methanol and air flow rates, are considered in this research. Experiments have been designed and conducted to determine the coefficients for this semi-empirical model. The semi-empirical model developed has also been validated through additional experiments.

2.3 DMFC Degradation

A key to commercially viable DMFCs is achieving a reliable long life. Presently, the performance range of the state-of-the-art DMFCs can compete with hydrogen-fueled fuel cell systems for portable power [Larminie and Dicks 2003]. However, the long-term stability of power is still a problem due to the degradation of components. There is a growing body of literature regarding the long-term operation of DMFCs [Bett *et al.* 1976, Wang *et al.* 1996, Prabhuram *et al.* 2005, Uribe *et al.* 2002, Paik *et al.* 2004, Eickes *et al.* 2006, Piela *et al.* 2004, Schulze *et al.* 2005, Park et al 2009] and several factors have been identified that influence the

stable performance of DMFC. These factors including gradual loss of active electrocatalyst surface area caused by sintering [Bett *et al.* 1976], poisoning due to reaction intermediates or impurities [Wang *et al.* 1996, Prabhuram *et al.* 2005], cathode activity loss due to surface oxide formation [Uribe *et al.* 2002, Paik *et al.* 2004, Eickes *et al.* 2006], degradation of membrane, ruthenium crossover from the anode to the cathode [Piela *et al.* 2004], changes of hydrophobic and hydrophilic properties in catalyst and gas diffusion layer [Schulze *et al.* 2005], etc.

The performance degradation of a DMFC appears to be a gradual process, the extent of which depends on time as well as operating conditions [Park *et al.* 2009]. The overall degradation in cell performance might be due to both temporary losses and permanent changes in the components of the system. The performance degradation which originates from temporary losses can be recovered partially or fully. Still, the degradation mechanisms are not fully understood and there is a lack of sufficient information about the detailed changes occurring in the cell during long-term operation. It is also necessary that the optimized operating conditions are of importance in obtaining the stable fuel cell operation.

Degradation strongly affects the performance of DMFC systems over long periods of time. Degradation rates of DMFCs are generally higher than those of hydrogen PEMFCs [Knights *et al.* 2004]. Liu *et al.* [2003] experimentally investigated the performance degradation of a DMFC in a 4,500-minute period and identified about a 50% increase in the high frequency impedance of the cell. Knights *et al.* [2004] investigated the aging mechanism of PEMFC and DMFC at different operating conditions and reported that the main reason for performance degradation is an irreversible change in the chemical kinetic and transport properties in the cell. Piela *et al.* [2004] found ruthenium crossed the fuel cell membrane from the Pt-Ru anode to the Pt cathode, with an increase in the level of ruthenium crossover over time. Chen *et al.* [2006]

found during the 30,000-minute life of a single cell DMFC that the particle size of electro-catalysts increased in the anode, and more so in the cathode, and confirmed the ruthenium crossover between anode to cathode, leading to a decrease in the catalyst's efficiency.

Wu *et al.* [2008] reviewed the mechanism of degradation in PEM fuel cells. They stated that the performance degradation is due to the failure in different components of the cell including the membrane, catalyst layers, gas diffusion layers (GDL), bipolar plates and the sealing gasket. According to the studies on the degradation of membrane electrode assembly (MEA), this kind of degradation can be classified as three categories of mechanical, thermal, and electrochemical. The catalyst degradation can happen in different modes such as loss of activation, conductivity loss, and decrease in mass transport rate of reactants. Also the pores in GDL can become clogged because of the impurities in the fuels, and this decreases mass transport and the conductivity of the system and lessens the performance. Further, conductivity loss and fracture can happen in the bipolar plates over time, which can reduce performance.

Modeling of the degradation considering the effect of operating conditions has been rarely investigated. The degradation model is needed to predict the performance loss in the system and its life time, analyze the system behaviour in long term operation. Bae *et al.* [2009] developed a model to predict the degradation rate of MEA using a bi-exponential function with random coefficients. Their analysis indicated that the reliability estimation of the model can be substantially improved by using the nonlinear random-coefficients model to incorporate two heterogeneous degradation characteristics of MEA performance during continuous operation of DMFC. Although their model can predict the degradation rate, the operating parameters are not considered and the experiments were conducted under the same operating conditions.

To address the deficiencies in the system degradation modeling, the durability study in this thesis investigates the degradation behaviour in DMFC performance over time considering the effect of fuel cell operating parameters and their interactions on the overall performance of a DMFC. It is proposed that a series of experiments be conducted on a single-cell DMFC system to observe the effect on cell performance and the interaction between four operational parameters: the internal fuel cell temperature, the methanol concentration, and the air and methanol flow rates. If a polarization model can estimate the performance change as a function of the operating conditions regardless of the degradation in the system. The same general polarization model can, therefore, be used to develop a degradation model that explains the loss mechanism of the polarization curve over its operating time and investigates the effects of changes on system performance. This model when coupled with raw experimental data, including the performance loss of the system over time, then formed the basis from which the changes in coefficients over time could be examined, providing insight into the degradation of system performance. Two empirical models, one for polarization and one for degradation, needed to be developed from experimentally measured DMFC performance data to predict the DMFC system behaviour from the four operating parameters.

2.4 Effects of DMFC Flow Fields and CFD Simulations

Although improvement has been made over the last few years, major technical challenges, such as slow electrochemical kinetics of methanol oxidation, methanol cross-over, cathode flooding, and CO_2 gas management, still prevent DMFCs to be commercial. In order to circumvent these problems, efforts have been made to develop more active electrocatalysts [Gurau *et al.* 1998, Liu *et al.* 1998, Choi *et al.* 2004, Carmo 2005], to modify and fabricate alternative membranes [Yoshida 1998, Peled *et al.* 1998, Pivovar *et al.* 1999, Staiti e al. 2000, Jia

et al. 2000, Libby *et al.* 2001, Finsterwalder *et al.* 2001, Ma *et al.* 2003, Kima *et al.* 2004], to investigate water management on the cathode [Ren *et al.* 2000, Mench and Wang 2003, Blum and Duvdevani 2003, Lu and Wang 2004], as well as to study flow field on the anode of a DMFC [Arico *et al.* 2000, Scott *et al.* 2001, Amphlett *et al.* 2001, Bewer *et al.* 2004, Yang and Zhao 2005, Wong *et al.* 2006].

In a DMFC, the distribution of the fuel on the electrode should be as uniform as possible to guarantee a uniform performance across the electrode surface [Wong *et al.* 2006] and the main component affecting the fuel distribution is the flow field. A few papers have reported on the optimal design of the anode flow field of DMFCs. Arico *et al.* [2000] inspected the effects of serpentine and interdigitated flow fields on the DMFC performance. Their experimental results showed that the serpentine design had a lower methanol crossover, higher fuel utilization, and marginally larger voltage efficiency at low current densities, while the interdigitated design enhanced mass transfer and membrane humidification, thus increasing power densities. However, methanol vapor was used in their experiments.

Amphlett *et al.* [2001] studied the performance of a DMFC equipped with an anode flow field width parallel rectangular channels. Their experiment indicated that a flow channel with a medium depth has a better performance than both shallower and deeper channels. Scott *et al.* [Scott 2001] used stainless steel mesh material as the flow field of a DMFC. Their experiment showed that this type of flow field has capable characteristics for gas removal and electrical performance.

Bewer *et al.* [2004] proposed a novel technique of simulating two-phase flow in a DMFC by using an aqueous H_2O_2 solution. The influence of the flow field on bubble creation and flow uniformity was investigated. Their experiment indicated that splayed manifolds provide a

uniform flow and thus a better performance when compared to other designs. Yang *et al.* [2005] investigated the effect of the single serpentine and parallel flow fields on the cell performance of a DMFC experimentally. In situ images show that CO_2 bubble behaviour varies in different flow fields as shown in Figure 2.2. They found that the single serpentine flow field exhibited a better performance than the parallel flow field. They also found that gas bubbles blocked the flow channels in the parallel flow field at low methanol solution flow rates and high current densities, but this channel-blocking issue was never found in the single serpentine flow field and could be the main reason of a better performance in serpentine channel flow field.

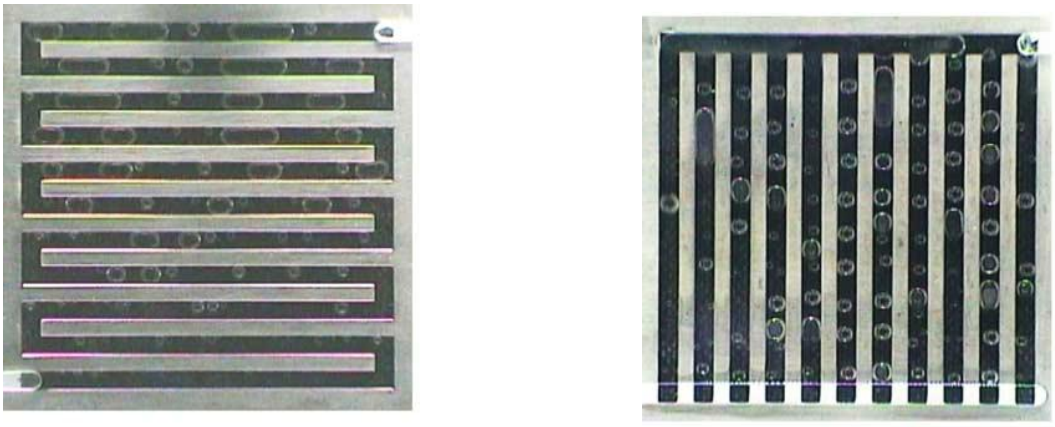

(a) (b)

Figure 2.2 In Situ Images of CO_2 Gas Bubble Behaviour in Single Serpentine Flow Field(A) and Parallel Flow Field (B) from Yang *et al.'s* [2005] Study

The effect of the bipolar/end plate channel width on the performance of the DMFC is proposed to be investigated. Since the optimum design has been reported to be serpentine flow field, the focus will be on the investigation of this design. Three different bipolar/end plates with a single-channel serpentine configuration are proposed to be fabricated with various channel widths, but maintaining the effective flow areas to be approximately the same by varying the lengths of the channels. A series of experiments will be designed to evaluate the performance of

the cell for each of the three geometric configurations. It is proposed that in the experiments, each bipolar/end plate geometry will be used on both the anode and the cathode and the performance curve for that geometry be measured to observe the effect of the geometry.

It is hypothesized that the change in performance using different types of geometries is mainly due to the flow characteristics inside the bipolar/end plate channels. In order to explain the performances between the different widths, a single-phase computational fluid dynamics (CFD) model for the flow in the channel is proposed to be developed. The comparison between the flow CFD simulations could reveal the causes of the different performances due to the change in the geometry.

Oliveira *et al.* [2007] classified the DMFC modeling methods into three types: analytical, semi-empirical, and mechanistic models. Analytical models are effective tools for understanding the influence of design and operating variables on fuel cell performance. Many assumptions are established to simplify mathematical models that describe fuel cell behaviour such as the relationship between current density and cell voltage. Semi-empirical models are developed by approximating theoretical relationships using empirical equations whose coefficients are trained by experimental data.

Mechanistic models are transport models with differential and algebraic equations developed based on electrochemical and physical governing phenomena. In mechanistic models, the phenomena of heat, momentum, multi-component mass transport, multi-phase transportation, and electrochemical processes are considered. Mechanistic models developed based on CFD can be classified into three categories: one-dimensional (1D), two-dimensional (2D), and three-dimensional (3D) models. In 1D models, the physical and chemical behaviours are considered only along a single direction, i.e., the X-direction from the anode to the cathode. In 2D models,

the physical and chemical behaviours are considered along both X-direction and Y-direction. Three-dimensional models are complete models where the physical and chemical behaviours are considered in all three directions. Computational fluid dynamics (CFD) is an effective tool for building mechanistic models in research on DMFCs.

Baxter *et al.* [1999] developed a one-dimensional model that considers the anode as a porous electrode consisting of an electronically conducting catalyst structure thinly coated with an ion-selective polymer electrolyte. Scott and Argyropoulos [2004] introduced another one-dimensional model to focus on DMFC anode catalyst. This model used a metal mesh supported electro-catalysts structure and analyzed the multi-reaction paths of methanol oxidation. Ko *et al.* [2010] presented a one-dimensional, two-phase model (i.e., liquid and air phases) in which the two-phase species transport behaviour through the porous DMFC components was formulated based on the Maxwell-Stefan multi-component diffusion equations, while the capillary-induced liquid flow in the porous media was described by Darcy's law.

Kulikovsky [2000] introduced a two-dimensional numerical model based on mass and current conservation equations. The velocity of the liquid in this model is governed by the gradients of membrane phase potential and pressure. Birgersson *et al.* [2003] developed an isothermal two-dimensional liquid phase model for the conservation of mass, momentum, and species in the anode of a DMFC. Divisek *et al.* [2003] developed a two-dimensional model that treats the diffusion layer as a water-gas system in the pore space, with saturation and permeability varying according to capillary effects. Bigersson *et al.* [2004] further introduced an isothermal two-phase ternary mixture model that takes into account conservation of mass, momentum, and species in the anode of the DMFC. Rice and Faghri [2006] developed a 2-dimensional, transient, multi-phase, multi-component model for a passive DMFC. This model

can capture evaporative effects, as water and fuel management issues are crucial. Yang and Zhao [2007] introduced an isothermal, two-dimension, two-phase transport model for liquid-feed DMFC. The two-phase mass transport behaviours in the anode and cathode porous regions were formulated based on the classical multiphase flow in porous media without invoking the assumption of constant gas pressure in the unsaturated porous medium flow theory.

Although the one-dimensional and two-dimensional CFD models are easier to use, they are not as accurate as three-dimensional CFD models. Ge and Liu [2006] developed a three-dimensional single phase (i.e., liquid phase at the anode and gas phase at the cathode), multi-component model of a DMFC. Danilov *et al.* [2006] presented a three-dimensional, two-phase CFD model for describing gas evolution and current distribution in a DMFC. Ge and Liu [2007] improved their previous three-dimensional single phase model into a three-dimensional, two-phase, multi-component model. Liu and Wang [2007] developed a three-dimensional, two-phase, isothermal model for DMFC to investigate the effect of electron transport through the backing layer and the land in bipolar plates. Yang *et al.* [2007] developed a three-dimensional steady-state model.

Despite progress in DMFC modeling, most models found in the literature consider only a single channel of simple geometric shape at the anode and cathode sides. The impact of geometric parameters at the anode and cathode on performance has not been well studied in DMFCs. Although Ge and Liu [2006] stated their models have the potential to predict DMFC performance with new geometries, only data collected from a DMFC with the same geometric configuration were used in their model. In addition, often physical and/or chemical model parameters have to be calibrated manually to match models with experimental data.

To address the above problems, a single-phase 3D CFD model is proposed to be developed in this research to study the causes of the different performance of single-cell DMFC with serpentine flow channels at the anode side. In this research, the impact of channel geometric parameters and fuel cell operating parameters on performance will be investigated. It is proposed that three geometric configurations of single-cell DMFC stacks be used to collect the experimental data and investigate the flow characteristics such as flow velocity and pressure.

2.5 Summary

As seen in the literature review, the DMFC has become a popular research topic, but some issues still prevent DMFCs from coming to market. Some of the challenges that have been investigated include slow electrochemical kinetics of methanol oxidation, methanol cross-over through polymer membranes, cathode flooding, as well as CO_2 gas management. However, compared to the other types of fuel cells, less research attention has been directed toward the durability of the DMFC systems and the geometry design of bipolar/end plates, which is the main focus of this thesis.

While in previous studies on the operating parameters in DMFCs, the effect of individual operating parameters on the performance is investigated, the effect of the four parameters of temperature, methanol concentration, methanol and air flow rate will be combined in this research. In addition, the interaction between different parameters and the interaction effect on the performance of the cell will be analyzed by varying all of the operating factors.

While durability and degradation in DMFCs has been also investigated by a few previous researchers, the systematic change in the system during the operating hours has been seldom modeled. The objective of the degradation study is to investigate the degradation behaviour in DMFC performance over time considering the effect of fuel cell operating parameters and their

interactions on the overall performance of a DMFC and also model the performance loss in the system. The required models for polarization and degradation will be developed from experimentally measured DMFC performance data to predict the DMFC system behaviour over time and study the causes of the systematic changes in the DMFC.

Beside the durability studies, the effect of the bipolar/end plate channel width on the performance of the DMFC is investigated. A couple of studies investigated the effect of flow fields in the performance of DMFCs and most of them agree that the serpentine flow field shows a better performance in the system. Based on this, three different bipolar/end plates with a single-channel serpentine configuration will be fabricated at various channel widths, but the effective flow areas are maintained to be approximately the same by varying the lengths of the channels. A series of experiments is needed to evaluate the performance of the cell for each of the three geometric configurations. The change in performance due to different geometries is hypothesized to originate from the flow characteristics of the fluid inside the bipolar/end plate channels. In order to explain the performances between the different widths, a single-phase computational fluid dynamics (CFD) model will be developed for the flow in the channel. The comparison between the flow simulations for the three used bipolar/end plates geometries can then be used to investigate the roots of the difference in polarization behaviour of the cell.

Previous studies have been reviewed and the DMFC challenges introduced. Among those challenges, durability and the design of the flow field for DMFCs seem to be areas that need more investigation. Therefore, the focus of this thesis has been brought to these two issues. The degradation is investigated by performing several experiments and measuring the response of the system. Moreover, an empirical model is developed to predict the performance loss in the system and relate the model to the possible causes of the degradation in the performance. Further, flow

field design has been rarely studied before. Therefore three different designs are fabricated and tested to investigate the effect of the width of the channel in the overall performance of the cell. Finally, a CFD model will be also developed to understand the causes of the change in the performance of different designs.

Chapter 3: EXPERIMENTS

Several experiments are needed to investigate the degradation behaviour of the system and measure the performance of different flow field designs in operation. In this chapter, the experimental setup is described and a design of experiments to investigate the durability and study the flow field is explained.

An experimental setup for a DMFC system was designed to control cell temperature, methanol concentration, and methanol and air flow rates, and measure the responses of the system at different operating conditions. Further, the impedance of the system has been measured at different operating conditions since its values are needed in developing the polarization model. Moreover, two series of experiments are designed to individually study the degradation and flow field of bipolar plate, respectively.

3.1 Experimental Setup

In the degradation study, performance and the electrical impedance of the system need to be measured to develop the polarization and degradation model. In addition, a performance measurement is required to study the difference between different flow fields. Therefore, the experiments required for this study can be divided into two types of measurements: polarization measurements and impedance measurements.

3.1.1 Polarization Measurements Experiments

Polarization measurement experiments evaluate the performance of the system under the running conditions. These experiments were carried out with a single-cell stack DMFC. To investigate the effect of the operating parameters on the performance, the setup had to control the

operating conditions and electrical load of the system. The measured output variables are voltage (V) and current density (j) of the polarization curves of the system.

The experimental setup is illustrated in Figure 3.1. In this setup, the pump and the air compressor are used to provide the desired fuel and air flows, respectively. An electronic load is used to consume the electric power produced by the fuel cell at different operating conditions.

The fuel cell is composed of a 10 cm^2 MEA with Pt-Ru/C catalyst on the anode, Pt/C catalyst on the cathode, the catalyst loading of 4 mg/cm^2, The used 5-layer MEA is from the TekStak educational fuel cell kit which uses PEMEAS/E-TEK, with a Nafion®-117 proton exchange membrane and 2 DLs with a porosity of 0.2. . Air is fed into the fuel cell at a controlled rate using an air compressor and regulated by a rotameter (Omega FL-3861SA). The methanol with purity of 99.9% is mixed with deionized water and pumped into the DMFC using a peristaltic pump (VWR 54856-070) right after the dilution of solution to avoid the concentration change in the solution. The air and methanol were supplied by 6.35 mm polypropylene tubing.

An aluminum housing with Teflon^{TM} current insulators was designed and fabricated to transfer the heat to the bipolar plates in the fuel cell for controlling the internal cell temperature. The temperature of the fuel cell is regulated by a hot plate below the DMFC with a thermal controller (Omega CSC32).

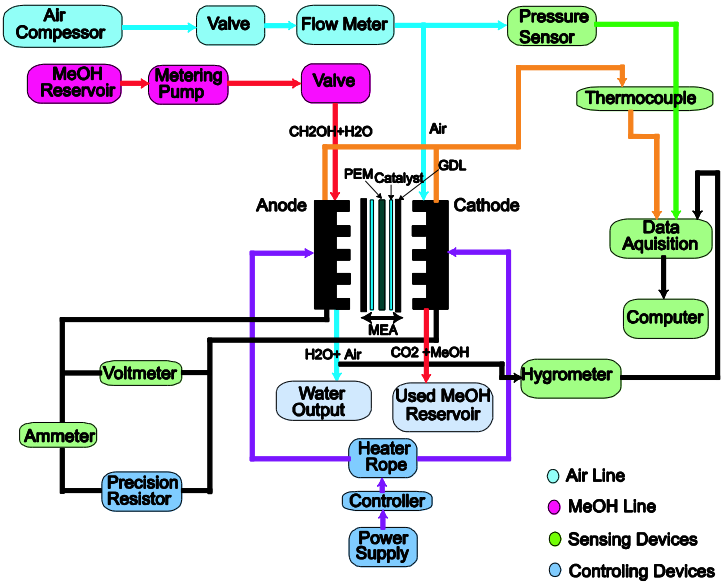

(a)

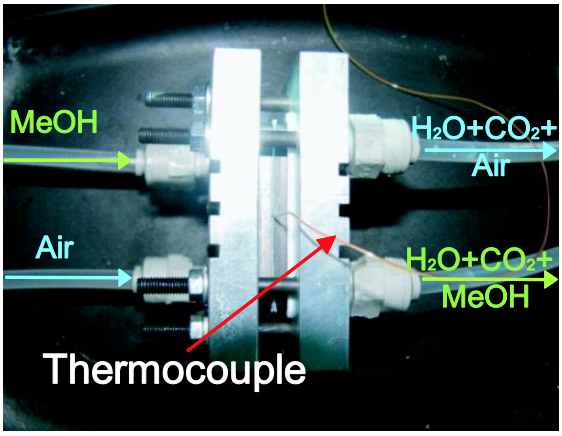

(b)

Figure 3.1. Experimental Setup: (a) Schematics of the Experimental Setup, (b) Pictorial View of the Setup

Pressure in the air stream is measured using a pressure transducer (Validyne P300D) and displayed by an electronic device. The temperatures of the methanol, air inlet and outlet, and the temperature inside the cell are recorded with a data acquisition unit. Voltage and current are measured using a high precision digital multimeter (Agilent 3478A). For electrical loading of the fuel cell, an electronic load (BK Precision 8540) is used. Accordingly, the operating parameters

of the cell will be adjusted to the desired value by the equipment, then the system is allowed to reach steady state. The polarization curve of the system then will be measured by changing the attached electric load. The parameters will be maintained the same during each run to evaluate the performance while the system is running.

3.1.2 Impedance Measurements

The oohmic internal resistance is the electrical resistance of the cell itself regardless of the attached electric load. The oohmic internal resistance of electrical systems plays an important role in system performance and should be measured carefully to determine the performance characteristics of the system. The impedance of the DMFC cell is necessary to model the system polarization curves, and ohmic resistance (R_e) is also a key performance driver of fuel cells [Larminie and Dicks 2003, Barbir 2005]. The ohmic resistance against DC voltage production can be estimated from the cell's impedance.

Three sources of ohmic voltage loss are resistance to ion movement in the electrolyte, resistance to electron passage in the cell components (electrodes, diffusion layers, etc.), and contact resistance. The total internal resistance of a fuel cell is an imperative factor, as a small change of ohmic resistance (in the order of milliohms) has a significant effect on the overall performance because of the high current densities at which DMFCs are generally operated [Larminie and Dicks 2003]. As a result, it is required to measure the resistance of the cell during its operation.

The fuel cell can be modeled by the Randles equivalent circuit shown in Figure 3.2a [Cooper and Smith 2006]. This model circuit is normally practical for electrochemical systems in which contact resistance are small enough to be ignored. Polarization resistance equivalent to the reaction, the capacitance is the interfacial capacitance of the cathode, and the ohmic resistance is

the resistive component of the fuel cell to be measured. The voltage source element is an ideal DC voltage source with zero internal resistance and a potential equal to the open circuit voltage of the cell.

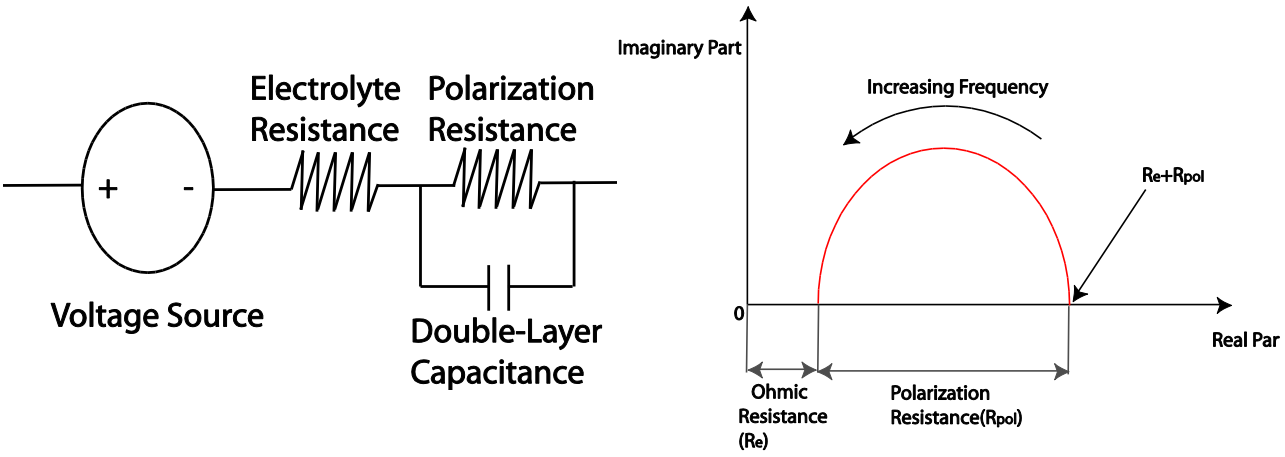

(a) (b)

Figure 3.2 (a) Equivalent Circuit for a PEM Fuel Cell, (b) Nyquist Plot of the Impedance of the Equivalent Circuit shown in (a) [redrawn from Cooper and Smith 2006]

Electrochemical impedance spectroscopy (EIS) was used to measure the impedance of the cell at different frequencies. In EIS, a potentiostat or a load bank combined with a Frequency Response Analyzer (FRA) are used. [Yuan *et al.* 2010]. The FRA will generate an AC current sinusoidal signal. The response to the signal from the fuel cell will enter to the FRA for analysis to obtain the AC impedance. To obtain the system impedance at different frequencies, the frequency of the excited sine wave can be swept across the frequency range of interest.

Therefore, EIS involves imposing an alternating current perturbation over a broad range of frequencies and observing the resulting differences in magnitude and phase of the cell voltage and current in order to obtain the impedance of the DMFC. Several parameters are extracted via

equivalent circuit modeling [Larminie and Dicks 2003]. These parameters contain electrode properties such as ohmic resistance and polarization resistance, double-layer capacitance, and transport properties [Cooper and Smith 2006, Springer *et al.* 1996, Makharia *et al.* 2005, Guo *et al.* 2003]. The equipment used for the EIS was a potentiostat/galvanostat at frequencies of 10 kHz to 10 Hz with 10 mA of current amplitude (Gamry instrument, Reference 600 / Biologic SP150). The resistance of the operating cell was measured at different conditions to determine the high frequency resistance of the cell. A table of conditions of the impedance measurement is provided in Appendix A.

Thus, the required experiments are divided to polarization measurements and impedance measurements. The experimental setup to measure the polarization was designed with the ability to control and change the operating parameters and evaluate the performance of the cell. In addition, EIS method was used to measure the impedance of the cell, which is a significant characteristic of the DMFC.

3.1.3 Preparation of the DMFC

After the stack has been assembled for the first run, it is necessary to break-in the membranes in order to achieve optimal performance according to the TekStak manual. The purpose of this process is to ensure that the MEAs are hydrated and to activate the catalyst layers to maximize the ionic conductivity of MEAs.

The followed break-in procedure outlined here is based on the procedure suggested by PEMEAS/E-TEK to achieve optimal MEA conditions which has two steps. The first step is to fully humidify the MEAs. Based on E-TEK recommendation, hot (90°C) deionized water was fed to the anode side of the cell and saturated air at 80°C was provided to the cathode side for about an hour.

The purpose of the second step is to activate the catalyst layers in the cell. E-TEK suggests that the catalyst layers can be activated using a 1-2 M methanol-water solution. Based on the procedure, the fuel solution was heated to 85°C and injected to the stack at a relatively high flow rate of 5 ccm. The air flow was about 750 ccm. The DMFC operated for 3 hours under a current load such that the output cell voltage is 0.2 to 0.3V. According to the TekStak educational kit manual, after 3 hours, catalyst activation should be complete. To ensure that the break in procedure is complete and the MEAs are fully activated, the performance of the cell has been measured and the polarization curve was compared to the presented curve in the manual. Figure 3.3 shows the comparison of the performance of the DMFC stack extracted from its manual and the performance of the tested DMFC in this study after the break-in procedure. The test conditions in Figure 3.3 are temperature of 50^0C, methanol concentration of 1M methanol flow rate of 5ccm, and air flowrate of 400ccm. The results show that the experimental data after the break-in process is close to the polarization curve and the power range is similar, therefore the MEA has been activated and can be used to proceed the experiments for this study. The difference in the two curves in Figure 3.3 can be due to the other conditions that can be different based on the laboratory conditions. The power density measure in this study is comparable to other existing DMFC experimental studies with low power densities ranging at 30-80 mW/cm2 [Wong *et al.* 2006, Yang and Zhao 2005, Rice and Faghri 2006]. The experimental data in this study were also matched with the data provided in the TekStak kit manual. The low power output of this cell is due to its low MEA catalyst loading compared to high output cells.

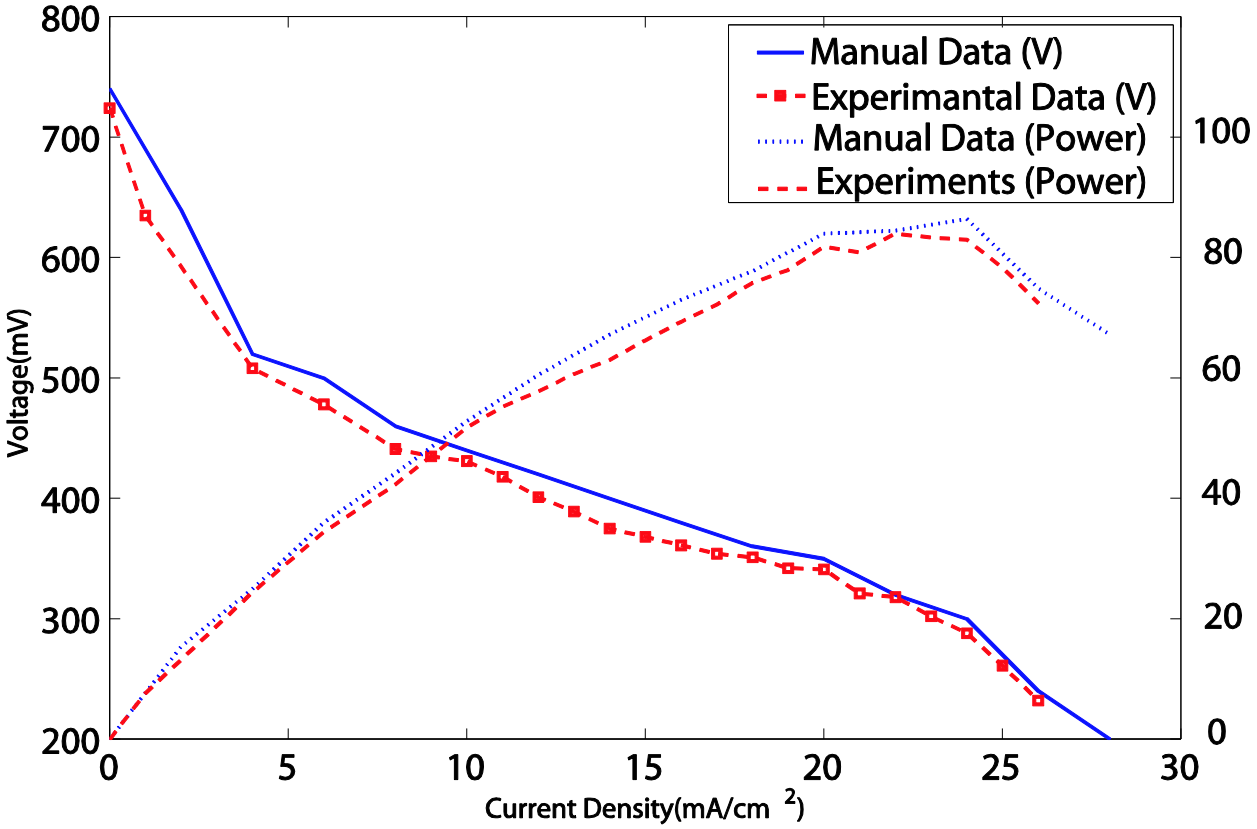

Figure 3.3 Comparison of the Performance Curves of DMFC after Break-In Procedure with the Performance Data of TekStak Manual (Temperature of 50^0C, Methanol Concentration of 1M Methanol Flow Rate of 5ccm, and Air Flow Rate of 400ccm.)

3.2 Performance Modeling and Durability Experiments

Performance modeling and durability experiments need to be conducted to evaluate the performance of the DMFC at different operating conditions and the influence of these conditions and their interaction on the polarization and degradation of the system. The conscious design of experiments helps to extract the useful data from the experiments and reduces the consumed time in the experimenting procedure. Therefore, the uniform design method was used to reduce the number of test cases for the different operating conditions [Fang and Yang 2000].

Table 3.1 Parameters Values for the Modeling and Durability Experiments

Level / Parameter	1	2	3	4	5
Temperature (K)	298	313	323	333	343
Methanol Concentration (M)	0.25	0. 5	1	1.5	2
Air Flow Rate (ccm)	81.2	93.6	108.7	125.2	140.8
Methanol Flow Rate (ccm)	3.5	4	4.5	5	5.5

Uniform design specifies test points that are uniformly scattered in the domain, which gives an even distribution of selected test points, and it is an easy to use method design of experiments. For a uniform design considering four factors at five levels, one of eleven different test configurations, ranging from five to fifty-five experimental tests, can be selected from the design of experiment table. In this study, 45 test cases were selected considering the efficiency and quality of numerical data fitting. Table 3.1 shows the values of the four operating parameters for the closed circuit experiments. The values chosen for each of the parameters were based on the structure of the DMFC system under investigation and the limitations of the experimental setup. Table 3.2 shows the design of the experiments of the 45 runs with different conditions. The time of each run is about one hour then the operating conditions are adjusted ti the design values based of design of experiments. Some runs have been chosen to be repeated in over the operating time of the cell to investigate the effect degradation at the same operating condition. The repeated runs are test 15, 30, and 45 which have been repeated three times over the operating time of the cell after every 15 runs respectively.

Table 3.2 Design of Experiments for the Durability Study

No.	T (level)	M_f (level)	C_{me} (level)	A_f (level)	No.	T (level)	M_f (level)	C_{me} (level)	A_f (level)
1	1	5	3	2	24	1	5	4	5
2	4	3	3	4	25	1	1	5	4
3	3	2	5	1	26	2	5	1	4
4	4	1	1	1	27	4	4	1	3
5	3	4	4	2	28	2	3	2	2
6	1	2	4	1	29	5	5	2	1
7	3	2	2	4	30	4	5	3	5
8	3	3	2	4	31	5	4	1	5
9	5	1	5	2	32	4	2	5	5
10	2	2	3	3	33	5	1	2	5
11	1	3	2	4	34	4	3	1	2
12	5	3	4	1	35	5	4	4	3
13	4	5	2	3	36	1	4	1	1
14	2	3	4	3	37	3	2	3	2
15	3	4	4	4	38	4	3	5	2
16	3	5	1	2	39	1	2	1	5
17	2	3	5	5	40	5	2	1	3
18	4	1	4	3	41	5	5	5	4
19	2	1	3	1	42	2	4	3	5
20	3	1	4	5	43	1	4	5	3
21	2	5	5	1	44	3	4	2	3
22	1	1	2	2	45	5	2	3	4
23	2	1	1	3					

Thus, the number of experiments is 45 runs with different conditions, which will be used to study the interaction between the parameters of the cell on the polarization behaviour. In each run, the conditions are set to the designed value and the voltage and current density in the cell are measured experimentally. Moreover, the operating time of each experiment has been recorded to

investigate the effect of degradations in the system while the cell is working with different conditions.

3.3 Flow Field Designs Experiments

The overall efficiency of fuel cells greatly depends on the performance of the bipolar/end plates in their stack [Besmann *et al.* 2000]. In this experimental setup, graphite bipolar/end plates were used. Graphite is a material common to these plates, due to its good thermal conductivity (25-470 W/m.K), low density (1.3-1.95 g/cm^3), and high corrosion resistivity compared to other alternatives such as stainless steel. The channels in the graphite bipolar/end plates are single-path serpentine flow channels machined on the graphite plates at different widths using 0.737 and 0.889 mm milling tools with the feedrate of about 0.00762 mm per revolution. The grooves on the three bipolar/end plates were designed such that the cross-sectional flow areas were approximately the same for the different channel widths. Flow area is defined as the total machined planar area of the graphite plate that feeds fuel or air to the Diffusion Layer (DL). Both the anode and the cathode have the same bipolar/end plate geometry and configuration. The dimensions of each bipolar/end plate are shown in Table 3.3, and the bipolar/end plates tested are shown in Figure 3.3. As can be seen from Table 3.3, the flow areas of the bipolar/end plates differed at most by 9% and therefore the factor in the experiments was the effect of the width of the channel on the performance.

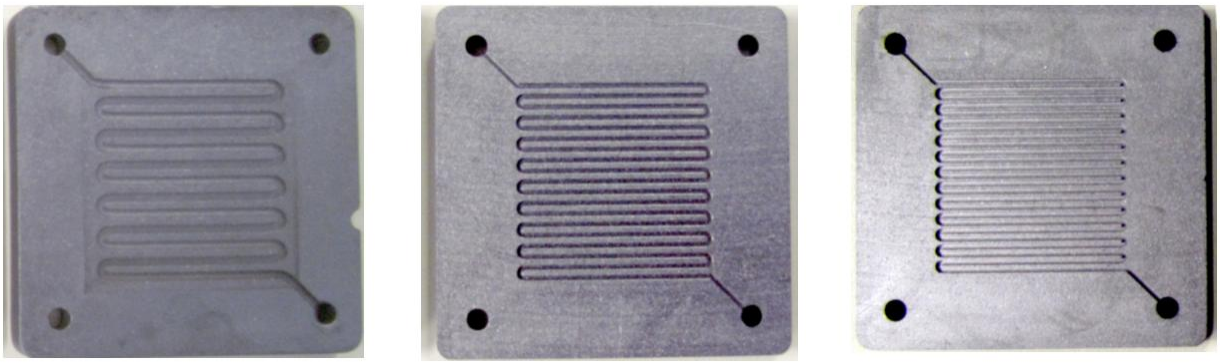

Design A Design B Design C

Figure 3.3 Three Fabricated Bipolar Plates for the DMFC experiments.

Table 3.3 Dimensions of Three Different Designed Bipolar/end plates

Design	Number of Switchbacks	Flow Area (mm^2)	Channel		
			Width (mm)	Depth (mm)	Hydraulic Diameter (mm)
A	12	558.1	1.37	0.5	0.733
B	18	512.7	0.889	0.5	0.640
C	24	544.7	0.737	0.5	0.596

In addition, the operating conditions have been changed for each design to see the effect of the operating conditions and to have enough data to model the performance. For each design, 10 conditions have been performed as shown in Table 3.4. The 10 selected experiments in this study chosen among the 45 tests in Section 3.2 in which two experiments for each of the five levels of the parameters will be conducted. The operating conditions were the same for the three flow field designs to compare the performance at the same operating conditions.

Table 3.4 Design of Experiments for the Flow Field Study

No.	Temp. (K)	Methanol Flow (ccm)	Methanol Conc. (mol/L)	Air Flow (ccm)
1	298	2.27	1.5	287
2	298	4.05	0.5	72
3	313	3.48	1	186
4	313	4.05	2	402
5	323	2.27	0.25	118
6	323	4.4	0.25	287
7	333	3.06	2	72
8	333	3.48	1	186
9	343	3.06	0.5	402
10	343	4.4	1.5	118

Thus, three various serpentine-channel flow fields were designed and fabricated. The width of the channel is different for each design but the open areas of the bipolar/end plates are approximately the same since the width of the channel is under investigation as a design factor. The widths of the three designs are 1.37, 0.889, and 0.737 mm for designs A, B and C respectively. These fabricated bipolar/end plates will be tested for the performance analysis and the operating conditions for each design should be known. To define the operating conditions, 10 tests were chosen from the design of experiments in Section 3.2 with the two runs for each level of parameters. Therefore, 10 tests at different operating conditions will be done for each design to observe the different performance of each design at these 10 operating conditions.

3.4 Summary

Investigation of the durability and flow field of DMFCs requires a series of experimental data. In this thesis, the experimental setup consists of a single-cell DMFC and the controlling apparatus to adjust the operating conditions, which are temperature, methanol concentration, methanol flow rate, and air flow rate. The impedance of the system is also measured, since it is needed to develop the polarization model.

In the performance durability study, five levels and four operating factors have been considered. Using a uniform design of experiment, a plan of 45 runs is used to observe the effect of the operating conditions and their interaction on the performance loss of the system.

For the geometry analysis, three bipolar plates with different widths have been designed and manufactured. The bipolar/end plates have been designed to have the same open area but different channel width. Based on a design of experiment, data was collected from 10 runs at different operating conditions for each geometry. Therefore, a total of 30 tests have been conducted to investigate the effect of the operating conditions and the flow filed design on the performance of the DMFC. The performance measurements at different operating conditions with the operational time will be used to model the degradation of the DMFC system, which is discussed in Chapter 4. The experiments on different flow fields will be used to observe the difference in the performance due to different channel width and also model the polarization curve, which is explained in Chapter 5.

Chapter 4: DEGRADATION ANALYSIS OF A SINGLE-CELL DIRECT METHANOL FUEL CELL SYSTEM

The goal of the durability study is to investigate the degradation behaviour in DMFC performance over time considering the effect of fuel cell operating parameters and their interactions on the overall performance of a DMFC. A series of experiments was conducted on a single-cell DMFC system to observe the effect on cell performance of the interaction between four operational parameters: the internal fuel cell temperature, the methanol concentration, and the air and methanol flow rates. In order to evaluate the degradation in the performance of the cell over its operating time, a model is required to estimate the performance change as a function of the operating conditions and the operating time of the cell. Assuming there is negligible degradation in the observed data, a model that accurately represents the basic performance of the cell can be formulated from that data independent of any performance degradation. This model, when coupled with raw experimental data which includes the performance loss of the system over time, then forms the basis to examine how the coefficients in the model change over time and give insight into the degradation of system performance. Two empirical models, one for polarization and one for degradation, have been developed from experimentally measured DMFC performance data to predict the DMFC system behaviour from the four operating parameters.

The aim in the polarization model is to predict the voltage-current curve of the system considering data compensated for changes over time, and determine the polarization behaviour of the system from operational factors independent of degradation. The four operational

parameters were empirically fitted to the polarization curves based on time-compensated experimental data. Some of experimental data that was not used in the fitting was used to validate how well the model predicts the polarization curve. The polarization model is capable of predicting the voltage-current curve of the cell independent of degradation (for time-compensated data). This confirmed that the raw experimental data can be used to study the degradation behaviour of the system and explain the loss mechanism of the polarization curve over its operating time.

4.1 Semi-Empirical Polarization Model

A semi-empirical polarization model was developed with curve coefficients that were fit from experimental data. However, during the experiment, a considerable decrease in the DMFC performance was observed. Tests were performed with the same conditions at points throughout the 3,000 minutes of its operation to investigate the degradation of the performance, and the accumulated operating time at each run was recorded. The degradation of the fuel cell performance over time must be compensated for before the experimental data can be used to build a semi-empirical model since the desired model will not have time embedded in its equations as one of its factors.

4.1.1 Time Compensation of the Experimental Data

The time-compensated data provides the polarization model with experimental data that shows its performance without the influence of system degradation.

The raw data from the experiments was compensated for its dependency on time based on the following algorithm:

(1) Select a common reference time point, t_c, at which the data will be observed.

(2) For each data observation time, subtracting off t_c.

(3) Use stepwise linear regression to fit a model with time and time's cross terms with voltage and the other four operating variables and the square root of the current density (j) as the dependent (predicted) variable. A square root transformation of the data was necessary to meet the normally distributed residual assumption for the regression. The linear regression model is shown in Equation 4.1 and the calculated coefficients are shown in Table 4.1.

$$j = \delta_1 T + \delta_2 C_{me} + \delta_3 M_f + \delta_4 A_f + \delta_5 V + \delta_6 M_f \times t + \delta_7 A_f \times t \qquad (4.1)$$

Table 4.1 Coefficients of the Time-Compensation Linear Regression Model (Equation 4.1)

Term	T	C_{me}	M_f	A_f	V	$M_f \times t$	$A_f \times t$
Coefficient	δ_1	δ_2	δ_3	δ_4	δ_5	δ_6	δ_7
Value	0.053	-3.46	0.428	0.063	0.036	-5.13e-5	5.97e-6

(4) Determine the model residuals.

(5) Use the model created from Step (3) to calculate an estimate of the output variable setting the time parameter as 0 and entering the test condition parameters and voltage for each observation. When time is 0, the model coefficients more meaningfully represent the state of the system at time t_c. The adjusted output estimates are labeled as y_{new}.

(6) Add the residual obtained in Step (4) to y_{new}. This reintroduces the variances to the standardized estimates.

(7) Square the output estimate to get it back to the original current measure, correcting for the square root transformation made in Step (3). Plot the repeated tests at the same condition to confirm the effectiveness of the data compensation

(8) Use the time compensated estimate to fit the semi-empirical model.

The flowchart of the compensation algorithm is illustrated in Figure 4.1. In the compensation algorithm, the data from each run is brought to a common reference time, t_c, which in this data set was 600 minutes from the beginning of the experiments. Six hundred minutes was selected as it could be assured that the system was fully broken in by this time. The break-in procedure is presented in Section 3.1.3. The linear regression model coefficients were acceptable at a 95% confidence level, and the R^2 value for this time compensation model was 0.92 which is shown in Table 4.1.

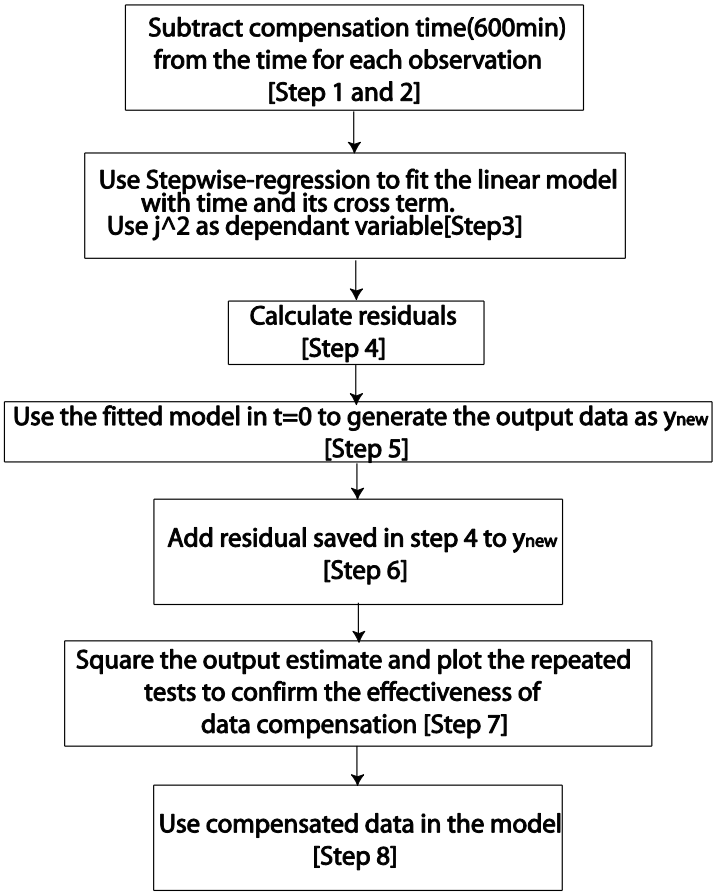

Figure 4.1 Flow Chart for Data Compensation Algorithm

To verify that the time-compensation algorithm can suppress the effects of time in the experimental data. We compared the results for the repeated test in the same conditions. As shown in Figure 4.2(a), the performance curve is degrading over time and the polarization curve in the same conditions but different operating time changes. After time-compensation, the time-compensated data for repeated tests are close to each other which means approximately the same performance curve after the time-compensation. Figure 4.2(b), shows the experimental data after time-compensation and the error in the three repeated test shown in Figure 4.2(a). To better show the range of error, these 68 data points were divided into 9 groups according to their current density values. The standard deviation, σ, for the data in each group was first calculated. The

−1.96σ and +1.96σ boundaries, corresponding to 95% of the confidence interval, were then used to plot the error bar for the selected data point group. This case also happened for the other two repeated tests and the results are similar to what is shown in Figure 4.2

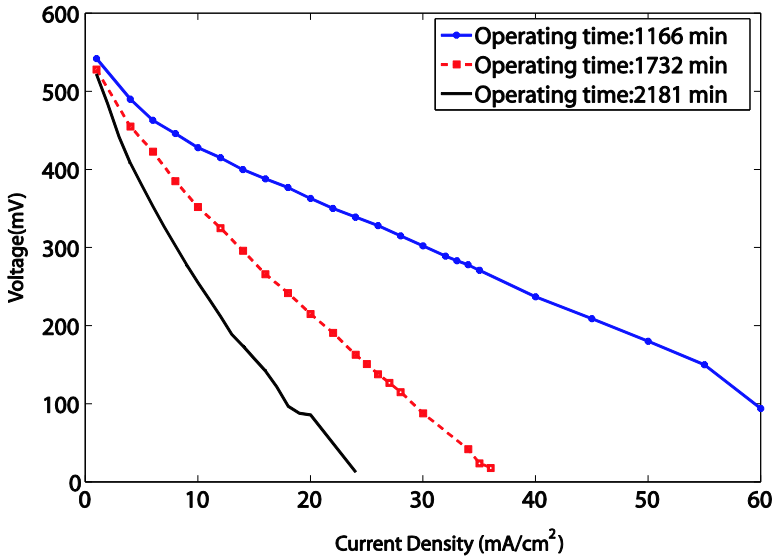

(a) Experimental Data of Run No. 15 in Different Operating Times

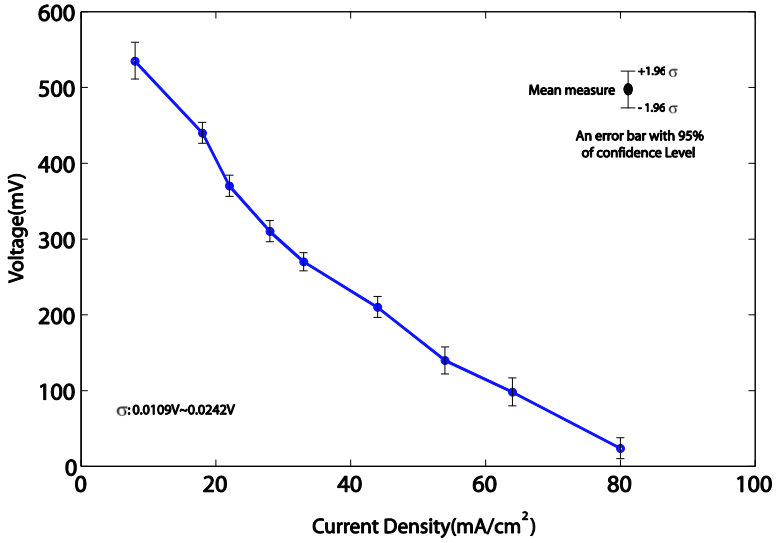

(b) Time-compensated Data after Compensation Algorithm

Figure 4.2 The Experimental Data before and after Applying Time-Compensation Algorithm (Temp.:323 K, MeOH Concentartion: 2M, Air Flow Rate: 140.8 ccm, MeOH Flow Rate: 5.5 ccm)

Thus, by applying the time-compensation algorithm to the raw experimental data, the performance loss in the system due to the degradation is suppressed. It can be assumed that the time-compensated data belongs to a DMFC system with the same properties but with negligible degradation effect. Therefore, the time-compensated data can be used in the semi-empirical polarization model to predict the basic performance of the tested DMFC regardless of degradation.

4.1.2 Semi-Empirical Polarization Model Formulation

Several models have been developed in the past to predict the polarization curves of DMFC systems. Srinivasan *et al.* [1988] used a simple model to describe the relationship between cell voltage and current density for a PEM fuel cell. Since a DMFC is a subset of the PEMFC family, the same model was selected for the DMFC [Scott *et al.* 2006]. Model Equation (4.2) describes the relationship between the cell voltage and the current density passing through the cell. In this equation, it is assumed that the oxidation of methanol does not occur under mass transport limitations and has no kinetic limitation.

$$E_{cell} = E_0^* - b_{cell} \ln j - R_e j \tag{4.2}$$

$$E_0^* = E_r + 2.303 \frac{RT}{\alpha F} \log j_0 \tag{4.3}$$

$$b_{cell} = \frac{RT}{\alpha F} \tag{4.4}$$

In Equation (4.2), E_{cell} is the potential of the cell, j is the current density of the cell, b_{cell} is the Tafel slope, an experimental value that represents the effect of loss in the voltage of the cell

and is related to the reaction rate in the system, and R_e is the slope of the linear region of the polarization curve representing the ohmic internal resistance of the cell. In Equation (4.3), E_r is the reversible potential of the cell and it can be calculated from the anode and cathode reactions in the cell. Although there are more complex and complete polarization models in the research literature, a simple model is used in this study since each coefficient can represent physical phenomena in the system. Therefore, if the model can be used to predict the performance of the tested DMFC, further investigation can be carried out especially for the degradation analysis. The anode reaction is defined by:

$$CH_3OH + H_2O \rightarrow 6H^+ + 6e^- + CO_2 \qquad (4.5)$$

The H^+ ions move through the electrolyte and the electrons move round the external circuit. Note that water is required at the anode, although it is produced at the cathode reaction:

$$1\frac{1}{2}O_2 + 6H^+ + 6e^- \rightarrow 3H_2O \qquad (4.6)$$

The ideal reversible cell voltage is calculated to be 1.21 V [Argyropoulos *et al.* 2003]. The practical voltage obtained is considerably smaller than the ideal voltage, and the losses in DMFCs are greater than those for other types of fuel cells, as considerable voltage loss has been observed at the anode of the DMFC to be caused by adsorption of partial decomposition products of methanol (e.g. CO), while the cathode losses are equivalent to other fuel cells [Appleby and Foulkes 1989].

The j_0 and α in Equation (4.3) are the exchange current density related to the reaction rate inside the system and transfer coefficient for the methanol oxidation, respectively. *T*, *R* and *F*

are the temperature of reaction, ideal gas constant (8.314472 J/mol · K), and Faraday constant (96,485 C/mol), respectively.

In addition, the resistance of the fuel cell can be modeled by [Scott *et al.* 2006]:

$$R_e = b_1 e^{\frac{b_2}{T}} \tag{4.7}$$

In Equation (4.7), R_e is the internal ohmic resistance of the fuel cell, which has been measured by the EIS measurement device, with empirical constants b_1 and b_2, and T is the absolute temperature of the cell.

The calculation procedure of the model coefficients listed in Table 4.2 is as follows: First, a set of coefficients for a log transformed Equation (4.7) have been obtained from a linear fit of the experimental data of the impedance measurements, and significant process parameters for Equations (4.10) and (4.11) were then determined from these values using stepwise regression, yielding a model fit of R^2 = 0.91. Using this resistance model to estimate R_e for each set of test conditions, forty-two $E_0^*$and b_{cell}, coefficients of the model in Equation (4.2) were then respectively obtained from a linear least squares data fit of the polarization curves from the test runs performed at the different test conditions of the uniform design of experiment. The minimum R^2 model fit observed when determining these $E_0^*$and b_{cell} values was 0.87. Note that three of the 45 experimental test runs were reserved for validation. The empirical coefficient α was calculated from Equation (4.4), which then permitted the calculation of j_0 from Equation (4.3), yielding 42 sets of values for $E_0^*$and b_{cell}.

A stepwise linear regression analysis was then performed to determine the significant empirical coefficients from the operating parameters T, the cell inner temperature, C_{me}, the molar methanol concentration, M_f, the methanol flow rate, and A_f, the air flow rate. With an adjusted R^2

value of 0.81, the step-wise regression analysis shows that methanol flow rate, air flow rate, the cross term for temperature and methanol flow rate, and the cross term for temperature and air flow rate are the significant factors to these coefficients, as shown in Equations (4.8) to (4.11). This reveals that methanol and air flow rates are important predictors to DMFC system performance, factors not captured in earlier DMFC models.

$$\alpha = \theta_1 A_f + \theta_2 T \times M_f + \theta_3 T \times A_f + \theta_4 M_f \times A_f \tag{4.8}$$

$$\ln(j_0) = \beta_1 A_f + \beta_2 T \times M_f + \beta_3 T \times A_f + \beta_4 M_f \times A_f \tag{4.9}$$

$$\ln(b_1) = \gamma_1 T + \gamma_2 M_f + \gamma_3 A_f + \gamma_4 T \times A_f + \gamma_5 M_f \times C_{me} + \gamma_6 M_f \times A_f \tag{4.10}$$

$$b_2 = \lambda_1 T + \lambda_2 M_f + \lambda_3 C_{me} + \lambda_4 M_f \times C_{me} \tag{4.11}$$

Table 4.2 Coefficients Values of Eqs. (4.8) to (4.11)

Eq. (4.8)	Term	A_f		T		$T \times A_f$	$M_f \times A_f$
	Coefficient	θ_1		θ_2		θ_3	θ_4
	Value$\times 10^6$	9.48		0.234		-0.025	-0.91
Eq. (4.9)	Term	A_f		$T \times M_f$		$T \times A_f$	$M_f \times A_f$
	Coefficient	β_1		β_2		β_3	β_4
	Value	36.421		2.010		-0.052	-4.636
Eq. (4.10)	Term	T	M_f	A_f	$T \times A_f$	$M_f \times C_{me}$	$M_f \times A_f$
	Coefficient	γ_1	γ_2	γ_3	γ_4	γ_5	γ_6
	Value$\times 10^4$	-0.231	-6.264	-0.281	0.019	-0.427	0.012
Eq. (4.11)	Term	T		M_f	C_{me}		$M_f \times C_{me}$
	Coefficient	λ_1		λ_2	λ_3		λ_4
	Value$\times 10^2$	0.032		5.01	0.62		0.21

4.1.3 Semi-Empirical Polarization Model Validation

The model was validated by comparing the polarization curves generated by the model to the 3 sets of experimental data reserved from the 45 uniform design test runs. Figure 4.3 shows three typical polarization curves of the experimental data. The error between the model and the

data, as represented by the standard deviation of error for the entire curve, was calculated and the results are shown in Table 4.3.

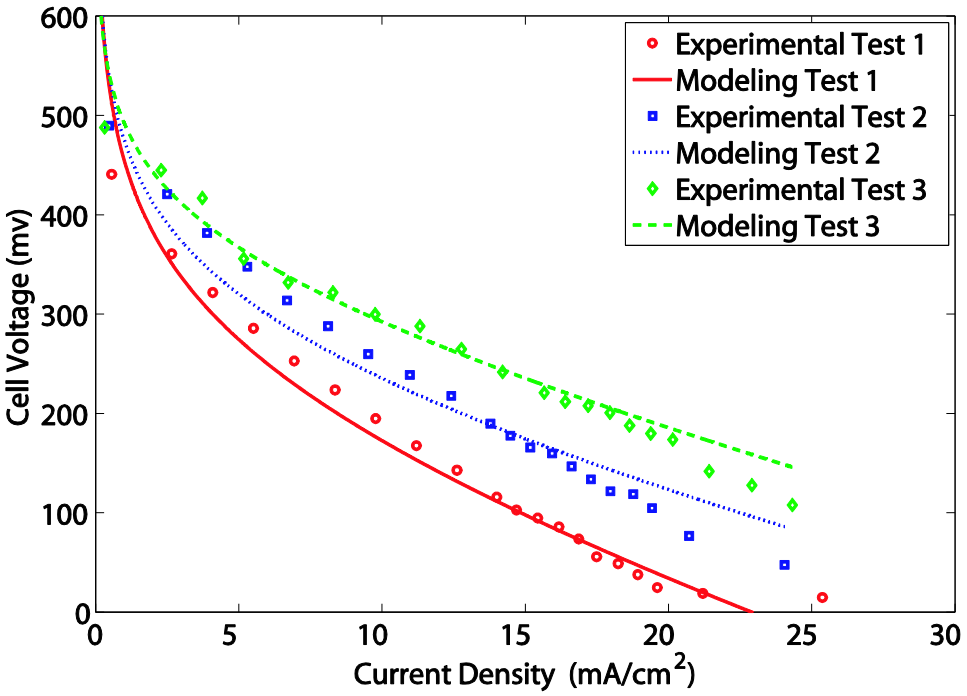

Figure 4.3 Validation of Model: The Comparison between the Experimental Data and DMFC Model in Three Different Conditions

Based on a comparison between the model and the experiments, it can be concluded that the model is effective for predicting the behaviour of the single-cell DMFC system. The maximum standard deviation in the three groups of data used in Figure 4.3 is 0.161V. For context, the average standard deviation of error for the 42 tests was 0.0533, and the three reserved tests represent different magnitudes of the error with an error percentile of 99th, 47th, and 14th for tests 1, 2, and 3, respectively. In Table 4.3, the Error Percentile column shows that the 3 reserved tests are from the three different ranges of model error according to the goodness

of the fit to the experimental data. This means that test 1 in Table 4.3 is among the poor fittings with R-squared of 0.88, test 2 is among the medium fittings with R-squared value of 0.90, and test 3 is among the good fittings of the model with the experimental data with R-Squared of 0.99. It is concluded that the empirical model has sufficient accuracy to estimate the polarization curve of the DMFC system when the temperature, methanol solution concentration, and methanol and air flow rates are provided.

Table 4.3 Prediction Error Analysis of the Modeled Experiments

Test No.	T (K)	C_{ME} (M)	A_f (ccm)	M_f (ccm)	*No. of Exp. Points*	Standard Deviation(V)	Fit Error Percentile	R-Squared
1	298	2	81.2	4	20	0.1607	99.5%	0.88
2	298	1	93.6	3.5	20	0.0499	46.7%	0.90
3	323	1.5	93.6	4	20	0.0091	14.1%	0.99

Some assumptions and limitations were made while developing this model. It is assumed that there is no constraint to mass transfer in the porous layer at the anode and cathode sides. However, in reality there are limitations for mass transfer of the fuels in the system, leading to a deviation of the model from the experimental data. In addition, this model should not be used for DMFC systems with geometric shapes that deviate from the tested system, nor outside the range of operational parameters tested. The model also should not be used for the stacked cells because the experiments in this study were carried out only for a single-cell DMFC.

Thus, the semi-empirical polarization model can predict the performance behaviour of the DMFC system based on the time-compensated data; therefore, the change in the coefficients while using the raw experimental data considering the existing degradation in the system can be used to achieve a degradation model which is discussed in Section 4.2.

4.2 Degradation Model

The degradation of the cell is investigated in this section by identifying the significant parameters that change over time during the operation of the system. Since the conditions of the tests varied over the time of the 45 uniform design experiments, the concept of moving averages has been used to analyze the experimental data to minimize the effect of changes in operational parameters other than operating time. Then, the data has been analyzed to develop a degradation model based on the change in the coefficients in the semi-empirical polarization model. The concept of moving average and the history indices is defined first, then the stepwise linear regression method to achieve the degradation model is discussed. Finally, the results of the degradation model and discussion of the possible reasons of the observed degradation is discussed.

4.2.1 Moving Average and History Indices

The fuel cell's degradation may be a result of systematic changes in the fuel cell over time. In order to understand short-term fluctuations and highlight longer-term trends or cycles, moving averages are commonly used to smooth out time series data. For example, it is often used in technical analysis of financial data over time [Chou 1969]. In this analysis, the experimental data was ordered in its chronological sequence. To observe long-term changes, the moving average of each experimental group has been calculated using a window size of three tests. As

illustrated in Figure 4.4, each group of three tests is assumed to have the conditions, time and response of the middle test, otherwise known as the pivot test. In other words, since only the overall trend is under investigation, grouping the time-sorted data and using the concept of the moving average provides a guide to the systematic changes in the system regardless of the change in the conditions of the tests.

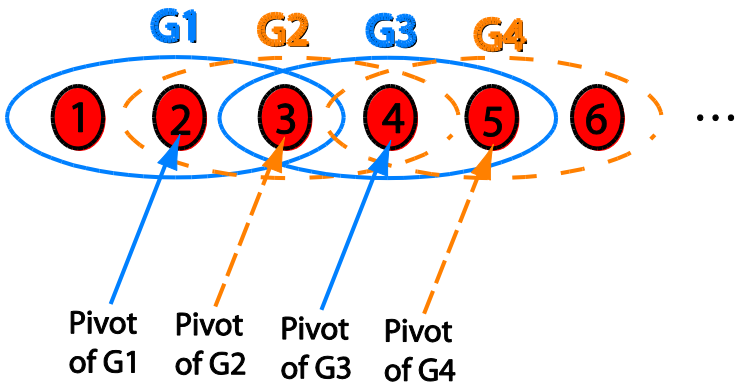

Figure 4.4 Moving Average Concept in the Analysis of Experimental Data

One hypothesis explaining the degradation in performance of the cell may be higher impedance from an increase in the size of the electro-catalyst particles in the catalyst layers [Bae *et al.* 2009], where this mass transfer could be explained by a time at a condition model, similar to how annealing is explained by time at temperature. The idea is to include the system operation history to predict its future performance. To include this history, a "History Index" is created, where the time of the operation at a specific condition is multiplied by an operating parameter, i.e. the temperature, methanol concentration, or methanol or air flow rate, and is represented by variables I_T, I_{Mf}, I_{Cme}, and I_{Af}. These terms are then added together as the system is operated under different conditions to provide a historic measure of exposure to the parameter for the next test. The history index for each parameter is calculated as shown in Equation (4.12), where $I_{X,i}$ is the history index for parameter X (temperature, methanol concentration, or methanol or air flow rate),

X_j is the value of the parameter setting for *j*th test, and t_j is the elapsed time for that test. Figure 4.5 illustrates the accumulative terms for each test. It can be seen that the History Indices (I_X) are the time integral of the operating parameter for the operational parameters at that condition and they actually represent what the system has gone through before performing the *j*th test.

$$I_{X,i} = \sum_{j=1}^{i} (X_j \times \Delta t_j) \tag{4.12}$$

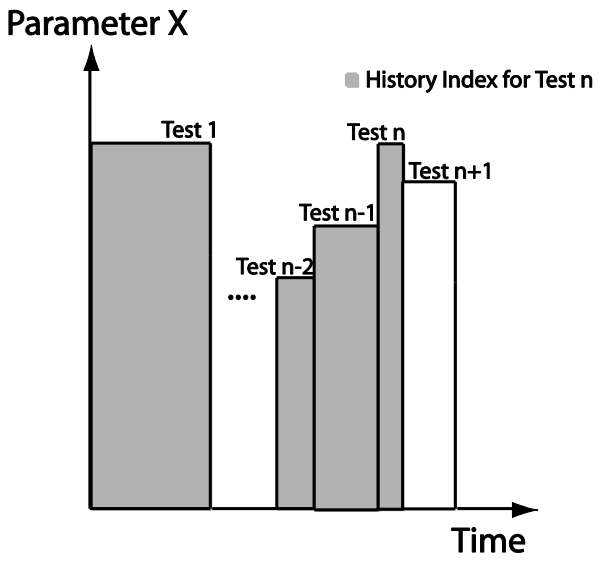

Figure 4.5History Index Illustration (the shaded area is the history index for each of the parameters for a specific test within an operating time)

4.2.2 Step-wise Linear Regression

The polarization curve relationship of Equation (4.2) was used to investigate the degradation behaviour of the DMFC system. The change in each coefficient of Equation (4.2) (E_0^*, b_{cell}, and R_e) over time can be used to characterize the change in performance in the DMFC since the model has been validated in Section 4.1.3. The model was developed by first fitting the

raw performance curves (not time compensated) for each of the experimental tests to Equation (4.2) and determining its coefficients. A relatively accurate prediction of the system performance was obtained from this fit, as the R^2 value is greater than 0.93 for all tests. In the next stage, these individual coefficients were used to model the degradation trend of each coefficient of Equation (4.2). A linear regression model has been used to achieve this degradation model for the cell.

The coefficients in Equation (4.2) calculated for each test condition were grouped following the moving average method discussed in Section 4.2.1. Equations (4.13) to (4.15) represent the potential linear model terms for the coefficients in Equation (4.2) based on the operating parameters (T, C_{me}, M_f, A_f) and the cross-terms of the operating parameters ($T \times C_{me}$, $T \times M_f$, $T \times A_f$, $C_{me} \times M_f$, $C_{me} \times A_f$,$M_f \times A_f$,), the operating time (t), and the history index for each of the operating parameters (I_T, I_{Mf}, I_{Cme}, I_{Af}).

$$\begin{aligned} E_0^* &= \eta_1 T + \eta_2 C_{me} + \eta_3 M_f + \eta_4 A_f \\ &+ \eta_5 T \times C_{me} + \eta_6 T \times M_f + \eta_7 T \times A_f + \eta_8 C_{me} \times M_f + \eta_9 C_{me} \times A_f + \eta_{10} M_f \times A_f \\ &+ \eta_{11} t + \eta_{12} I_T + \eta_{13} I_{M_f} + \eta_{14} I_{C_{me}} + \eta_{15} I_{A_f} \end{aligned} \quad (4.13)$$

$$\begin{aligned} b_{cell} &= \kappa_1 T + \kappa_2 C_{me} + \kappa_3 M_f + \kappa_4 A_f \\ &+ \kappa_5 T \times C_{me} + \kappa_6 T \times M_f + \kappa_7 T \times A_f + \kappa_8 C_{me} \times M_f + \kappa_9 C_{me} \times A_f + \kappa_{10} M_f \times A_f \\ &+ \kappa_{11} t + \kappa_{12} I_T + \kappa_{13} I_{M_f} + \kappa_{14} I_{C_{me}} + \kappa_{15} I_{A_f} \end{aligned} \quad (4.14)$$

$$\begin{aligned} R_e &= \mu_1 T + \mu_2 C_{me} + \mu_3 M_f + \mu_4 A_f \\ &+ \mu_5 T \times C_{me} + \mu_6 T \times M_f + \mu_7 T \times A_f + \mu_8 C_{me} \times M_f + \mu_9 C_{me} \times A_f + \mu_{10} M_f \times A_f \\ &+ \mu_{11} t + \mu_{12} I_T + \mu_{13} I_{M_f} + \mu_{14} I_{C_{me}} + \mu_{15} I_{A_f} \end{aligned} \quad (4.15)$$

To simplify the degradation model, a stepwise linear regression at a 90% confidence level was employed to determine which parameters are significant. The insignificant terms found from the stepwise regression with p-values more than 0.1 have been omitted from Equation (4.13) to (4.15). The number of coefficients has been reduced to 15 coefficients in Equations (4.16) to (4.18) from the 45 coefficients in Equations (4.13) to (4.15). The values of the regression coefficients using only the significant terms and the model fit R^2 term for these equations are listed in Table 4.4.

$$E_0^* = \eta_2 C_{me} + \eta_5 T \times C_{me} \tag{4.16}$$

$$b_{cell} = \kappa_2 C_{me} + \kappa_4 A_f + \kappa_5 T \times C_{me} + \kappa_{14} I_{C_{me}} + \kappa_{15} I_{A_f} \tag{4.17}$$

$$R_e = \mu_5 T \times C_{me} + \mu_{11} t + \mu_{12} I_T + \mu_{13} I_{M_f} + \mu_{15} I_{A_f} \tag{4.18}$$

Table 4.4 Coefficients Values of Eqs. (4.16) to (4.18)

Eq. (4.16)	Term	C_{me}		$T \times C_{me}$			*Adj.* R^2
	Coefficient	η_2		η_5			
	Value	510.80		-1.82			0.34
Eq. (4.17)	Term	C_{me}	A_f	$T \times C_{me}$	I_{Cme}	I_{Af}	*Adj.* R^2
	Coefficient	κ_2	κ_4	κ_5	κ_{14}	κ_{15}	
	Value	185.83	0.11	-0.60	0.13	-0.005	0.41
Eq. (4.18)	Term	$T \times C_{me}$	t	I_T	I_{Mf}	I_{Af}	*Adj.* R^2
	Coefficient	μ_5	μ_{11}	μ_{12}	μ_{13}	μ_{15}	
	Value$\times 10^3$	0.438	4.20	0.049	2.12	0.060	0.58

The model fit R^2 values for these degradation models indicate that about 35-60% of the variance can be predicted by the linear model. These values are the highest among the different methods of analysis that was explored during this study. The lower predictive power of these models indicates that other factors or parameters, possibly including the random sequential changes in operating parameters, were not included in the regression model.

4.2.3 Results and Discussions

As mentioned earlier, each of the coefficients in Equation (4.2) represents a specific characteristic in the system and their change over time can be investigated to observe the degradation in the system. Figures 4.6 to 4.8 show the change in the coefficients of Equation (4.2) based on the degradation model. The coefficients have been calculated from Equations (4.16) to

(4.18) for each test and a trend line has been plotted for the overall change in the calculated coefficients. In addition, the fitted coefficients in Equation (4.2) have been shown for both the moving average groups of data and raw uncompensated data.

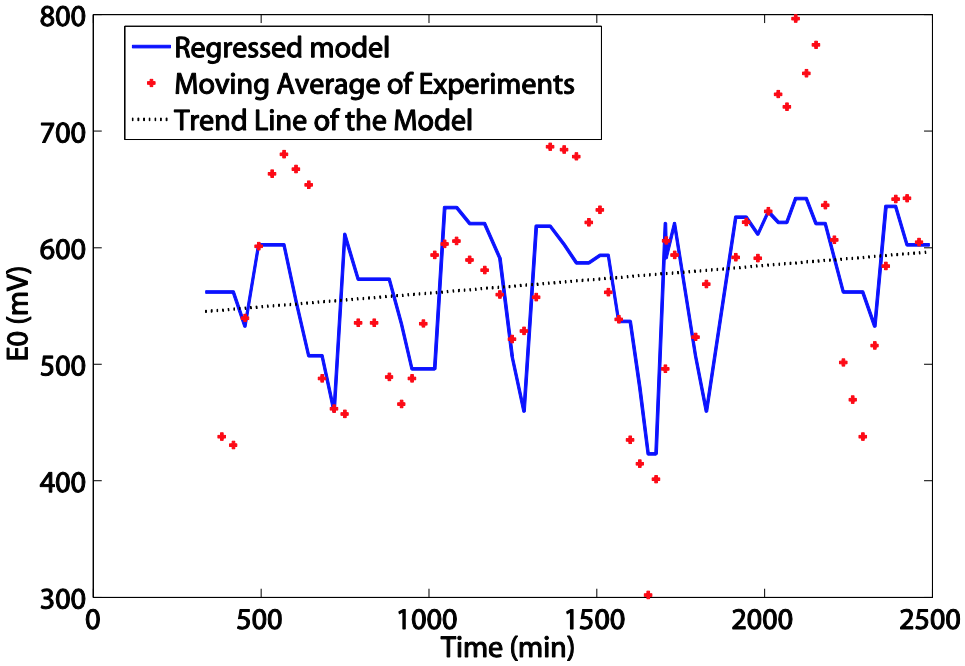

Figure 4.6 E_0^* versus the Operating Time for Each Data Group with the Degradation Model and the Trend Line of the Model

Equation (4.16) shows that the significant parameters in the change of E_0^* are the methanol concentration and the cross-term of temperature and methanol concentration. This has been also seen in a previous study [Yang *et al.* 2011] that among different operating conditions, temperature and methanol concentration are more significant in the DMFC performance than the other parameters such as methanol flow rate and air flow rate. As mentioned in Section 4.1.2, E_0^* represents the capability of the cell to generate voltage. Equation (4.16) shows that the history indices are not significant in the model, meaning that the capacity of the cell in voltage

generation does not change with cumulative exposure to any of the operating parameters. In other words, the capacity of the cell remains the same as the cell operates.

Figure 4.6 shows the trend of E_0^* in Equation (4.2). E_0^* has been calculated for each set of experimental conditions using the degradation model and a regressed trend line has been plotted from this data in the degradation model to show the change in E_0^* in the cell over time. The slope of the trend line is 0.0237 mV/min, which means a voltage change of 59 mV over the 2,500 minutes of operation. The p-value for the slope of the trend line is 0.32, compared to a p-value for its intercept of 0.001, which shows that the capacity of the cell for voltage generation is not changing significantly over time. As mentioned earlier, the model for this factor (E_o^*) does not include history indices, but is influenced by the methanol concentration and the temperature and methanol concentration cross-term. This means operating the cell at a specific concentration and temperature determines the capacity of the cell to produce voltage (E_o^*) and thus its capacity was not appreciably changed over the operating time of the DMFC.

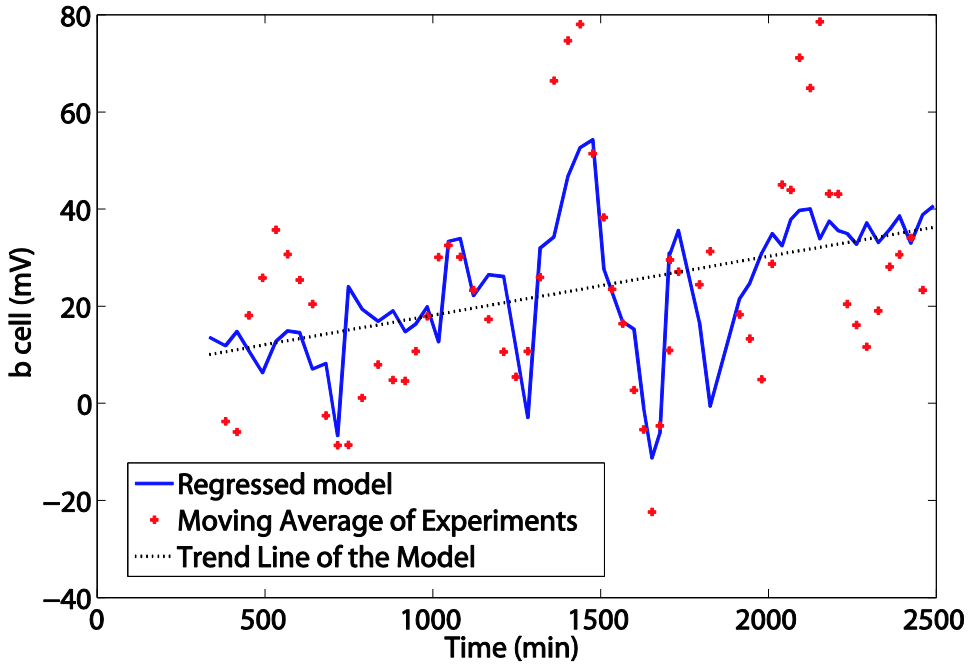

Figure 4.7 b_{cell} versus the Operating Time for Each Data Group with the Degradation Model and the Trend Line of the Model

Equation (4.17) shows that the significant factors in the change of b_{cell} are the methanol concentration, air flow rate, the cross-term of temperature and methanol concentration and the history indices of methanol concentration and air flow rate. The Tafel slope is represented by b_{cell} in Equation (4.2) and represents the chemical reaction rate inside the cell. Since the sign of b_{cell} is negative in Equation (4.2), if b_{cell} increases, the performance will degrade and vice versa. By looking at the history indices coefficients in Equation (4.17), methanol concentration history index (I_{CMe}) and air flow rate history index (I_{Af}) are significant terms. Based on the degradation model, it can be concluded that performance loss is higher at higher levels of methanol concentration. We speculate that this may be due to the exposure of the electro-catalyst layer in the cell to higher methanol concentrations degrading the efficiency of the electro-catalyst and thus the reaction rate. On the other hand, the negative coefficient of the air flow history index

predicts a decrease in b_{cell} with exposure to air. The change in b_{cell} over time will be discussed further later in this section.

As can be seen in Figure 4.7, the trend line indicates that b_{cell} is increasing over time. The slope of the trend line is 0.0121 mV/min, which causes a voltage loss of 138 mV during the operating time of the cell, and the p-values for both the slope and intercept are below 0.001. As the Tafel slope, b_{cell}, increases, the kinetics of the reaction decreases and the reaction rate slows. Thus, one reason for the observed degradation is a lower reaction rate related to the reduction of catalyst efficiency. Wu *et al.* [2008] counted several modes for the electro catalyst failure in PEM fuel cells over time, including activation loss, which appears in this model as well. The majority of studies observing a loss of activation in the catalyst layer agree that the main mechanism for this loss is sintering of the electro-catalyst. Several mechanisms have been proposed to explain the sintering in catalyst particle size as a PEM fuel cell operates. These include Ostwald ripening, where small Pt particles in the ionomer phase dissolve and deposit on the surface of large particles [Watanabe *et al.* 1994], a migration towards a minimization of the clusters' Gibbs free energy [Ascarelli *et al.* 2002], and the formation of metal oxides at the anode [Cheng *et al.* 2004] or cathode [Ahn *et al.* 2002] sides of the electro-catalysts. However, there is no agreement so far on which mechanism is dominantly responsible for the catalyst particle growth which leads to activation loss in the catalyst layer [Shao *et al.* 2007].

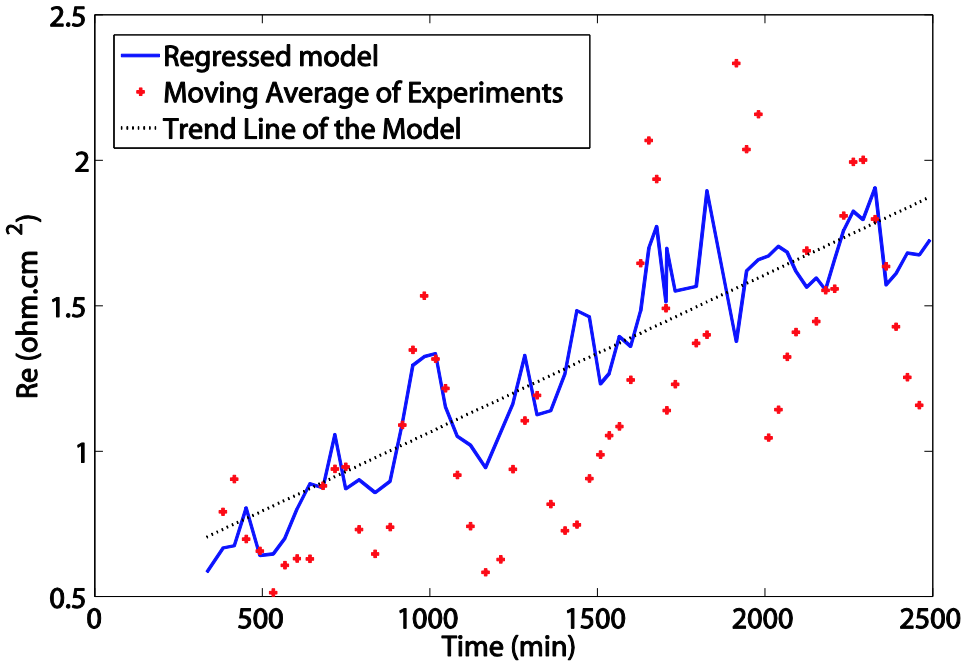

Figure 4.8 R_e versus the Operating Time for Each Data Group with the Degradation Model and the Trend Line of the Model

Equation (4.18) shows the significant factors in the change in R_e are the cross-terms of methanol concentration with temperature, the operating time, and the history indices of temperature, methanol and air flow rates. R_e is the ohmic resistance of the cell in Equation (4.2) and its coefficient has a negative sign, resulting in performance degradation when R_e increases, and vice versa when it decreases. It can be seen that the coefficient for the cross-terms of methanol concentration with temperature is positive meaning that as the methanol concentration increases the resistance of the cell increase. This is due to the fact that water is necessary to ensure the adequate ionic conductivity of the Nafion membrane. Thus, if the water concentration is lowered the ionic conductivity decreases and the ohmic cell resistance should increase. The coefficients of the history indices in Equation (4.18) indicate that all of the operational histories seem to increase the resistance of the cell.

Figure 4.8 shows the change in the ohmic resistance of the cell, R_e, over time. The trend of resistance change is increasing with the slope of 0.542 mOhm.cm^2/min, which causes a voltage loss of 138 mV over the operating time and the result agrees with the experimental study in Knights *et al.* [2004], who observed a 50% increase in resistance over the life time of their cell. Again the p-values for the linear trend line are less than 0.001 for both the intercept and the slope, and it can be concluded at a 95% of confidence that the trend is significant. An increase in ohmic resistance means there is a loss of electrical conductivity in the cell or the movement of the ions inside the cell is inhibited. Wu *et al.* [2008] reported that the increase in the conductive resistivity of the cell occurs in three components of the cell, the catalyst layer, the GDL, and the bipolar plate. Roen *et al.* [2004] and Du *et al.* [2006] reported accelerated corrosion in hydrogen-type PEM fuel cells. DMFCs also experience corrosion in the catalyst support which may result in the loss of the conductivity of the catalyst layer over time. Ru corrosion on the anode side is among the most damaging processes for DMFC lifetime [Piela *et al.* 2004]. Gancs *et al.* [2006] reported when the cell is working under load, Ru is dissolved and Ru ions are transported through the membrane to the cathode, and they are deposited onto the Pt surface. This process decreases the number of available active sites for methanol oxidation at the anode and reduces the activity of the cathode catalyst [Gancs *et al.* 2006]. Kulikovsky [2011] modeled the carbon and Ru corrosion in a DMFC anode under strong methanol depletion based on current conservation equation in the membrane. His calculations showed that 50–100 mV loss in the cell potential manifests quite a significant (above 50%) methanol-depleted fraction of the cell active area. Additionally, corrosion can cause the diffusion layer (DL) and bipolar plate to lose their electrical conductivity. While corrosion in metallic bipolar plates has also been reported as a reason of conductivity loss in PEM fuel cells, the bipolar plate used in this study is graphite

which is highly corrosion resistant and not expected to contribute significantly to degradation in our experiments.

Each history term in Equation (4.18) will be looked at separately to investigate possible causes of the resistance increase over time. The history index terms in Equation (4.18) which affect the resistance are temperature (I_T), methanol flow rate (I_{Mf}), and air flow rate (I_{Af}).

Temperature history index (I_T): In Equation (4.18), I_T is a parameter increasing the resistance which can be associated with thermal degradation in the MEA. Several studies report thermal degradation is an issue for Nafion membranes [Wilkie *et al.* 1991, Surowiec *et al.* 1988]. Mechanisms of MEA thermal degradation were proposed by Wilkie *et al.* [1991] and Samms *et al.* [1996], including rupture of the C–S bond to produce sulfur dioxide, OH^- radicals, and a left carbon-based radical for cleavage at higher temperatures. Cho *et al.* [2004] also reported that the contact resistance between the membrane and the electrode increase after thermal cycles, while membrane ionic conductivity was not affected significantly. However, McDonald *et al.*'s [2004] results show that after cycling between +80 and −40 °C, the ionic conductivity, gas impermeability, and the mechanical strength of Nafion membranes were harshly weakened.

Methanol and air flow rate history indices (I_{Mf}, I_{Af}): Parameters I_{Mf} and I_{Af} are mainly related to the cell's ability to transfer fuels to the desired locations in the cell. Mass transport of the reactants occurs in two main regions in DMFCs: the catalyst layer and the DL. Experimental results from Xie *et al.* [2005] have shown a change in the hydrophobic properties of the catalyst layer over time because of the dissolution of Nafion, which damagingly affects the and mass transport and water management ability of the electrode. In addition, a decrease in mass transport occurs in the DL due to a degradation of the backing material in the diffusion layer of the cell [Wu *et al.* 2008].

Thus, the proposed degradation model can be used to estimate the performance and its degradation by knowing the operating conditions over time. However, there are some limitations in the proposed degradation model. The degradation model has been validated in the tested DMFC and it may not be a universal model, since the tested cell has been tested under laboratory conditions with a sepcific single-cell DMFC. Finally, more tests with longer periods of operation are needed to model the performance loss more accurately. In addition, different testing environmental conditions such as humidity and pressure of the air, number of cells in the stack, the type of the MEA, and the test procedure may also affect the rate of the performance degradation and this model.

4.3 Summary

In this study, a single-cell DMFC system has been tested by varying temperature, methanol concentration, air flow rate, and methanol flow rate parameters to investigate their influences on system performance. A series of experiments have been conducted to measure fuel cell performance and investigate the effect of these operational parameters. To develop an empirical polarization model, the experimental data has been compensated for performance variation in time to a fixed time of 600 minutes. The compensated data is used to develop a model to predict the polarization curve of the system from the four operating parameters. A comparison between the experimental data and the data created by the model shows that the model is able to estimate the performance of the DMFC system and is therefore is suitable to investigate the degradation mechanism of a DMFC.

The degradation phenomenon in the performance of DMFC was investigated by ordering the experimental data based on its accumulated operating time of the system, grouping the tests into clusters of three runs to smooth out the minor fluctuations in the performance due to the

different operating conditions. The overall trend of the degradation was analyzed by using a simple model, Equation (4.2), that was fit to the experimental data for each of the raw data groups (without time compensation). The temporal change in the coefficients of the polarization curves was used as the criterion to investigate the degradation in its performance.

A regression model indicating the significant parameters that influence degradation in a DMFC has been proposed and the parameters of the model were examined in the context of published literature on fuel cell performance. The model used a stepwise regression analysis to determine the significant operational parameters for DMFC degradation that describe the change of each coefficient in Equation (4.2). The initial number of parameters was reduced by using stepwise regression which removes the insignificant parameters and keeps the significant ones in the analysis. In the polarization model, the number of parameters in the regression has been reduced from initial number of 10 to 4, 4, 6 and 4 significant parameters in Equations (4.8) to (4.11) which are shown in Table 4.2. On the other hand, in the degradation model, the number of parameters has been reduced from 15 to 2, 5 and 5 in Equations (4.16) to (4.18) which are shown in Table 4.3. In the conducted step-wise regression the R-squared value, which is a criterion for the accuracy and predictability of the model, increased considerably when the insignificant parameters were excluded from the regression. Also, achieving high R-squared values after the stepwise regressions shows that the model is compatible with the experimental data and this method can be used. The degradation model shows that the voltage generation capacity of the cell does not degrade significantly and influenced by the temperature and methanol concentration in the cell. However, two other coefficients in Equation (4.2), the Tafel coefficient and ohmic resistance, change over time.

The degradation model presented describes the performance loss trend in DMFCs and, with the support of previous studies, explains possible reasons for the terms present in the model equations. The degradation model indicates a reduction in the reaction rate of the system and an increase in the electrical resistance of the cell as time elapses. The loss in the reaction rate, shown in Equation (4.18), can be due to the loss of activation in the catalyst layer of the MEA. According to the literature, this degradation occurs in the catalyst layer due to the sintering and de-alloying of the electro-catalysts. In addition, some previous studies stated that the phenomena of thermal degradation of the membrane and loss of the capability of the cell in mass transport contribute to an increase in the resistance of the cell.

Chapter 5: INVESTIGATION OF BIPOLAR PLATE GEOMETRY ON DMFC PERFORMANCE

As mentioned in Chapter 2, the design of the bipolar/end plates flow field is an important aspect in investigating the design of DMFC system, as it influences the performance of DMFC. In this chapter, the effect of bipolar/end plate channel width on the performance of the DMFC is investigated. Three different single-channel serpentine configurations were fabricated at various channel widths but with approximately the same effective flow areas by varying the channel length. A series of experiments was designed to evaluate the performance of the cell for each geometric configuration. In these experiments, the same bipolar/end plate geometry was used on both the anode and the cathode and the current-voltage performance curve was measured to investigate the effect of geometry.

The change in performance due to geometry was mainly due to the flow characteristics of the fluid inside the bipolar/end plate channels. In order to elucidate the performance differences, a single-phase computational fluid dynamics (CFD) model for the flow in the serpentine channel was developed. A comparison between the flow simulations will be used to investigate differences in fuel flow inside the cell. The experimental results are first discussed in this chapter, and then the polarization curves are modeled for each design to investigate the performance characteristics. Finally, the CFD simulation results are explained and the results and findings are summarized.

5.1 Performance Comparison of Flow Fields

The comparison of the experimental data of DMFCs equipped with different designs shows which design(s) has (have) a higher performance. The experimental results for the three bipolar/end plates were compared for a specific condition, and the results are discussed. In addition, the effect of the change in the channels was investigated by calculating the Reynolds numbers in the channels. Since the same flow rate (Q_{in}) was used for all experiments, the Reynolds' numbers are different in the channels due to their different hydraulic diameters. The maximum power density from each experiment was obtained and compared for each test geometry.

The three bipolar/end plate designs were tested at the conditions listed in Table 3.4. Figure 5.1 shows an example polarization curve of the three bipolar/end plates at a cell temperature of 50°C, a methanol concentration of 1 M, an air flow rate of 140.8 cubic centimeters per minute (ccm), and a methanol flow rate of 4 ccm. The system was electronically loaded to give different current density values, and the corresponding voltage was measured. As can be seen in the figure, while open circuit cell voltage is approximately the same for each design, the overall cell performance increases as the channel becomes narrower. Narrower channels have higher voltage and current densities over their entire current density range. This trend was observed to be the same for all conditions operated in the experiments.

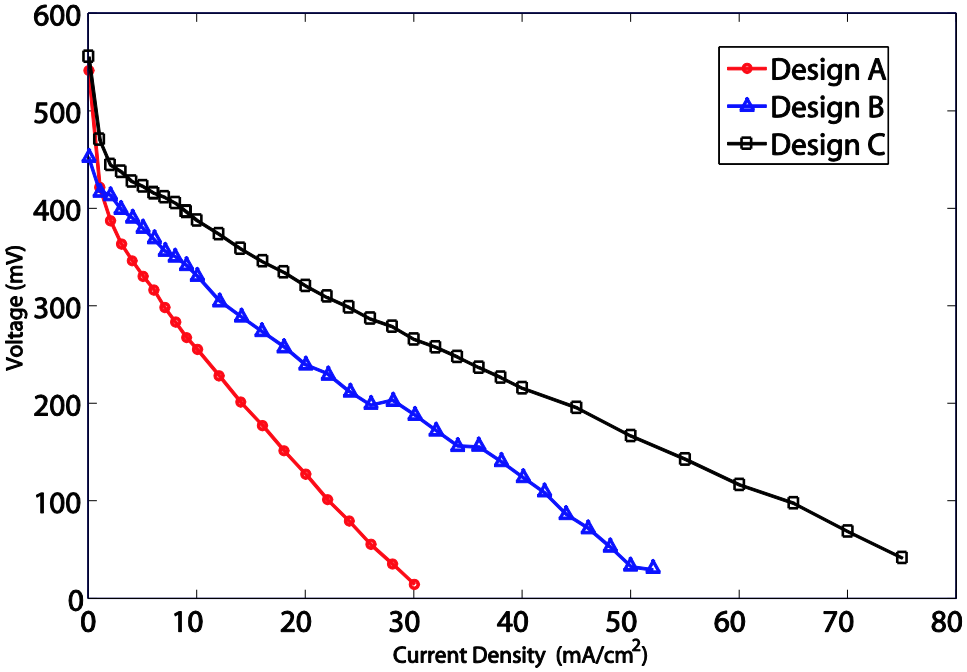

Figure 5.1 Comparison of the Polarization Curves of the Three Fabricated DMFCs.

The differences observed in the polarization curves could have been caused by differences in the flow velocity inside the channels, the distribution of fuel in the DL, and/or a pressure drop of the fluid inside the channel. While the flow rate for the three bipolar/end plate designs was constant in the experiments, the higher flow velocity in the narrower bipolar/end plate channel may have caused the fuel to penetrate more effectively into the DL and to improve the overall efficiency of the cell. To understand the effect of velocity better, the fluid flow characteristics inside the channel needed to be further investigated. Since air flow in the cathode side is compressible and more complex than the methanol flow, the investigation will be conducted only on the anode side of the DMFC.

The Reynolds number was selected as the criterion for describing the methanol solution flow in the channels and for comparison to the maximum power produced by the DMFC system [Yang and Zhao 2005], as calculated per Equation (5.1):

$$\mathrm{Re} = \frac{\rho Q_{in} D}{\mu A} \tag{5.1}$$

where Q_{in} is the methanol solution flow rate at the inlet of flow channel, D is the hydraulic diameter of the flow channel, A is the cross-sectional area of the flow channel (Table 3.4), μ is mixture viscosity (ranging from 0.7 to 1.23×10^{-3} kg $m^{-1}s^{-1}$, depending on temperature and concentration of methanol), and ρ is the density of the fluid.

Figure 5.2 shows the relationship between the maximum power of the cell and its Reynolds number at different test conditions. The maximum power was taken as the peak power of the power-current curve. Three different operating conditions are shown in Figure 5.2, where it can be seen that the maximum power output of the system was higher for narrower designs. As can be seen, as the Reynolds number increases the maximum power of the cell increases considerably. The maximum power in Design B was about 70% higher than Design A, and Design C was about 20% higher than Design B. Moreover, the Reynolds number for the narrower design was higher due to the higher velocity of the fluid at the same flow rate.

The difference in fuel cell performance in thin wall configurations may result from a more uniform fuel distribution in the DL since a thinner channel defuses fuel over a shorter distance under these thin walls. When the ribs are too wide, a non-uniform distribution of methanol in the DL reduces the methanol mass transfer, thereby causing degradation in cell performance [Yang and Zhao 2005]. However, longer channels also have a significant effect on

cell performance as they result in a larger pressure drop due to the channel friction. These reasons are further explored with CFD simulations in Section 5.3.

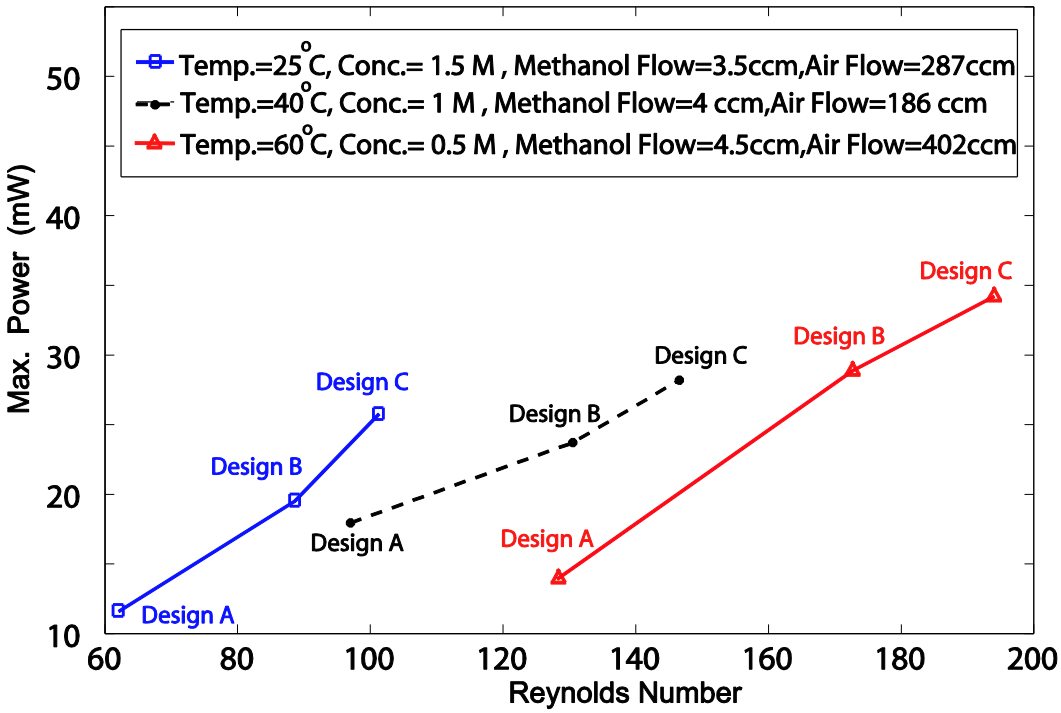

Figure 5.2 Maximum Power versus the Reynolds Number on the Anode Side for Different Operating Conditions (temperature, methanol concentration, methanol flow rate, and air flow rate)

Thus the experimental results showed that Design B and C have a higher maximum power and performance compared to design A. To investigate the reasons and causes for this difference, the polarization curves of each design are modeled by a simple model in which the change in the coefficients can be represented as the operational characteristics of different designs.

5.2 Polarization Model for Different Bipolar Geometry

In this section, the coefficients of the empirical model for the polarization curve, mentioned in Chapter 4, are used to investigate the performance of the three bipolar/end plate geometries. Several polarization models have been developed in the past to predict the voltage-current curves of DMFC systems. Srinivasan *et al.* [1988] used a simple model to describe the relationship between the cell voltage and the current density for a proton exchange member (PEM) fuel cell. Since a DMFC is a subset of the PEM fuel cell family, the same model was selected for this analysis [Scott *et al.* 2006]. Equation (5.2) describes the relationship between the cell voltage and the current density passing through the cell. In this equation it is assumed that a reduction of methanol does not occur under mass transport limitations.

$$E_{cell} = E_O^* - b_{cell} \ln j - R_e j \qquad (5.2)$$

In Equation (5.2), E_{cell} is the cell potential, j is the current density, b_{cell} is the Tafel slope, an experimental value that represents the effect of loss in the voltage of the cell, R_e is the slope of the linear region of the polarization curve representing the cell's ohmic internal resistance, and E_0^* is related to the reversible potential of the cell and is a measure of the open circuit voltage or the capacity of the cell to produce voltage.

Three coefficients (E_0^*, b_{cell} and R_e) from Equation (5.2) were investigated to evaluate the change in performance due to bipolar/end plate geometry. Experimental conditions were varied for each geometry and the polarization behaviour of the system was collected, with the operating conditions and model coefficients shown in Appendix A. The minimum R^2 (coefficient of determination) observed when the empirical models were fit was 0.89. A multi-variable analysis

of variance (ANOVA) was performed to investigate which coefficients change as an effect geometry at a confidence level of 95%.

The ANOVA results show that E_0^* does not significantly change (p-value = 0.509) with the width of the channel with the same effective area. As mentioned earlier, E_0^* is related to the open circuit voltage of the cell or the capacity of the cell for voltage generation. Figure 5.3(a) shows the fitted mean values of the calculated E_0^* from the experimental results for the three different geometries. As shown in the figure, the trend is not consistent from the wider channel to narrower one; and the difference of the fitted mean values of the minimum (Design B) and maximum (Design A) for E_0^* are about 10% which implies that the change in the geometry is not influencing E_0^* significantly. Thus, the difference in E_0^* was not significant for the three tested geometries.

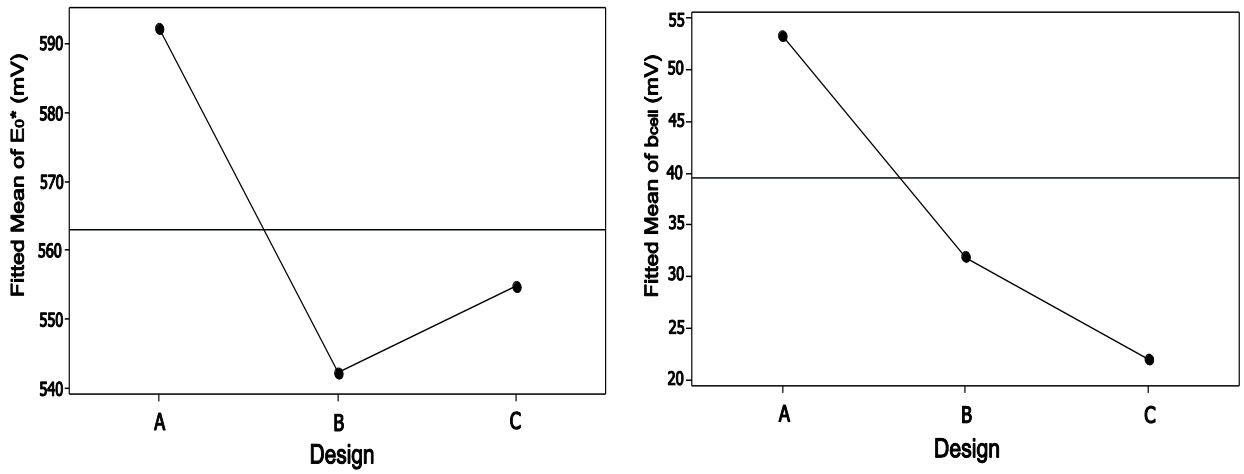

(a) (b)

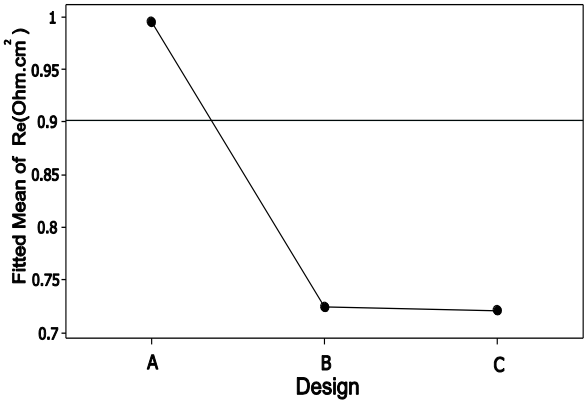

(c)

Figure 5.3 Fitted Mean Values from Experimental results (a) E_0* (b) b_{cell}(c) R_e for Designs A, B and C.

Unlike for E_0^*, b_{cell} changes significantly (p-value = 0.021) with the width of the channel with the same effective area. As mentioned earlier, b_{cell} is the Tafel slope related to the system reaction rate, implying a change in the channel width changes the chemical kinetics of the system. Figure 5.3(b) shows the mean fitted values of the calculated b_{cell} for the three tested

designs. As illustrated in the figure, the high fitted mean Tafel slope for Design A means it has the lowest reaction rate in the system and was significantly different to Design B (a 68% difference) and Design C (a 83% difference). However, fitted mean values for Designs B and C was not significantly different (23% difference) compared to the differences from Design C. This implies that making thinner channels improves the reaction rate, but does not significantly change in the two thinnest channels.

Finally, the geometry factor (p-value = 0.033) is significant to the ohmic resistance of system (R_e). Although the fitted mean of the ohmic resistance in Designs B and C was approximately the same (differ by 5%), it is higher for Design A, as shown in Figure 5.3(c). The change of the internal resistance (R_e) of Design A was about 53% higher than Designs B and C. These results show that the internal resistance of the cell decreases when the width of the channel is smaller. The results of the analysis of variance (ANOVA) analysis are summarized in Table 5.1.

The coefficients significantly affected by the change in the width of the channel were the reaction rate occurring inside the cell, represented by b_{cell}, and the ohmic resistance of the cell, represented by R_e in Equation (5.2). The mean values of b_{cell} and R_e of Designs A, B and C were 41.3, 29.88 and 21.40 mV, and 0.91, 0.72, and 0.78 ohm·cm^2, respectively. Therefore, the calculated values for Design B and C are approximately the same compared to their values for Design A. The reaction rate was highest in Design C, as the Tafel slope has a reverse relation to the reaction rate of the system. Better diffusion of fuel into the DL is one reason for changes to the reaction rate of the cell. In the next section, a CFD model to investigate methanol diffusion into the DL is used to understand the effect of channel width on flow velocity and pressure inside the DL.

Table 5.1 Summary of the multi-variable ANOVA for the operating parameters and geometry factor

Coefficient in Equation (5.2)	**Representation of Coefficient**	**Geometry Significance**	**p-Value**	**Adjusted R^2 (%)**
E_{0*}	Capacity of Voltage Generation	_	0.509	32.98
b_{cell}	Chemical Reaction Rate	✓	0.029	30.29
R_e	Internal ohmic Resistance	✓	0.033	80.37

5.3 CFD Modeling of Channels and Diffusion Layer

A CFD simulation is undertaken to understand why a decrease in channel width in the bipolar/end plates enhanced the performance of the DMFC system. The CFD simulation determined the velocity of the flow and the pressure distribution in the DL on the anode side of the bipolar/end plate. The physical domain of the CFD simulation, shown in Figure 5.4 included three fluid zones: the anode channel, the anode DL, and the anode catalyst layer. The anode catalyst layer was simplified as an infinitely thin interface. The electrochemical kinetics of the cell were ignored in this CFD model, since the aim of the simulation was only to understand the behaviour of the flow in the bipolar/end plates.

Some assumptions applied to the CFD model include all fluid flows are considered to be laminar, all fluids were incompressible, the fuel cell operates at a steady state and under an

isothermal condition, and the CO_2 generated by methanol oxidation is completely dissolved in the water, so only a liquid phase existed in the anode side. All porous media (i.e., the DL, membrane and catalyst layer) are assumed to be isotropic materials and the membrane operated at a fully hydrated state. The thickness of the anode diffusion layer was 0.2 mm with a porosity of 0.6, and the anode catalyst layer's thickness was 0.02 mm with a porosity of 0.4.

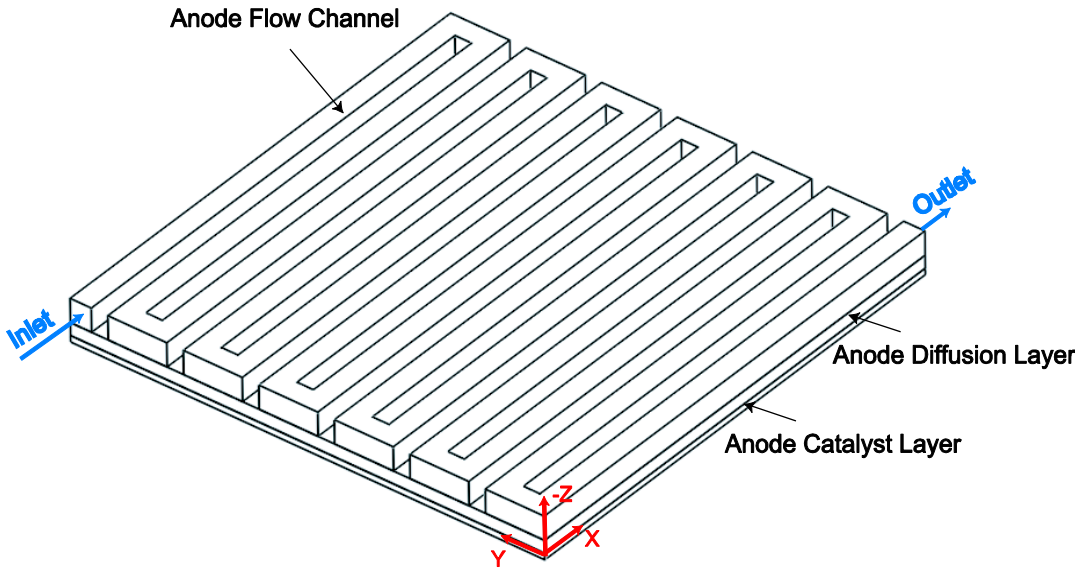

Figure 5.4 Physical Domains of the Created CFD Model (Design A).

Three types of principal equations were used in the CFD simulation, including the continuity, momentum and species equations, which were applied to all physical domains with their specific physical and chemical characteristics. The continuity equation describes that, in a steady-state process, the rate mass enters the control volume is equal to the rate at which mass leaves the system. The continuity equation is given in Equation (5.3) [He *et al.* 2009]:

$$\nabla \cdot (\varepsilon \rho \vec{v}) = 0 \tag{5.3}$$

where ε is the porosity of the physical domain (ε = 1 at the channel, ε = 0.6 at the DL, and ε = 0.4 at the catalyst layer), ρ is the fluid density (kg m^{-3}), and $\vec{v}$ is the velocity vector of mixture (m s^{-1}).

The momentum equation is defined by the relations given in Equations (5.4) and (5.5) [He *et al.* 2009]:

$$\nabla \cdot (\varepsilon \rho \vec{v}\vec{v}) = -\nabla(\varepsilon P) + \nabla \cdot (\varepsilon \mu \nabla \vec{v}) + S_{mom} \tag{5.4}$$

where P is the pressure (Pa), μ is the mixture viscosity (kg $m^{-1}s^{-1}$), and S_{mom} is the momentum source term ($N \cdot m^{-3}$), which is caused by the porous media and is 0 in the channel. S_{mom} is defined in Equation (5.5), where K is the permeability of porous media (m^2) [Le and Zhou 2008, He *et al.* 2009]:

$$S_{mom} = -\varepsilon^2 \frac{\mu}{K} \vec{v} \tag{5.5}$$

The species equations are defined in Equations (5.6) and (5.7) [Sivertsen and Djilali 2005]:

$$\nabla \cdot (\varepsilon \rho \vec{v} Y_k) = \nabla \cdot (\varepsilon \rho D_k^{eff} Y_k) \tag{5.6}$$

where Y_k is the mass fraction of species k, and D_k^{eff} is the effective diffusion coefficient of species k (m^2s^{-1}) [Ge and Liu 2006]:

$$D_k^{eff} = \begin{cases} D_k, & \text{In the channel} \\ \varepsilon^{1.5} D_k, & \text{In other zones} \end{cases} \quad (5.7)$$

where D_k is the diffusion coefficient in the channel. Since the CFD simulation just considers the anode side, the species in the model were methanol (CH_3OH) and water (H_2O). The physical parameters used for the CFD simulation are presented in Appendix B.

Figure 5.5 shows the CFD simulation for the flow velocity magnitude inside the DL at the anode side. For ease of comparison, the three CFD simulations use the same color scale. As can be seen, the magnitude of the resultant X-, Y- and Z-direction fluid velocities is higher in Design C than Design B. The resultant velocity of Design C is also more uniform, which could explain the higher performance of the narrower channel shown in Figure 5.2. These results also confirm the conclusions of Wong *et al.* [2006], who report higher performance because of more uniform flow distribution in cells equipped with narrower channels.

Figure 5.6 shows the CFD analysis of the Z-component of the velocity in the DL of the cell, representing the flow transporting reactants towards the catalyst layer. The Z-component of the velocity was the largest in the narrowest channel (Design C), and also larger in Design B than in Design A. Integrating the Z-velocity over the area of DL for Designs A, B and C gives values of 1.98, 2.30 and 5.05 $\times 10^{-8}$ $m^3 s^{-1}$, respectively, showing the amount of methanol passing through the DL is largest for the narrowest channels. Greater flow to the catalyst layer provides more methanol for the reactions and thus a higher performance.

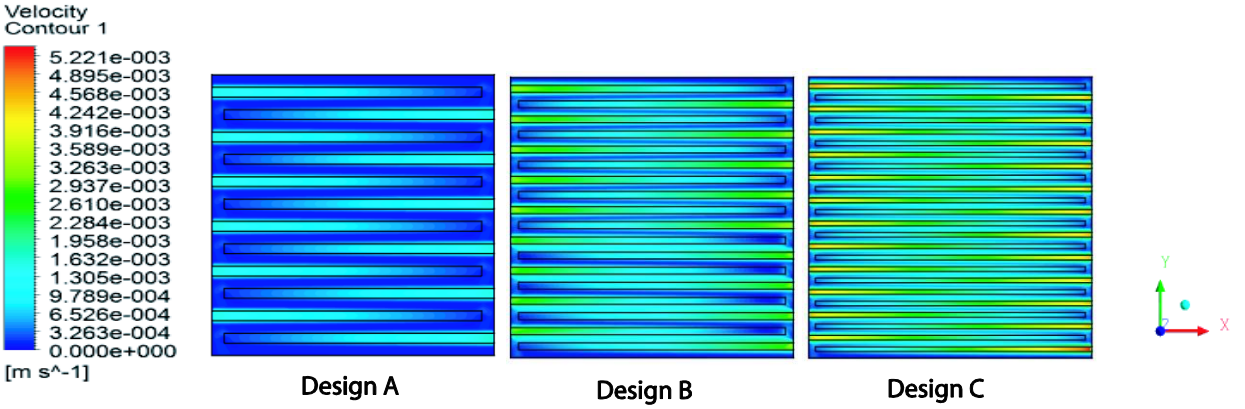

Figure 5.5 CFD Simulation for Resultant Velocity Magnitude inside the Diffusion Layer for Three Bipolar Plate Designs

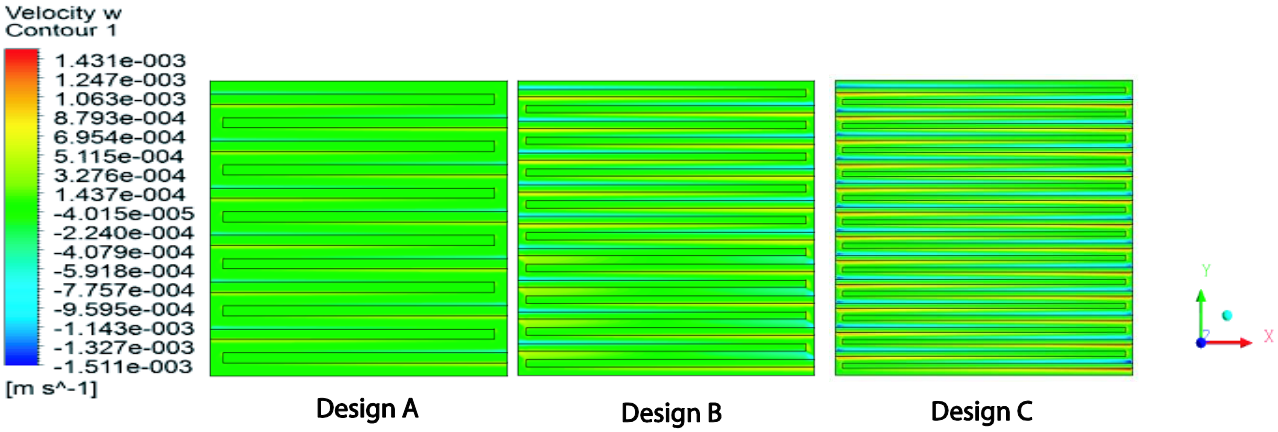

Figure 5.6 CFD Simulation for the Z-component of the Velocity inside the Diffusion Layer for Three Bipolar Plate Designs

The pressure of the flow also plays an important role in transporting reactants in the system and is different for the three bipolar/end plate geometries, as presented in Figure 5.7. High pressure can increase the velocity of methanol in the flow field. In addition, more CO_2 can be dissolved into the solution quicker under higher pressure. In other words, high pressure can improve the mass transfer efficiency in the DMFC. The pressure gradient is also higher in the

narrower channel due to the longer flow path and higher wall friction. The inlet-to-outlet pressure drop determined from the CFD in Designs A, B and C was 0.48, 1.45 and 1.94 kPa, respectively. While this pressure drop requires more pumping power to drive the fuel flow inside the channel, the higher pressure gradient also helps diffuse methanol in the DL and improves system performance.

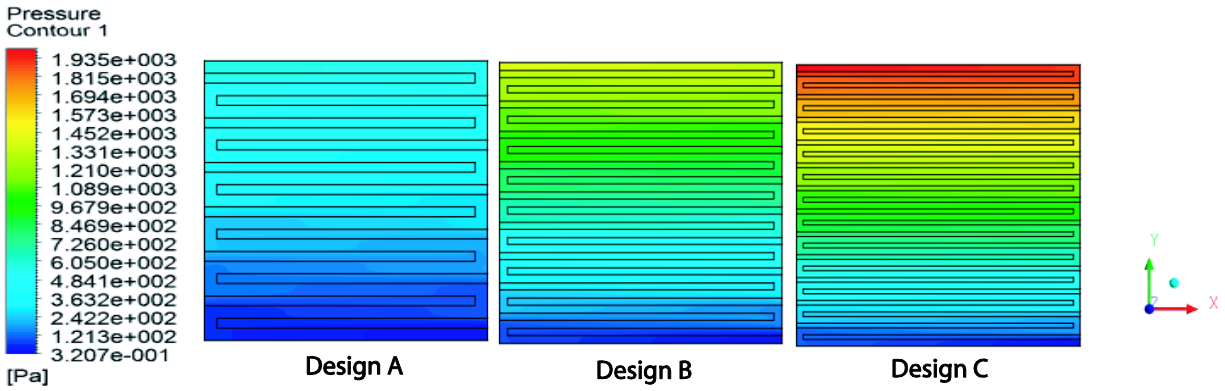

Figure 5.7 CFD Simulation for Pressure Distribution inside the Diffusion Layer for Three Designed Bipolar Plates.

The CFD simulations indicate that narrower channels increase flow velocity in the DL at the same system flow rate. In addition, the flow velocity perpendicular to the DL was also higher in narrower channels. Furthermore, the distribution of the flow becomes more uniform as the width of the channels narrowed. These reasons are likely cause for the higher reaction rate seen in Section 5.2. The CFD model also shows that the width of the channel changes the pressure distribution of the flow in the DL. The pressure drop is higher when the width of the channels is lower, but this drop requires more pumping power. The pressure was highest in the narrowest

groove design, directing the driving force of the flow towards the cathode and improving the performance of the cell.

The assumptions made for CFD modeling of the flow inside the channels may affect the above conclusions. Ignoring the reactions happening in the system could influence the flow of the reactants in the cell. For example, the flow inside the channels could be a two-phase, a combination of CO_2 bubbles and methanol solution, not like the assumption that the CO_2 was completely dissolved in the methanol solution. Although both the anode and cathode groove width were varied in the experimental tests, the effect of the flow on the cathode side (air side) was not investigated in the CFD due to the complexity of the modeling compressible flow.

5.4 Summary

In this chapter, the effect of bipolar/end plate channel width on the overall performance of a DMFC was investigated. The experimental results show that, under various operating conditions, a DMFC equipped with single-path serpentine groove with approximately the same planar flow area improves its overall performance as the width of the channel is reduced. The experimental results were fit to a polarization curve model at different operating conditions. An ANOVA analysis on the polarization model coefficients found that changes in bipolar/end plate channel width does not significantly affect the capacity of the cell for voltage generation (E_0^*). However, the width of the channel does significantly influence the reaction rate in the cell (b_{cell}) and its ohmic resistance (R_e). Thinner channels appear to improve the reaction kinetics occurring inside the system. However, the change in reaction rate and ohmic resistance is not significant between the cells with the thinnest channels (Designs B and C). Finally, a CFD simulation was developed to investigate flow behaviour due to changes in channel width that may affect

performance. The CFD simulation showed higher performance in narrower channels results from: (1) a greater diffusion of the methanol to the MEA due to higher flow velocity in the channels; (2) a more uniform fuel distribution due to the thinner ribs; and (3) a higher inlet-to-outlet pressure drop making CO_2 bubbles removal easier. However, the higher inlet-to-outlet pressure drop in thinner channels requires more pumping power for the cell. Overall, the experimental results showed that the narrowest channel tested improved the DMFC's maximum power by 20% over that of the middle channel width, and 70% over that of widest width bipolar.

Chapter 6: SUMMARY AND FUTURE WORK

Despite the many advantages of DMFC systems, such as high efficiency, easy acquisition, transportation and storage of fuels, and operation at room temperature, DMFCs still encounter some challenges. These challenges, which were investigated by others in past studies, include methanol cross-over through the MEA, slow electrochemical kinetics of methanol oxidation, cathode flooding, and CO_2 gas management.

In this study, we have focused on the durability and design issues associated with the performance of DMFCs, considering the ultimate goal which is a commercially viable DMFC system. A better understanding of the causes for DMFC performance degradation would enable us to predict the performance loss of DMFC systems and also help to determine solutions that would facilitate their prolonged life. In addition, the bipolar plates are one of the major components of DMFCs, and their channel designs influence the overall performance of the system. Therefore, the flow field design within the bipolar plate is an important factor in optimization of the system design. Summaries of the methodology, findings and contributions of this thesis are discussed in this chapter.

In the durability study, four parameters – temperature, methanol concentration, air flow rate, and methanol flow rate – were varied to investigate their influences on the overall system performance. A series of experiments was performed to measure DMFC performance, and the effects of these operational parameters were analyzed. The experimental data was compensated for performance variations in time to a fixed time of 600 minutes. A comparison between the experimental data and the data created by the model shows that the model is able to estimate the

performance of the DMFC system and was, therefore, suitable for investigation of the degradation mechanisms of a DMFC.

The degradation phenomenon in the performance of DMFCs was investigated by sorting the experimental data chronologically and grouping the tests into clusters of three runs to smooth out the minor fluctuations in the performance due to the different operating conditions. The overall trend of degradation was analyzed by using a simple model that was fit to the experimental data for each of the raw data groups (without time compensation). The temporal change in the coefficients of the polarization curves was used as the criterion for the investigation of performance degradation.

A regression model indicating the significant parameters that influence degradation in a DMFC was proposed, and the parameters of the model were examined in the context of the published literature on fuel cell performance. The model used a step-wise regression analysis to determine the dominant operational parameters for DMFC degradation that describe the change of each coefficient of the polarization curve model of the DMFC, as depicted in Equation (4.2). The regression analysis showed that the voltage generation capacity of the cell (E_0^*) did not change significantly during the operating time. However, two other coefficients in polarization curve model, the Tafel coefficient and ohmic resistance, did change over time.

The presented degradation model describes the performance loss trend in DMFCs and, with the support of previous studies, explains possible reasons for the coefficients present in the model equations. The degradation model can be used for the tested DMFC to predict the performance curve of the cell at an operating time and under certain conditions by just measuring the output polarization curve of the DMFC. The methodology in achieving the degradation model can be tested for other cells and might be a compatible model to predict the performance

loss over time and obtaining operating conditions with lower degradation rates. The degradation model indicates a reduction in the reaction rate of the system and an increase in the electrical resistance of the cell as time elapses. Based on the studies in the literature, the loss in the reaction rate is speculated to be due to the loss of activation in the catalyst layer of the MEA. According to Wu et al. [2008], this degradation occurs in the catalyst layer, due to the sintering and de-alloying of the electro-catalysts. In addition, the phenomenon of thermal degradation of the membrane and the loss of the mass transport capability of the cell have been observed in the previous studies [Wu et al. 2008] as the reasons that can add to an increase in the resistance of the cell.

In the flow field study, the effect of bipolar plate channel width on the overall performance of a DMFC was investigated. The experimental results showed that, under various operating conditions, a DMFC equipped with single-path serpentine groove with approximately the same planar flow area improved its overall performance as the width of the channel was reduced. The experimental results were fit to a polarization curve model at different operating conditions.

An analysis of variation (ANOVA) of the polarization model's coefficients found that changes in the bipolar plate channel width did not significantly affect the capacity of the cell for voltage generation (E_0^*). However, the width of the channel did significantly influence the reaction rate in the cell (b_{cell}) and its ohmic resistance (R_e). Thinner channels appeared to improve the reaction kinetics occurring inside the system. However, the changes in the reaction rate and ohmic resistance were not significant between two thinner width cells (Designs B and C).

A CFD simulation was developed to investigate the flow behaviour due to changes in the channel width that have may affected performance. The results from the CFD simulation show higher diffusion of solution to the membrane, more uniform distribution of flow in the diffusion layer and higher pressure drop when the channel is narrower. Overall, the experimental results showed that the narrowest tested channel improved the DMFC's maximum power by 20% over that of the middle channel width, and 70% over that of widest channel bipolar/end plate.

In summary, the findings and answers to the research questions are as follows:

- The polarization behaviour of the tested DMFC system can be accurately modeled and predicted by a semi-empirical polarization model.
- The temperature and methanol concentration are the two main operating parameters that affect the performance of the DMFCs, although the methanol and air flow rate also influenced the performance, but less significantly.
- Degradation in performance was observed as the DMFC operated, and the performance loss was modeled in the operating time of the system.
- The degradation model indicated a reduction in the reaction rate of the system, due to the loss of activation in the catalyst layer of the MEA, and an increase in the electrical resistance of the cell as time passed.
- The bipolar plate's role in the performance of the DMFC was significant. In the serpentine flow field design, the channel width was a key design parameter; and, the experiments showed that thinner channels had increased performance, due to greater diffusion into and a more uniform distribution of flow in the diffusion layer. On the other hand, the required pumping power was higher in the thinner channel.

6.1 Novel Scientific Contributions

Among the DMFC studies conducted, this research addressed the investigation of the durability and flow field of DMFCs, which have not had been the focus of many other studies. Novel contributions have been made to performance modeling of DMFCs by considering the operating parameters of temperature, methanol concentration, and methanol and air flow rates, which have not been investigated before. With an appropriate experimental design, the effects of the interactions between the parameters were observed.

Other contributions include the use of the concept of a moving average and history index to build a degradation model that improved the accuracy of predicting the performance loss from experimental data. In addition, the open area of the DMFC has not been investigated by previous researchers. Finally, a CFD simulation was developed to examine this open area, which showed a greater diffusion of the methanol from the anode side, a more uniform distribution of flow, and a higher pressure drop across the inlet and outlet. Further explanations of these contributions are discussed in the following subsections.

6.1.1 Operating Parameters and Their Interaction

The interactional effect of operating parameters on DMFC performance has not been studied. In this thesis, four parameters – temperature, methanol concentration, and methanol and air flow rates – were varied simultaneously, instead of just varying one or two of these parameters. By considering all of these operating parameters with a proper experimental design, the interactions between the changes in the parameters were observed from the measured performance in different operating conditions. These interactions had not been previously

researched. The results showed that some interaction terms influenced the performance and its model.

The results of the degradation and polarization modeling, at a confidence level of 95%, showed that the significant parameters in the change of the voltage generation (E_0^*) capacity of the cell were the methanol concentration and the interaction (cross term) between the temperature and the methanol concentration. The significant factors in the reaction rate inside the cell, b_{cell}, were the methanol concentration, air flow rate and the interaction between the temperature and the methanol concentration. Finally, for the electrical resistance of the cell, R_e, the interaction between the temperature and the methanol concentration was significant. Thus, simultaneously varying the operating conditions has shown the presence of interaction terms in polarization and degradation modeling.

6.1.2 Degradation Modeling

Fuel cell degradation is a result of systematic changes in the fuel cell over time. To analyze the systematic changes that may have a long-term effect, moving averages were used, which had not yet been used to model the degradation behaviour of DMFCs. Moving averages highlight long-term trends and are commonly used to smooth out time series data. The moving average of each experimental group was calculated using a window size of three tests. In other words, when the overall trend was under investigation, grouping the time-sorted data and using the concept of moving average provided a guide to the systematic changes in the system, regardless of changes in the conditions of the tests.

Another novel idea regarding the degradation modeling was the inclusion of a system operational history parameter to model its next performance. A history index was formed, where the time of the operation at a specific condition was multiplied by an operating parameter. The basis of this concept is the hypothesis that degradation in the performance of the cell may originate from an increase in the size of the electro-catalyst particles in the catalyst layers [Bae *et al.* 2009], which is similar to the explanation of annealing. Cumulative exposure to operational parameters as the system was operated under different conditions provided a historic measure that influenced performance during the next test.

Several statistical and analytical methods were tried in the modeling of the experimental data for degradation, such as step-wise regression without using moving average and/or history indices with different configurations of data. It was observed that the proposed method to establish the degradation model decreased the error and was effective in improving the accuracy of the degradation model, which resulted in R^2 (coefficient of determination) values equal to 0.34, 0.41 and 0.58 for E_0^*, b_{cell} and R_e, respectively. Therefore, use of a moving average and history indices for the degradation modeling of the tested DMFC improved the accuracy of the model in performance loss prediction.

6.1.3 Flow Field Design Experiments and CFD Simulation of Flow in the Diffusion Layer

A few researchers have studied the effect of flow field design in DMFCs, some of whom compared the performance of different designs; however, the separate study of design parameters within a specific design has rarely been investigated. Previous studies have reported that the optimal design is a serpentine flow field; therefore, the focus of this study was on the investigation of this design.

The width of the channel in the bipolar plate of a DMFC is a significant design parameter in the geometry of the flow field. The open area (the grooved area in the bipolar/end plate) of each design was kept approximately the same, in order to minimize the change in the performance due to different effective areas and to study the width in the channel individually. Previous studies changed the width of the channels without considering the effect on the open area of the plate.

Another contribution of the flow field study is the modeling of the performance of each design at different operating conditions using a simple performance model. Since each coefficient of the model represents a specific property of the working fuel cell, a comparison of the model coefficients can describe performance differences in the designs.

ANOVA results showed that the reaction rate and electrical resistance coefficient in the model changed significantly with a change in the width of the channel in the bipolar/end plate. The calculated reaction rate factor in Design A (widest channel width) was significantly lower than in the other two designs, as the changes of this factor in Designs B and C were negligible. The electrical resistance coefficient was significantly higher in Design A compared those of Designs B and C, and the values for the two narrower designs (B and C) were quite close.

Only a few studies of the flow field geometry in DMFCs have performed CFD simulations and experiments together [Birgersson et al. 2004, Ge and Liu 2006, Yang and Liang 2009]. In this thesis, a three-dimensional CFD simulation of the diffusion layer was conducted to investigate flow behaviour due to changes in the channel width. The CFD simulations showed increased performance in narrower channels, resulting from a greater diffusion of methanol to the MEA, a more uniform fuel distribution, due to the thinner ribs, and a higher inlet-to-outlet pressure drop, making CO_2 bubble removal easier. Hence, there was novelty in the CFD

simulation of the geometry and the fabrication and testing of three different widths in the bipolar/end plates geometry design, with the same open area, in order to consider the effect of the channel width of the bipolar/end plate.

6.2 Limitations and Assumptions

This research had several assumptions and limitations that need to be addressed. First, the models proposed in this research, including the semi-empirical polarization model, the degradation model and the CFD simulation are limited to the tested DMFC configuration and are not universal models. Therefore, the model coefficients and accuracy should be determined and calibrated for other DMFC systems. Also, when a semi-empirical model for a different DMFC is required, new experiments need to be conducted to obtain the coefficients of the semi-empirical model.

The semi-empirical polarization model assumed that there was no mass transport limitation, which is not the case in DMFCs, however the model is a simple study of the degradation phenomenon and considering other effects such as mass transport limitations and methanol cross over adds to the complication of the model The operating parameters, such as the temperature and methanol concentration, could not be changed over a wide range during the experiments, due to limitations of the system. For example, the highest operating temperature for the system was 80°C, which was limited by the MEA. Therefore, the semi-empirical polarization model that predicts the V-I curve of the system would not be reliable with the operating conditions out of the range of the conducted experiments.

In the degradation study, the time of each experiment was recorded. The degradation tests could not be conducted continuously, because the operating parameters changed for each condition and because of the long hours of operation. Therefore, there were periods during the experiments when the system was shut down, which may have caused errors in the data collected in the derivation of the degradation model. Having the data for the continuous operation of the cell may give more accurate model for the degradation study.

An assumption in the calculations of the degradation model was that the conditions for each test remained the same, while performing the test and collecting the data. However, some of the parameters may have changed slightly during some tests. Another assumption was the use of the middle test in the moving average data as the pivot test in each group for the regression analysis. Further, the degradation model only explains a portion of the degradation behaviour (with a maximum R^2 of 0.58) and may not be accurate in some regions, due to the uncertainties in the degradation phenomenon. Also, it should be mentioned that the degradation phenomenon in DMFC is not fully understood and there is a lack of sufficient and up-to-date information about the detailed changes occurring in the cell during long-term operation.

In the geometry study, the fabricated bipolar plates were to have the same effective area, so that the effects of the channel width on the performance of the system could be compared. While the open area of each design was not exactly the same, due to the available machine tools, the maximum deviation was about 9%, which is considered acceptable for this research.

Some assumptions were also applied to the CFD model, including that all fluid flows were considered to be laminar, all fluids were incompressible, the fuel cell operated at a steady state and under an isothermal condition, and the CO_2 generated by methanol oxidation was completely dissolved in the water so only a liquid phase existed in the anode side. A single-phase

simulation was considered sufficient since CO_2 bubbles do not change the performance significantly when the current density is low [Ge and Liu 2007] since part of the generated CO_2 can be dissolved in the water (CO_2 solubility in water, 1.45 g/L at 25 °C, 100 kPa) [Yang and Zhao 2005]. Furthermore, as a preliminary study, the additional complication in the CFD simulation of a two-phase flow in a porous media would not yield additional insight at these lower current density levels. All porous media (i.e. the diffusion layer, membrane and catalyst layer) were assumed to be isotropic materials, and the membrane was assumed to operate at a fully hydrated state. The thickness of the anode diffusion layer was 0.2 mm with a porosity of 0.6, and the anode catalyst layer's thickness was 0.02 mm with a porosity of 0.4.

6.3 Future Work

Although this study addressed its objectives, some future work is recommended to make this study more complete and for further investigation. The ultimate goal is commercially viable DMFCs. Considering this goal, several suggestions can be made from the experience in this research.

The current semi-empirical model is limited to the TekStak^{TM} DMFC and cannot be used for DMFCs with different geometries. To resolve this issue, future work should focus on the development of models that simultaneously consider the influence of both operating parameters and geometric parameters on DMFC performance. By adding geometric parameters to these models, the optimal design parameters, in addition to the optimal operating parameters, can also be achieved.

A single-cell DMFC was studied in this thesis; however, in practice, several cells are stacked together to increase the power and provide higher electrical power demands. The stacked cell should be studied to investigate their performance compared to that of a single-cell system. Similarly, the degradation and design of stacked cells can be investigated in future works to check the linearity relation of the model to the number of stacks and the degree of degradation.

Further investigation of the MEA should be considered for future research, since the MEA is also affected by the degradation. A comparison of scanning electron microscopy (SEM) images of unused and degraded MEA samples can be used to observe the change in the catalyst particles' size and agglomeration during the operating time. Moreover, mitigation strategies to slowdown or suppress degradation effects can be studied. For instance, determination of the optimal operating conditions to minimize degradation and the use of new materials in the MEA and as a catalyst to increase the fuel cell's lifetime can be further investigated.

Multiple phase CFD simulation that considers the reaction between the anode and cathode should be investigated. The development of a three-dimensional CFD performance model with multiple phases that can predict the performance of the cell equipped with several geometries would be a big step in modeling the system.

Future investigations should add geometric parameters to the performance modeling of stacked cell studies, SEM imaging of the degraded MEA should be conducted, and a performance model coupled with CFD simulation of the flow in the system should be developed. These suggestions for future work would contribute to the findings of this thesis and further enhance the DMFCs' durability and design.

References

Ahn SY, Shih SJ, Ha HY, Hong SA, Lee YC, Lim TW, Oh IH. Investigation of the performance decay of anodic Pt/Ru catalyst with working time of direct methanol fuel cells. J Power Sources 2002; 106: 295-303.

Amphlett JC, Peppley BA, Halliop E, Sadip A. The effect of anode flow characteristics and temperature on the performance of a direct methanol fuel cell. J Power Sources 2001; 96: 204-213.

Appleby AJ, Foulkes FR, Fuel Cell Handbook, New York: Van Nostrand Reinhold; 1989.

Argyropoulos P, Scott K, Shukla AK, Jackson C. A semi-empirical model of the direct methanol fuel cell performance: part I - model development and verification, J Power Sources 2003; 123(2): 190-9.

Aricò AS, Cretì P, Baglio V, Modica E, Antonucci V. Influence of flow field design on the performance of a direct methanol fuel cell. J Power Sources 2000; 91: 202-9.

Ascarelli P, Contini V, Giorgi R. Formation process of nanocrystalline materials from x-ray diffraction profile analysis: Application to platinum catalysts, J Appl Phys 2002; 91: 4556-61.

Bae SJ, Kim S, Um S , Park J , Lee J, Cho H, A prediction model of degradation rate for membrane electrode assemblies in direct methanol fuel cells. Int J Hydrogen Energy 2009; 34(14): 5749-58.

Barbir F. PEM fuel cells: theory and practice, Burlington:Elsevier Academic Press; 2005: 39-45.

Baxter SF, Battaglia VS, White RE. Methanol fuel cell model: anode. J Electrochem Soc 1999; 146: 437-47.

Besmann TM, Klett JW, Henry JJ Jr, Lara-Curzio E.Carbon/Carbon composite bipolar plate for PEM fuel cells. J Electrochem Soc 2000; 147: 4083-6.

Bett JAS, Kinoshita K, Stonehart P. Crystallite growth of platinum dispersed on graphitized carbon black II. Effect of liquid environment. J Catalysis 1976; 41: 124-33.

Bewer T, Beckmann T, Dohle H, Mergel J, Stolten D. Novel method for investigation of two-phase flow in liquid feed direct methanol fuel cells using an aqueous H_2O_2 solution. J Power Sources 2004; 125: 1-9.

Birgersson E, Nordlund J, Ekström H, Vynnycky M, Lindbergh G. Reduced two-dimensional one-phase model for analysis of the anode of a DMFC. J Electrochem Soc 2003; 150: 1368-76.

Birgersson E, Nordlund J, Vynnycky M, Picard C, Lindbergh G. Reduced two-phase model for analysis of the anode of a DMFC. J Electrochem Soc 2004; 151: 2157-72.

Blum A, Duvdevani T, Philosoph M, Rudoy N, Peled E. Water-neutral micro direct-methanol fuel cell (DMFC) for portable applications. J Power Sources 2003; 117: 22-5.

Carmoa M, Santosa AR, Spinacéa EV, Fuessc H, Pocob JGR, Linardia M. Alternative supports for catalysts preparation for low-temperature fuel cells using the alcohol reduction method 2006; 162: 1009–1016, Scientific Bases for the Preparation of Heterogeneous Catalysts, Proceedings of the 9th International Symposium.

Casalegno A, Marchesi R. DMFC anode polarization: Experimental analysis and model validation. J Power Sources 2008; 175: 372–82.

Celik S, Mat MD. Measurement and estimation of species distribution in a direct methanol fuel cell. Int J Hydrogen Energy 2010; 35: 2151–9.

Cheddie D, Munroe N. Review and comparison of approaches to proton exchange membrane fuel cell modeling. J Power Sources 2005; 147(1-2): 72-84.

Chen J, Asano M, Maekawa Y, Sakamura T, Kubota H, Yoshida M. Preparation of ETFE-based fuel cell membranes using UV-induced photografting and electron beam-induced crosslinking techniques. J Membrane Sci 2006; 283 (1-2): 373-9.

Chen W, Sun G, Guo J, Zhao X, Yan S, Tian J, Tang S, Zhou Z, Xin Q. Test on the degradation of direct methanol fuel cell, Electrochim Acta 2006; 51: 2391-9.

Cheng X, Chen L, Peng C, Chen Z, Zhang Y, Fan Q. Catalyst microstructure examination of PEMFC membrane electrode assemblies vs. time, J Electrochem Soc 2004; 151: A48-A52.

Cho EA, Ko JJ, Ha HY, Hong SA, Lee KY, Lim TW, Oh IH. Effects of water removal on the performance degradation of PEMFCs repetitively brought to [less-than] 0[degree]C, J Electrochem Soc 2004; 151: A661-5.

Choi JH, Park KW, Park IS, Nam WH, Sung YE. Methanol electro-oxidation and direct methanol fuel cell using Pt/Rh and Pt/Ru/Rh alloy catalysts. Electrochimica Acta 2004; 50: 787-90.

Choi JS, Chung WS, Ha HY, Lim TH, Oh IH, Hong SA, Lee HI. Nano-structured Pt-Cr anode catalyst over carbon support, for direct methanol fuel cell. J Power Sources2006, 156 (2): 466-71.

Chou Y. Statistical analysis: with business and economic applications, 2nd ed. New York: Holt, Rinehart and Winston; 1969: 556.

Cooper KR, Smith M. Electrical test methods for on-line fuel cell ohmic resistance measurement. J Power Sources 2006; 160(2): 1088-95.

Cropper MAJ, Geiger S, Jollie DM. Fuel cells: a survey of current developments. J Power Sources 2004; 131: 57-61.

Danilov VA, Lim J, Moon I, Chang H. Three-dimensional, two-phase, CFD model for the design of a direct methanol fuel cell. J Power Sources 2006; 162: 992-1002.

Dillon R, Srinivasan S, Aricò AS, Antonucci V. International activities in DMFC R&D: status of technologies and potential applications. J Power Sources 2004; 127(1-2): 112-26.

Divisek J, Fuhrmann J, Gärtner K, Jung R. Performance modeling of a direct methanol fuel cell. J Electrochem Soc 2003; 150: 811-25.

Dohle H, Wippermann K. Experimental evaluation and semi-empirical modeling of U/I characteristics and methanol permeation of a direct methanol fuel cell. J Power Sources 2004; 135(1-2): 152-64.

Du B, Pollard R, Elter J. Proceedings of Fuel Cell Seminar 2006, Honolulu, Hawaii, USA, November, 2006: 61-4.

Dyer CK. Fuel cells for portable applications. J Power Sources 2002; 106: 31-4.

Eickes C, Piela P, Davey J, Zelenay P. Recoverable cathode performance loss in direct methanol fuel cells. J Electrochem Soc 2006; 153: A171-8.

Fang K, Yang Z. On uniform design of experiments with restricted mixtures and generation of uniform distribution on some domains. Stat Probabil Lett 2000; 46(2): 113-20.

Figueiredo JL, Pereira MFR, Serp P, Kalck P, Samant PV, Fernandes JB. Development of carbon nanotube and carbon xerogel supported catalysts for the electro-oxidation of methanol in fuel cells. Carbon2006; 44 (12): 2516-22.

Finsterwalder F, Hambitzer G. Proton conductive thin films prepared by plasma polymerization. J Membr Sci 2001; 185: 105-24.

Fowler M, Amphlett JC, Mann RF, Peppley BA, Roberge PR. Issues associated with voltage degradation in a polymer electrolyte fuel cell stacks. J New Mater Electrochem Syst 2002; 5: 255-62.

Gancs L, Hakim N, Hult BN, Mukerjee S. Dissolution of Ru from PtRu electrocatalysts and its consequences in DMFCs. ECS Transactions 2006; 3: 607-18.

Ge J, Liu H. A three-dimensional mathematical model for liquid-fed direct methanol fuel cells. J Power Sources 2006; 160(1): 413-21.

Ge J, Liu H. A three-dimensional two-phase flow model for a liquid-fed direct methanol fuel cell. J Power Sources 2007; 163: 907-15.

Gottesfeld S, Zawodzinski TA. In: Alkire RC, editor. Advances in electrochemical science and engineering. Weinheim, New York: Wiley-VCH, 1997. 5. p. 195-301.

Gubler L. Operating Polymer Electrolyte Fuel Cells with Reformed Fuel. ETH Zurich, Dissertation, Diss ETH No. 13954, 2001.

Guo Q, Cayetano M, Tsuo Y, De Castro ES, White R E. Study of ionic conductivity profiles of the air cathode of a PEMFC by AC impedance spectroscopy. J Electrochem Soc 2003; 150: 1440-9.

Gurau B, Smotkin ES. Methanol crossover in direct methanol fuel cells: a link between power and energy density. J Power Sources 2002; 112: 339-52.

Gurau B, Viswanathan R, Liu R, Lafrenz TJ, Ley KL, Smotkin ES. Structural and Electrochemical Characterization of Binary, Ternary, and Quaternary Platinum Alloy Catalysts for Methanol Electro-oxidation. J Phys Chem B 1998; 102: 9997-10003.

Hamnett A, Kennedy BJ, Weeks SA. Base metal oxides as promotors for the electrochemical oxidation of methanol. J Electroanal Chem 1988; 240: 349-53.

Han K, Lee J, Kim H. Preparation and characterization of high metal content Pt-Ru alloy catalysts on various carbon blacks for DMFCs. Electrochimica Acta 2006; 52 (4): 1697-702.

He YL, Li XL, Miao Z, Liu YW. Two-phase modeling of mass transfer characteristics of a direct methanol fuel cell. Appl Therm Eng 2009; 29: 1998-2008.

Iwasita T, Nart FC, Vielstich W. An FTIR Study of the Catalytic Activity of a 85-15 Pt-Ru Alloy for Methanol Oxidation. Ber Bunsenges Phys Chem 1990; 94: 1030-4.

Jia N, Lefebvre MC, Halfyard J, Qi Z, Pickup PG. Modification of Nafion Proton Exchange Membranes to Reduce Methanol Crossover in PEM Fuel Cells. Electrochem Solid-State Lett 2000; 3: 529-31.

Jiang Z, Zheng X, Wu H, Wang J, Wang Y. Proton conducting CS/P(AA-AMPS) membrane with reduced methanol permeability for DMFCs. J of Power Sources 2008; 180 (1): 143-153.

Kim YS, Hicknerc MA, Dongd L, Pivovara BS, McGrathb JE. Sulfonated poly(arylene ether sulfone) copolymer proton exchange membranes: composition and morphology effects on the methanol permeability. J Membr Sci 2004; 243: 317.

Knights SD, Colbow KM, St-Pierre J, Wilkinson P. Aging mechanisms and lifetime of PEFC and DMFC. J Power Sources 2004; 127(1–2): 127-34.

Ko J, Chippar P, Ju H. A one-dimensional, two-phase model for direct methanol fuel cells - part I: model development and parametric study. Energy 2010; 35: 2149-59

Kordesch K, Simader G. Fuel Cells and Their Applications, Weinheim: Wiley-VCH; 1996.

Kulikovsky AA. A model for carbon and Ru corrosion due to methanol depletion in DMFC. Electrochimica Acta 2011; 56: 9846–50

Kulikovsky AA. Analytical model of the anode side of DMFC: The effect of non-Tafel kinetics on cell performance. Electrochem Commun 2003; 5 (7): 530-8.

Kulikovsky AA. Two-dimensional numerical modeling of a direct methanol fuel cell, J Appl Electrochem 2000; 30: 1005-14.

Lamy C, Léger JM, Srinivasan S. Direct Methanol Fuel Cells: From a Twentieth Century Electrochemist's Dream to a Twenty-first Century Emerging Technology.Modern Aspects of Electrochemistry, Ed. by J.O'M. Bockris, B.E. Conway, and R.E. White, New York: Kluwer Academic / Plenum Publishers; 2001: 53-118.

Larminie J, Dicks A. Fuel Cell Systems Explained, 2nd ed. West Sussex: John Wiley & Sons Ltd.; 2003.

Le AD, Zhou, B. A general model of proton exchange membrane fuel cell. J of Power Sources 2008; 182: 197-222.

Lee C, Mérida W. Gas diffusion layer durability under steady-state and freezing conditions. J Power Sources 2007; 164: 141-53.

Li X, Sabir I. Review of bipolar plates in PEM fuel cells: Flow-field designs. Int J Hydrogen Energ 2005; 30: 359-371.

Libby B, Smyrl WH, Cussler EL. Composite Membranes for Direct Methanol Fuel Cells. Electrochem Solid-State Lett 2001; 4: A197-9.

Liu J, Zhou Z, Zhao X, Xin Q, Sun G, Yi B. Studies on performance degradation of a direct methanol fuel cell (DMFC) in life test. PCCP online journal (2003).

Liu W, Wang CY. Electron transport in direct methanol fuel cells, J Power Sources 2007; 164: 561-6.

Lu GQ, Wang CY. Electrochemical and flow characterization of a direct methanol fuel cell. J Power Sources 2004; 134: 33-40.

Ma ZQ, Cheng P, Zhao TS. A palladium-alloy deposited Nafion membrane for direct methanol fuel cells. J Membr Sci 2003; 215: 327-36.

Makharia R, Mathias MF, Baker DR. Measurement of catalyst layer electrolyte resistance in PEFC using electrochemical impedance spectroscopy. J Electrochem Soc 2005; 152: A970-7.

McDonald RC, Mittelsteadt CK, Thompson EL. Effects of deep temperature cycling on Nafion® 112 membranes and membrane electrode assemblies. Fuel Cells 2004; 4: 208-13.

McNicol BD, Rand DAJ, Williams KR. Direct methanol-air fuel cells for road transportation. J Power Sources 1999; 83: 15-31.

Mench MM, Wang CY. An In Situ Method for Determination of Current Distribution in PEM Fuel Cells Applied to a Direct Methanol Fuel Cell, J Electrochem Soc 2003; 150: A79-85

Munichandraiah N, McGrath K, Prakash G, Aniszfeld R, Olah G, J Power Sources 2003; 117: 98-101.

Oliveira VB, Falcãoa DS, Rangelb CM, Pinto AMFR. A comparative study of approaches to direct methanol fuel cells modeling. Int J Hydrogen Energy 2007; 32: 415-424

Paik CH, Jarvi TD, O'Grady WE. Extent of PEMFC cathode surface oxidation by oxygen and water measured by CV. Electrochem Solid-State Lett 2004; 7: A82-4.

Park J, Lee J, Kang S, Sauk J, Song I. Mass balance research for high electrochemical performance direct methanol fuel cells with reduced methanol crossover at various operating conditions. J Power Sources 2008; 178(1): 181-7.

Park JY, Lee JH, Sauk J, Son IH. The operating mode dependence on electrochemical performance degradation of direct methanol fuel cells. Int J Hydrogen Energy 2008; 33: 4833-43.

Park JY, Scibioh MA, Kim SK, Kim HJ, Oh IH., Lee TG, Ha HY. Investigations of performance degradation and mitigation strategies in direct methanol fuel cells. Int J Hydrogen Energy 2009; 34 (4): 2043-51.

Paulson, L. D. Will fuel cells replace batteries in mobile devices?. Computer 2003; 36: 10-2.

Peled E, Duvdevani T, Melman A. A Novel Proton-Conducting Membrane. Electrochem Solid-State Lett 1998; 1: 210-11.

Piela P, Eickes C, Brosha E, Garzon F, Zelenay P. Ruthenium crossover in direct methanol fuel cell with Pt–Ru black anode. J Electrochem Soc 2004; 151(12): 2053-9.

Piela P, Eickes C, Brosha E, Garzon F, Zelenay P. Ruthenium crossover in direct methanol fuel cell with Pt-Ru black anode. J Electrochem Soc 2004; 151: A2053-9.

Pivovar BS, Wang Y, Cussler EL. Pervaporation membranes in direct methanol fuel cells. J Membr Sci 1999; 154: 155-62.

Prabhuram J, Zhao TS, Yang H. Methanol adsorbates on the DMFC cathode and their effect on the cell performance. J Electroanal Chem 2005; 578: 105-12.

Ren X, Springer TE, Gottesfeld S. Water and Methanol Uptakes in Nafion Membranes and Membrane Effects on Direct Methanol Cell Performance. J Electrochem Soc 2000; 147: 92-8.

Rice J, Faghri A. A transient, multi-phase and multi-component model of a new passive DMFC. Int J Heat and Mass Transfer 2006; 49: 4804-20.

Roen LM , Paik CH , Jarvi TD. Electrocatalytic corrosion of carbon support in PEMFC cathodes. Electrochem Solid St 2004; 7: A19-22.

Samms SR, Wasmus S, Savinell RF. Thermal stability of proton conducting acid doped polybenzimidazole in simulated fuel cell environments, J Electrochem Soc 1996;143: 1498-504.

Schultz T, Zhou S, Sundmacher K. Current status and recent developments of the direct methanol fuel cell. Chem Eng Tech 2001; 24: 1223-33.

Schulze M, Christenn C. XPS investigation of the PTFE induced hydrophobic properties of electrodes for low temperature fuel cells. Appl Surf Sci 2005; 252: 148.

Scott K, Argyropoulos P, Yiannopoulos P, Taama WM. Electrochemical and gas evolution characteristics of direct methanol fuel cells with stainless steel mesh flow beds. J Appl Electrochem 2001; 31: 823-32.

Scott K, Argyropoulos P. A one dimensional model of a methanol fuel cell anode. J Power Sources 2004; 137: 228-38.

Scott K, Jackson C, Argyropoulos P. A semi empirical model of the direct methanol fuel cell - part II: parametric analysis. J Power Sources 2006; 161(2): 885-92..

Scott K, Taama WM, Argyropoulos P. Engineering aspects of the direct methanol fuel cell system. J Power Sources 1999; 79(1): 43-59.

Shao Y, Yin G, Gao Y. Understanding and approaches for the durability issues of Pt-based catalysts for PEM fuel cell. J Power Sources 2007; 171: 558-66.

Sivertsen BR, Djilali N. CFD-based modelling of proton exchange membrane fuel cells. J Power Sources 2005; 141: 65-78.

Song M, Park S, Kim Y, Kim K, Min S, Rhee H. Characterization of polymer-layered silicate nanocomposite membranes for direct methanol fuel cells. Electrochim Acta 2004; 50(2-3): 639-43.

Song SQ, Zhou WJ, Li WZ, Sun G, Xin Q, Konton S, Tsiakaras P. Direct methanol fuel cells : Methanol crossover and its influence on single DMFC performance. Ionics 2004; 10: 458-62.

Springer TE, Zawodzinski TA, Wilson MS, Gottesfeld S. Characterization of polymer electrolyte fuel cells using AC impedance spectroscopy. J Electrochem Soc 1996: 143: 587-99.

Srinivasan S, Ticianelli E A, Derouin CR, Redondo A. Advances in solid polymer electrolyte fuel cell technology with low platinum loading electrodes. J Power Sources 1988; 22(3-4): 359-75.

Staiti P, Minutoli M, Hocevar S. Membranes based on phosphotungstic acid and polybenzimidazole for fuel cell application. J Power Sources 2000; 90: 231-5.

Surowiec J, Bogoczek R. Studies on the thermal stability of the perfluorinated cation-exchange membrane Nafion-417. J Therm Anal 1988; 33: 1097-102.

Tian AH, Kim JY, Shi JY, Kim K, Lee K. Surface-modified Nafion membrane by oleylamine-stabilized Pd nanoparticles for DMFC applications. J Power Sources 2007; 167 (2): 302-8.

Uribe FA, Zawodzinski Jr TA. A study of polymer electrolyte fuel cell performance at high voltages. Dependence on cathode catalyst layer composition and on voltage conditioning. Electrochim Acta 2002; 47: 3799-806.

Vera M. A single-phase model for liquid-feed DMFCs with non-Tafel kinetics. J Power Sources 2007; 171: 763-77.

Vielstich W, Lamm A, Gasteiger HA. Handbook of Fuel Cells: Fundamentals, Technology and Applications. Chichester: Wiley; 2003.

Wang JT, Wasmus S, Savinell RF. Real-time mass spectrometric study of the methanol crossover in a direct methanol fuel cell. J Electrochem Soc 1996; 143: 1233-9.

Wang R, Qi L, Xie X, Ding Q, Li C, Ma CM, Modeling of a 5-cell direct methanol fuel cell using adaptive-network-based fuzzy inference systems, J Power Sources 2008; 185(2): 1201-8.

Wang ZH, Wang CW. Mathematical modeling of liquid-feed direct methanol fuel cells. J Electrochem Soc 2003; 150: 508-19.

Washington K. Development of 250kW class polymer electrolyte fuel cell stack. Proceedings of Fuel Cell Seminar 2000, Portland, USA, November, 2000, pp. 468–472.

Wasmus S, Küver A. Methanol oxidation and direct methanol fuel cells: a selective review. J Electroanal Chem 1999; 461: 14-31.

Watanabe M, Tsurumi K, Mizukami T, Nakamura T, Stonehart P. Activity and stability of ordered and disordered Co-Pt alloys for phosphoric acid fuel cells. J Electrochem Soc 1994; 141: 2659-68.

Wilkie CA, Thomsen JR, Mittleman ML. Gas diffusion layer durability under steady-state and freezing conditions. J Appl Polym Sci 1991; 42: 901-9.

Wong CW, Zhao TS, Ye Q, Liu JG. Experimental investigations of the anode flow field of a micro direct methanol fuel cell. J Power Sources 2006; 155: 291-6.

Wu J, Yuana XJ, Martina JJ, Wanga H, Zhanga J, Shena J, Wua Sh, Meridaa W. A review of PEM fuel cell durability: Degradation mechanisms and mitigation strategies, J Power Sources 2008; 184: 104-19.

Xie J, Wood III DL, Wayne DM, Zawodzinski TA, Atanassov P, Borup RL. Durability of PEFCs at high humidity conditions, J Electrochem Soc 2005; 152: A104-13.

Xu B, Yang X, Wang X, Guo J, Liu X. A novel catalyst support for DMFC: Onion-like fullerenes. J Power Sources 2006; 162 (1): 160-4.

Yan TZ, Jen TC. Two-phase flow modeling of liquid-feed direct methanol fuel cell. International Journal of Heat and Mass Transfer 2008; 51: 1192–204.

Yang H, Zhao TS. Effect of anode flow field design on the performance of liquid feed direct methanol fuel cells. Electrochemica Acta 2005; 50: 3243-52.

Yang Q, Kianimanesh A, Freiheit T, Park SS, Xue D, A semi-empirical model considering the influence of operating parameters on performance for a direct methanol fuel cell. J Power Sources 2011; 196(24): 10640-51.

Yang S, Chen C, Wang W. An impedance study for the anode micro-porous layer in an operating direct methanol fuel cell. J Power Sources 2010; 195(11): 3536-3545.

Yang WW, Zhao TS, Xu C. Three-dimensional two-phase mass transport model for direct methanol fuel cells. Electrochimica Acta 2007; 53: 853-862.

Yang WW, Zhao TS. A two-dimensional, two-phase mass transport model for liquid-feed DMFCs. Electrochimica Acta 2007; 52: 6125-40.

Yoshida N, Ishisaki T, Watakabe A, Yoshitake M. Characterization of Flemion® membranes for PEFC. Electrochim Acta 1998; 43: 3749-54.

Yuan XZ, Song C, Wang H, Zhang J. Electrochemical Impedance Spectroscopy in PEM Fuel Cells, London: Springer Press; 2010: 312.

Zenith F, Krewer U. Modelling, dynamics and control of a portable DMFC system. Journal of Process Control 2010; 20: 630–42.

Zhang J, Yin GP, Lai QZ, Wang ZB, Cai KD, Liu P. The influence of anode gas diffusion layer on the performance of low-temperature DMFC. J Power Sources 2007; 168 (2): 453-8.

Appendix A: Performance Measurements Experiments

Design of Experiments for Impedance Measurement

No.	T(K)	M_f(ccm)	C_{me}(M)	A_f(ccm)	R_{ohmic}(Ω.cm^2)
1	298	3.5	0.5	81.2	1.42
2	313	3.5	0.5	81.2	1.39
3	313	3.5	0.5	125.2	1.16
4	313	3.5	2	81.2	1.31
5	313	3.5	2	125.2	1.23
6	323	3.5	0.5	81.2	1.11
7	333	3.5	0.5	81.2	1.02
8	343	3.5	0.5	81.2	0.98
9	343	3.5	0.5	125.2	0.91
10	343	3.5	2	81.2	1.05
11	343	3.5	2	125.2	1.17
12	343	4.5	2	125.2	1.15
13	343	5.5	2	125.2	1.09

Operating conditions and model coefficients of the tests for Designs A, B and C

No.	Temp. (K)	Methanol Flow (ccm)	Methanol Conc. (mol/L)	Air Flow (ccm)	Design A			Design B			Design C		
					E_0^* (mV)	b_{cell} (mV)	R_e ($\Omega.cm^2$)	E_0^* (mV)	b_{cell} (mV)	R_e ($\Omega.cm^2$)	E_0^* (mV)	b_{cell} (mV)	R_e ($\Omega.cm^2$)
1	298	2.27	1.5	287	825.6	120.1	0.50	623.8	62.0	1.07	532.0	31.3	1.01
2	298	4.05	0.5	72	508.6	29.6	1.21	572.2	41.5	1.07	570.1	33.2	1.09
3	313	3.48	1	186	516.7	24.6	1.09	537.6	24.0	0.76	547.6	28.3	0.56
4	313	4.05	2	402	457.0	25.8	0.84	380.1	10.6	0.86	510.0	25.3	0.67
5	323	2.27	0.25	118	593.8	27.5	0.77	575.0	17.5	0.61	611.5	11.1	1.10
6	323	4.4	0.25	287	822.5	83.6	0.92	634.5	32.2	0.56	581.9	12.7	1.03
7	333	3.06	2	72	413.4	31.9	0.98	501.8	24.3	0.70	390.4	13.4	0.96
8	333	3.48	1	186	498.6	18.3	0.83	613.6	46.5	0.51	557.8	21.2	0.51
9	343	3.06	0.5	402	556.7	20.9	0.86	573.3	20.7	0.42	581.0	17.9	0.43
10	343	4.4	1.5	118	503.9	31.2	1.05	480.6	19.3	0.63	521.2	19.7	0.46

Appendix B: CFD Simulation Parameters

Physical parameters for the CFD simulation

Parameter	Value	Reference
Water density, ρ_{H2O}	1,000 kg m^{-3}	
Water viscosity, μ_{H2O}	$0.458509-5.30474\times10^{-3}T+2.31231\times10^{-5}T^2-4.49161\times10^{-8}T^3+3.27681\times10^{-11}T^4$ kg $m^{-1}s^{-1}$	Wang and Wang [2003]
Diffusion coefficient of methanol in water, D_{CH3OH}	$10^{-5.4163-(999.778/T)}$ m^2s^{-1}	Wang and Wang [2003]
Permeability of anode diffusion layer, K_{adl}	1×10^{-11} m^2	Assumed
Permeability of anode catalyst layer, K_{acl}	1×10^{-11} m^2	Assumed
Porosity of anode diffusion layer, ε_{adl}	0.6	Assumed
Porosity of anode catalyst layer, ε_{acl}	0.4	Assumed
Molecular weight of methanol, M_{CH3OH}	0.032 kg mol^{-1}	Vera [2007]
Molecular weight of water, M_{H2O}	0.018 kg mol^{-1}	Vera [2007]

Appendix C: Experimental Datasheet

Temp. (K)	MeOH Flow Rate (ccm)	MeOH Conc.(M)	Air Flow Rate(ccm)	Time(min)	Current (mA)	Voltage(mV)	Test No.
313	3.5	0.5	108.7	1121	0	548	1
313	3.5	0.5	108.7	1121	10	535	1
313	3.5	0.5	108.7	1121	40	493	1
313	3.5	0.5	108.7	1121	60	477	1
313	3.5	0.5	108.7	1121	80	475	1
313	3.5	0.5	108.7	1121	100	448	1
313	3.5	0.5	108.7	1121	120	432	1
313	3.5	0.5	108.7	1121	130	425	1
313	3.5	0.5	108.7	1121	140	423	1
313	3.5	0.5	108.7	1121	160	417	1
313	3.5	0.5	108.7	1121	180	395	1
313	3.5	0.5	108.7	1121	200	380	1
313	3.5	0.5	108.7	1121	220	370	1
313	3.5	0.5	108.7	1121	240	356	1
313	3.5	0.5	108.7	1121	260	346	1
313	3.5	0.5	108.7	1121	280	332	1
313	3.5	0.5	108.7	1121	300	318	1
313	3.5	0.5	108.7	1121	320	304	1
313	3.5	0.5	108.7	1121	330	298	1
313	3.5	0.5	108.7	1121	340	292	1
313	3.5	0.5	108.7	1121	350	285	1

313	3.5	0.5	108.7	1121	400	252	1
313	3.5	0.5	108.7	1121	450	220	1
313	3.5	0.5	108.7	1121	500	187	1
313	3.5	0.5	108.7	1121	550	157	1
313	3.5	0.5	108.7	1121	600	129	1
313	3.5	0.5	108.7	1703.5	0	550	1
313	3.5	0.5	108.7	1703.5	10	528	1
313	3.5	0.5	108.7	1703.5	40	465	1
313	3.5	0.5	108.7	1703.5	60	426	1
313	3.5	0.5	108.7	1703.5	80	395	1
313	3.5	0.5	108.7	1703.5	100	361	1
313	3.5	0.5	108.7	1703.5	120	335	1
313	3.5	0.5	108.7	1703.5	140	300	1
313	3.5	0.5	108.7	1703.5	160	273	1
313	3.5	0.5	108.7	1703.5	180	246	1
313	3.5	0.5	108.7	1703.5	200	215	1
313	3.5	0.5	108.7	1703.5	220	195	1
313	3.5	0.5	108.7	1703.5	240	166	1
313	3.5	0.5	108.7	1703.5	260	143	1
313	3.5	0.5	108.7	1703.5	280	115	1
313	3.5	0.5	108.7	1703.5	300	90	1
313	3.5	0.5	108.7	1703.5	320	72	1
313	3.5	0.5	108.7	1703.5	330	65	1
313	3.5	0.5	108.7	1703.5	340	54	1
313	3.5	0.5	108.7	1703.5	350	38	1

313	3.5	0.5	108.7	1703.5	365	18	1
313	3.5	0.5	108.7	2152.5	0	568	1
313	3.5	0.5	108.7	2152.5	10	531	1
313	3.5	0.5	108.7	2152.5	20	489	1
313	3.5	0.5	108.7	2152.5	30	463	1
313	3.5	0.5	108.7	2152.5	40	435	1
313	3.5	0.5	108.7	2152.5	50	411	1
313	3.5	0.5	108.7	2152.5	60	386	1
313	3.5	0.5	108.7	2152.5	70	361	1
313	3.5	0.5	108.7	2152.5	80	338	1
313	3.5	0.5	108.7	2152.5	90	315	1
313	3.5	0.5	108.7	2152.5	100	293	1
313	3.5	0.5	108.7	2152.5	110	275	1
313	3.5	0.5	108.7	2152.5	120	254	1
313	3.5	0.5	108.7	2152.5	130	234	1
313	3.5	0.5	108.7	2152.5	140	214	1
313	3.5	0.5	108.7	2152.5	150	194	1
313	3.5	0.5	108.7	2152.5	160	174	1
313	3.5	0.5	108.7	2152.5	170	155	1
313	3.5	0.5	108.7	2152.5	180	135	1
313	3.5	0.5	108.7	2152.5	190	116	1
313	3.5	0.5	108.7	2152.5	200	96	1
313	3.5	0.5	108.7	2152.5	240	16	1
313	5.5	0.5	125.2	1166	0	560	2
313	5.5	0.5	125.2	1166	10	542	2

313	5.5	0.5	125.2	1166	40	490	2
313	5.5	0.5	125.2	1166	60	463	2
313	5.5	0.5	125.2	1166	80	446	2
313	5.5	0.5	125.2	1166	100	428	2
313	5.5	0.5	125.2	1166	120	415	2
313	5.5	0.5	125.2	1166	140	400	2
313	5.5	0.5	125.2	1166	160	388	2
313	5.5	0.5	125.2	1166	180	377	2
313	5.5	0.5	125.2	1166	200	363	2
313	5.5	0.5	125.2	1166	220	350	2
313	5.5	0.5	125.2	1166	240	339	2
313	5.5	0.5	125.2	1166	260	328	2
313	5.5	0.5	125.2	1166	280	315	2
313	5.5	0.5	125.2	1166	300	302	2
313	5.5	0.5	125.2	1166	320	289	2
313	5.5	0.5	125.2	1166	330	283	2
313	5.5	0.5	125.2	1166	340	278	2
313	5.5	0.5	125.2	1166	350	271	2
313	5.5	0.5	125.2	1166	400	237	2
313	5.5	0.5	125.2	1166	450	209	2
313	5.5	0.5	125.2	1166	500	180	2
313	5.5	0.5	125.2	1166	550	150	2
313	5.5	0.5	125.2	1166	600	94	2
313	5.5	0.5	125.2	1731.5	0	552	2
313	5.5	0.5	125.2	1731.5	10	528	2

313	5.5	0.5	125.2	1731.5	40	455	2
313	5.5	0.5	125.2	1731.5	60	423	2
313	5.5	0.5	125.2	1731.5	80	385	2
313	5.5	0.5	125.2	1731.5	100	352	2
313	5.5	0.5	125.2	1731.5	120	325	2
313	5.5	0.5	125.2	1731.5	140	296	2
313	5.5	0.5	125.2	1731.5	160	266	2
313	5.5	0.5	125.2	1731.5	180	242	2
313	5.5	0.5	125.2	1731.5	200	215	2
313	5.5	0.5	125.2	1731.5	220	191	2
313	5.5	0.5	125.2	1731.5	240	163	2
313	5.5	0.5	125.2	1731.5	250	151	2
313	5.5	0.5	125.2	1731.5	260	138	2
313	5.5	0.5	125.2	1731.5	270	127	2
313	5.5	0.5	125.2	1731.5	280	115	2
313	5.5	0.5	125.2	1731.5	300	88	2
313	5.5	0.5	125.2	1731.5	340	42	2
313	5.5	0.5	125.2	1731.5	350	24	2
313	5.5	0.5	125.2	1731.5	360	18	2
313	5.5	0.5	125.2	2180.5	0	554	2
313	5.5	0.5	125.2	2180.5	10	522	2
313	5.5	0.5	125.2	2180.5	20	484	2
313	5.5	0.5	125.2	2180.5	30	442	2
313	5.5	0.5	125.2	2180.5	40	408	2
313	5.5	0.5	125.2	2180.5	50	380	2

313	5.5	0.5	125.2	2180.5	60	353	2
313	5.5	0.5	125.2	2180.5	70	327	2
313	5.5	0.5	125.2	2180.5	80	302	2
313	5.5	0.5	125.2	2180.5	90	278	2
313	5.5	0.5	125.2	2180.5	100	255	2
313	5.5	0.5	125.2	2180.5	110	234	2
313	5.5	0.5	125.2	2180.5	120	212	2
313	5.5	0.5	125.2	2180.5	130	189	2
313	5.5	0.5	125.2	2180.5	140	174	2
313	5.5	0.5	125.2	2180.5	150	158	2
313	5.5	0.5	125.2	2180.5	160	142	2
313	5.5	0.5	125.2	2180.5	170	122	2
313	5.5	0.5	125.2	2180.5	180	97	2
313	5.5	0.5	125.2	2180.5	190	88	2
313	5.5	0.5	125.2	2180.5	200	86	2
313	5.5	0.5	125.2	2180.5	240	13	2
313	4.5	1	93.6	1211	0	558	3
313	4.5	1	93.6	1211	10	541	3
313	4.5	1	93.6	1211	40	494	3
313	4.5	1	93.6	1211	60	475	3
313	4.5	1	93.6	1211	80	455	3
313	4.5	1	93.6	1211	100	437	3
313	4.5	1	93.6	1211	120	423	3
313	4.5	1	93.6	1211	140	408	3
313	4.5	1	93.6	1211	160	402	3

313	4.5	1	93.6	1211	180	386	3
313	4.5	1	93.6	1211	200	372	3
313	4.5	1	93.6	1211	220	359	3
313	4.5	1	93.6	1211	240	345	3
313	4.5	1	93.6	1211	260	335	3
313	4.5	1	93.6	1211	270	328	3
313	4.5	1	93.6	1211	280	323	3
313	4.5	1	93.6	1211	290	315	3
313	4.5	1	93.6	1211	300	308	3
313	4.5	1	93.6	1211	350	275	3
313	4.5	1	93.6	1211	400	240	3
313	4.5	1	93.6	1211	450	209	3
313	4.5	1	93.6	1211	500	178	3
313	4.5	1	93.6	1211	550	146	3
313	4.5	1	93.6	1211	600	115	3
313	4.5	1	93.6	1706.5	0	534	3
313	4.5	1	93.6	1706.5	10	513	3
313	4.5	1	93.6	1706.5	40	442	3
313	4.5	1	93.6	1706.5	50	425	3
313	4.5	1	93.6	1706.5	60	420	3
313	4.5	1	93.6	1706.5	80	393	3
313	4.5	1	93.6	1706.5	100	360	3
313	4.5	1	93.6	1706.5	120	329	3
313	4.5	1	93.6	1706.5	140	296	3
313	4.5	1	93.6	1706.5	160	268	3

313	4.5	1	93.6	1706.5	180	244	3
313	4.5	1	93.6	1706.5	200	221	3
313	4.5	1	93.6	1706.5	220	198	3
313	4.5	1	93.6	1706.5	230	186	3
313	4.5	1	93.6	1706.5	240	175	3
313	4.5	1	93.6	1706.5	250	166	3
313	4.5	1	93.6	1706.5	260	155	3
313	4.5	1	93.6	1706.5	280	129	3
313	4.5	1	93.6	1706.5	300	104	3
313	4.5	1	93.6	1706.5	350	40	3
313	4.5	1	93.6	1706.5	370	18	3
313	4.5	1	93.6	2207.5	0	540	3
313	4.5	1	93.6	2207.5	10	494	3
313	4.5	1	93.6	2207.5	20	465	3
313	4.5	1	93.6	2207.5	30	437	3
313	4.5	1	93.6	2207.5	40	411	3
313	4.5	1	93.6	2207.5	50	387	3
313	4.5	1	93.6	2207.5	60	368	3
313	4.5	1	93.6	2207.5	70	349	3
313	4.5	1	93.6	2207.5	80	330	3
313	4.5	1	93.6	2207.5	90	308	3
313	4.5	1	93.6	2207.5	100	290	3
313	4.5	1	93.6	2207.5	110	274	3
313	4.5	1	93.6	2207.5	120	256	3
313	4.5	1	93.6	2207.5	130	238	3

313	4.5	1	93.6	2207.5	140	222	3
313	4.5	1	93.6	2207.5	150	205	3
313	4.5	1	93.6	2207.5	160	190	3
313	4.5	1	93.6	2207.5	170	177	3
313	4.5	1	93.6	2207.5	180	162	3
313	4.5	1	93.6	2207.5	190	143	3
313	4.5	1	93.6	2207.5	200	126	3
313	4.5	1	93.6	2207.5	240	57	3
313	4	1.5	108.7	334.5	0	457	4
313	4	1.5	108.7	334.5	10	445	4
313	4	1.5	108.7	334.5	20	435	4
313	4	1.5	108.7	334.5	40	420	4
313	4	1.5	108.7	334.5	60	411	4
313	4	1.5	108.7	334.5	80	396	4
313	4	1.5	108.7	334.5	100	376	4
313	4	1.5	108.7	334.5	120	358	4
313	4	1.5	108.7	334.5	130	356	4
313	4	1.5	108.7	334.5	135	355	4
313	4	1.5	108.7	334.5	140	351	4
313	4	1.5	108.7	334.5	145	350	4
313	4	1.5	108.7	334.5	150	346	4
313	4	1.5	108.7	334.5	155	342	4
313	4	1.5	108.7	334.5	160	337	4
313	4	1.5	108.7	334.5	165	328	4
313	4	1.5	108.7	334.5	170	327	4

313	4	1.5	108.7	334.5	175	324	4
313	4	1.5	108.7	334.5	180	323	4
313	4	1.5	108.7	334.5	190	319	4
313	4	1.5	108.7	334.5	200	312	4
313	4	1.5	108.7	334.5	210	306	4
313	4	1.5	108.7	334.5	220	292	4
313	4	1.5	108.7	334.5	230	284	4
313	4	1.5	108.7	334.5	240	270	4
313	4	1.5	108.7	334.5	250	262	4
313	4	1.5	108.7	334.5	260	260	4
313	4	1.5	108.7	334.5	270	256	4
313	4	1.5	108.7	334.5	280	250	4
313	4	1.5	108.7	334.5	290	240	4
313	4	1.5	108.7	2234	0	474	4
313	4	1.5	108.7	2234	10	442	4
313	4	1.5	108.7	2234	20	398	4
313	4	1.5	108.7	2234	30	375	4
313	4	1.5	108.7	2234	40	347	4
313	4	1.5	108.7	2234	50	318	4
313	4	1.5	108.7	2234	60	292	4
313	4	1.5	108.7	2234	70	280	4
313	4	1.5	108.7	2234	80	250	4
313	4	1.5	108.7	2234	90	228	4
313	4	1.5	108.7	2234	100	210	4
313	4	1.5	108.7	2234	110	185	4

313	4	1.5	108.7	2234	120	164	4
313	4	1.5	108.7	2234	130	143	4
313	4	1.5	108.7	2234	140	126	4
313	4	1.5	108.7	2234	150	86	4
313	4	1.5	108.7	2234	160	80	4
313	4	1.5	108.7	2234	170	62	4
313	4	1.5	108.7	2234	180	36	4
313	4	1.5	108.7	2234	190	34	4
313	4	1.5	108.7	2234	200	12	4
313	3.5	1.5	81.2	382.5	0	531	5
313	3.5	1.5	81.2	382.5	10	456	5
313	3.5	1.5	81.2	382.5	20	402	5
313	3.5	1.5	81.2	382.5	40	426	5
313	3.5	1.5	81.2	382.5	60	408	5
313	3.5	1.5	81.2	382.5	80	401	5
313	3.5	1.5	81.2	382.5	100	397	5
313	3.5	1.5	81.2	382.5	120	360	5
313	3.5	1.5	81.2	382.5	140	337	5
313	3.5	1.5	81.2	382.5	160	335	5
313	3.5	1.5	81.2	382.5	180	308	5
313	3.5	1.5	81.2	382.5	200	290	5
313	3.5	1.5	81.2	382.5	220	275	5
313	3.5	1.5	81.2	382.5	225	272	5
313	3.5	1.5	81.2	382.5	230	270	5
313	3.5	1.5	81.2	382.5	235	268	5

313	3.5	1.5	81.2	382.5	240	265	5
313	3.5	1.5	81.2	382.5	245	258	5
313	3.5	1.5	81.2	382.5	250	248	5
313	3.5	1.5	81.2	382.5	260	242	5
313	3.5	1.5	81.2	382.5	270	232	5
313	3.5	1.5	81.2	382.5	280	225	5
313	3.5	1.5	81.2	2262.5	0	390	5
313	3.5	1.5	81.2	2262.5	10	368	5
313	3.5	1.5	81.2	2262.5	20	347	5
313	3.5	1.5	81.2	2262.5	30	332	5
313	3.5	1.5	81.2	2262.5	40	312	5
313	3.5	1.5	81.2	2262.5	50	276	5
313	3.5	1.5	81.2	2262.5	60	264	5
313	3.5	1.5	81.2	2262.5	70	252	5
313	3.5	1.5	81.2	2262.5	80	228	5
313	3.5	1.5	81.2	2262.5	90	200	5
313	3.5	1.5	81.2	2262.5	100	170	5
313	3.5	1.5	81.2	2262.5	110	160	5
313	3.5	1.5	81.2	2262.5	120	138	5
313	3.5	1.5	81.2	2262.5	130	116	5
313	3.5	1.5	81.2	2262.5	140	94	5
313	3.5	1.5	81.2	2262.5	150	71	5
313	3.5	1.5	81.2	2262.5	160	50	5
313	3.5	1.5	81.2	2262.5	170	24	5
313	3.5	1.5	81.2	2262.5	180	16	5

313	5	1.5	140.8	416.5	0	458	6
313	5	1.5	140.8	416.5	10	435	6
313	5	1.5	140.8	416.5	20	432	6
313	5	1.5	140.8	416.5	40	418	6
313	5	1.5	140.8	416.5	60	402	6
313	5	1.5	140.8	416.5	80	376	6
313	5	1.5	140.8	416.5	100	362	6
313	5	1.5	140.8	416.5	120	352	6
313	5	1.5	140.8	416.5	140	339	6
313	5	1.5	140.8	416.5	160	324	6
313	5	1.5	140.8	416.5	180	315	6
313	5	1.5	140.8	416.5	200	298	6
313	5	1.5	140.8	416.5	220	285	6
313	5	1.5	140.8	416.5	225	282	6
313	5	1.5	140.8	416.5	230	277	6
313	5	1.5	140.8	416.5	235	273	6
313	5	1.5	140.8	416.5	240	274	6
313	5	1.5	140.8	416.5	245	271	6
313	5	1.5	140.8	416.5	250	263	6
313	5	1.5	140.8	416.5	255	258	6
313	5	1.5	140.8	416.5	260	256	6
313	5	1.5	140.8	416.5	270	249	6
313	5	1.5	140.8	416.5	280	238	6
313	5	1.5	140.8	416.5	300	206	6
313	5	1.5	140.8	2292.5	0	458	6

313	5	1.5	140.8	2292.5	10	418	6
313	5	1.5	140.8	2292.5	20	394	6
313	5	1.5	140.8	2292.5	30	375	6
313	5	1.5	140.8	2292.5	40	354	6
313	5	1.5	140.8	2292.5	50	318	6
313	5	1.5	140.8	2292.5	60	292	6
313	5	1.5	140.8	2292.5	70	265	6
313	5	1.5	140.8	2292.5	80	237	6
313	5	1.5	140.8	2292.5	90	213	6
313	5	1.5	140.8	2292.5	110	175	6
313	5	1.5	140.8	2292.5	120	153	6
313	5	1.5	140.8	2292.5	130	134	6
313	5	1.5	140.8	2292.5	140	116	6
313	5	1.5	140.8	2292.5	150	98	6
313	5	1.5	140.8	2292.5	160	80	6
313	5	1.5	140.8	2292.5	170	46	6
313	5	1.5	140.8	2292.5	180	28	6
313	5	1.5	140.8	2292.5	190	12	6
313	4.5	2	108.7	451.5	0	523	7
313	4.5	2	108.7	451.5	10	450	7
313	4.5	2	108.7	451.5	20	422	7
313	4.5	2	108.7	451.5	40	397	7
313	4.5	2	108.7	451.5	60	378	7
313	4.5	2	108.7	451.5	80	373	7
313	4.5	2	108.7	451.5	100	348	7

313	4.5	2	108.7	451.5	120	321	7
313	4.5	2	108.7	451.5	140	310	7
313	4.5	2	108.7	451.5	180	261	7
313	4.5	2	108.7	451.5	200	272	7
313	4.5	2	108.7	451.5	220	251	7
313	4.5	2	108.7	451.5	225	246	7
313	4.5	2	108.7	451.5	230	236	7
313	4.5	2	108.7	451.5	235	224	7
313	4.5	2	108.7	451.5	240	223	7
313	4.5	2	108.7	451.5	245	217	7
313	4.5	2	108.7	451.5	250	225	7
313	4.5	2	108.7	451.5	255	207	7
313	4.5	2	108.7	451.5	260	182	7
313	4.5	2	108.7	451.5	270	174	7
313	4.5	2	108.7	451.5	280	143	7
313	4.5	2	108.7	451.5	300	83	7
313	4.5	2	108.7	2327.5	0	430	7
313	4.5	2	108.7	2327.5	10	380	7
313	4.5	2	108.7	2327.5	20	352	7
313	4.5	2	108.7	2327.5	30	316	7
313	4.5	2	108.7	2327.5	40	295	7
313	4.5	2	108.7	2327.5	50	271	7
313	4.5	2	108.7	2327.5	60	258	7
313	4.5	2	108.7	2327.5	70	227	7
313	4.5	2	108.7	2327.5	80	202	7

313	4.5	2	108.7	2327.5	90	193	7
313	4.5	2	108.7	2327.5	100	173	7
313	4.5	2	108.7	2327.5	110	153	7
313	4.5	2	108.7	2327.5	120	136	7
313	4.5	2	108.7	2327.5	130	118	7
313	4.5	2	108.7	2327.5	140	106	7
313	4.5	2	108.7	2327.5	150	87	7
313	4.5	2	108.7	2327.5	160	41	7
313	4.5	2	108.7	2327.5	170	22	7
313	4.5	2	108.7	2327.5	180	8	7
313	4.5	0.25	140.8	2361	0	597	8
313	4.5	0.25	140.8	2361	10	560	8
313	4.5	0.25	140.8	2361	20	528	8
313	4.5	0.25	140.8	2361	30	502	8
313	4.5	0.25	140.8	2361	40	477	8
313	4.5	0.25	140.8	2361	50	455	8
313	4.5	0.25	140.8	2361	60	450	8
313	4.5	0.25	140.8	2361	70	444	8
313	4.5	0.25	140.8	2361	80	420	8
313	4.5	0.25	140.8	2361	90	393	8
313	4.5	0.25	140.8	2361	100	373	8
313	4.5	0.25	140.8	2361	110	354	8
313	4.5	0.25	140.8	2361	120	337	8
313	4.5	0.25	140.8	2361	130	319	8
313	4.5	0.25	140.8	2361	140	300	8

313	4.5	0.25	140.8	2361	150	282	8
313	4.5	0.25	140.8	2361	160	264	8
313	4.5	0.25	140.8	2361	170	248	8
313	4.5	0.25	140.8	2361	180	233	8
313	4.5	0.25	140.8	2361	190	217	8
313	4.5	0.25	140.8	2361	200	203	8
313	4.5	0.25	140.8	2361	220	186	8
313	4.5	0.25	140.8	2361	250	122	8
313	5.5	0.25	81.2	2390	10	554	9
313	5.5	0.25	81.2	2390	20	531	9
313	5.5	0.25	81.2	2390	30	492	9
313	5.5	0.25	81.2	2390	40	464	9
313	5.5	0.25	81.2	2390	50	435	9
313	5.5	0.25	81.2	2390	60	414	9
313	5.5	0.25	81.2	2390	70	390	9
313	5.5	0.25	81.2	2390	80	368	9
313	5.5	0.25	81.2	2390	90	345	9
313	5.5	0.25	81.2	2390	100	325	9
313	5.5	0.25	81.2	2390	110	312	9
313	5.5	0.25	81.2	2390	120	292	9
313	5.5	0.25	81.2	2390	130	276	9
313	5.5	0.25	81.2	2390	140	257	9
313	5.5	0.25	81.2	2390	150	238	9
313	5.5	0.25	81.2	2390	160	210	9
313	5.5	0.25	81.2	2390	170	200	9

313	5.5	0.25	81.2	2390	180	184	9
313	5.5	0.25	81.2	2390	190	175	9
313	5.5	0.25	81.2	2390	200	150	9
313	5.5	0.25	81.2	2390	220	113	9
313	5.5	0.25	81.2	2390	250	53	9
313	5.5	0.25	81.2	2390	270	18	9
333	3.5	0.5	81.2	492.5	10	663	10
333	3.5	0.5	81.2	492.5	20	553	10
333	3.5	0.5	81.2	492.5	40	512	10
333	3.5	0.5	81.2	492.5	60	485	10
333	3.5	0.5	81.2	492.5	80	460	10
333	3.5	0.5	81.2	492.5	100	441	10
333	3.5	0.5	81.2	492.5	120	420	10
333	3.5	0.5	81.2	492.5	140	401	10
333	3.5	0.5	81.2	492.5	180	364	10
333	3.5	0.5	81.2	492.5	200	357	10
333	3.5	0.5	81.2	492.5	220	344	10
333	3.5	0.5	81.2	492.5	225	344	10
333	3.5	0.5	81.2	492.5	230	342	10
333	3.5	0.5	81.2	492.5	235	341	10
333	3.5	0.5	81.2	492.5	240	325	10
333	3.5	0.5	81.2	492.5	245	341	10
333	3.5	0.5	81.2	492.5	250	348	10
333	3.5	0.5	81.2	492.5	255	346	10
333	3.5	0.5	81.2	492.5	260	342	10

333	3.5	0.5	81.2	492.5	270	334	10
333	3.5	0.5	81.2	492.5	280	325	10
333	3.5	0.5	81.2	492.5	300	297	10
333	3.5	0.5	81.2	2424	0	572	10
333	3.5	0.5	81.2	2424	10	535	10
333	3.5	0.5	81.2	2424	20	512	10
333	3.5	0.5	81.2	2424	30	488	10
333	3.5	0.5	81.2	2424	40	466	10
333	3.5	0.5	81.2	2424	50	448	10
333	3.5	0.5	81.2	2424	60	438	10
333	3.5	0.5	81.2	2424	70	422	10
333	3.5	0.5	81.2	2424	80	403	10
333	3.5	0.5	81.2	2424	90	386	10
333	3.5	0.5	81.2	2424	100	369	10
333	3.5	0.5	81.2	2424	110	355	10
333	3.5	0.5	81.2	2424	120	341	10
333	3.5	0.5	81.2	2424	130	325	10
333	3.5	0.5	81.2	2424	140	308	10
333	3.5	0.5	81.2	2424	150	293	10
333	3.5	0.5	81.2	2424	160	288	10
333	3.5	0.5	81.2	2424	170	274	10
333	3.5	0.5	81.2	2424	180	262	10
333	3.5	0.5	81.2	2424	190	245	10
333	3.5	0.5	81.2	2424	200	230	10
333	3.5	0.5	81.2	2424	220	195	10

333	3.5	0.5	81.2	2424	260	160	10
333	3.5	0.5	81.2	2424	280	152	10
333	3.5	0.5	81.2	2424	300	83	10
333	5	0.5	108.7	532.5	0	713	11
333	5	0.5	108.7	532.5	10	566	11
333	5	0.5	108.7	532.5	20	547	11
333	5	0.5	108.7	532.5	40	520	11
333	5	0.5	108.7	532.5	60	499	11
333	5	0.5	108.7	532.5	80	489	11
333	5	0.5	108.7	532.5	100	458	11
333	5	0.5	108.7	532.5	120	440	11
333	5	0.5	108.7	532.5	140	422	11
333	5	0.5	108.7	532.5	180	388	11
333	5	0.5	108.7	532.5	200	374	11
333	5	0.5	108.7	532.5	220	362	11
333	5	0.5	108.7	532.5	225	361	11
333	5	0.5	108.7	532.5	230	357	11
333	5	0.5	108.7	532.5	235	354	11
333	5	0.5	108.7	532.5	240	360	11
333	5	0.5	108.7	532.5	245	360	11
333	5	0.5	108.7	532.5	250	355	11
333	5	0.5	108.7	532.5	255	352	11
333	5	0.5	108.7	532.5	260	347	11
333	5	0.5	108.7	532.5	270	338	11
333	5	0.5	108.7	532.5	280	334	11

333	5	0.5	108.7	532.5	300	318	11
333	5	0.5	108.7	532.5	320	295	11
333	5	0.5	108.7	532.5	340	286	11
333	5	0.5	108.7	532.5	350	275	11
333	5	0.5	108.7	2460	0	573	11
333	5	0.5	108.7	2460	10	541	11
333	5	0.5	108.7	2460	20	508	11
333	5	0.5	108.7	2460	30	489	11
333	5	0.5	108.7	2460	40	471	11
333	5	0.5	108.7	2460	50	453	11
333	5	0.5	108.7	2460	60	437	11
333	5	0.5	108.7	2460	70	422	11
333	5	0.5	108.7	2460	80	406	11
333	5	0.5	108.7	2460	90	392	11
333	5	0.5	108.7	2460	100	378	11
333	5	0.5	108.7	2460	110	366	11
333	5	0.5	108.7	2460	120	354	11
333	5	0.5	108.7	2460	130	341	11
333	5	0.5	108.7	2460	140	327	11
333	5	0.5	108.7	2460	150	314	11
333	5	0.5	108.7	2460	160	301	11
333	5	0.5	108.7	2460	170	289	11
333	5	0.5	108.7	2460	180	279	11
333	5	0.5	108.7	2460	190	267	11
333	5	0.5	108.7	2460	200	255	11

333	5	0.5	108.7	2460	220	235	11
333	5	0.5	108.7	2460	240	211	11
333	5	0.5	108.7	2460	260	185	11
333	5	0.5	108.7	2460	280	162	11
333	5	0.5	108.7	2460	300	140	11
333	5	0.5	108.7	2460	350	83	11
333	4.5	0.5	93.6	567.5	0	584	12
333	4.5	0.5	93.6	567.5	10	563	12
333	4.5	0.5	93.6	567.5	20	532	12
333	4.5	0.5	93.6	567.5	40	504	12
333	4.5	0.5	93.6	567.5	60	478	12
333	4.5	0.5	93.6	567.5	80	457	12
333	4.5	0.5	93.6	567.5	100	441	12
333	4.5	0.5	93.6	567.5	140	405	12
333	4.5	0.5	93.6	567.5	180	379	12
333	4.5	0.5	93.6	567.5	200	365	12
333	4.5	0.5	93.6	567.5	220	353	12
333	4.5	0.5	93.6	567.5	225	352	12
333	4.5	0.5	93.6	567.5	230	350	12
333	4.5	0.5	93.6	567.5	235	347	12
333	4.5	0.5	93.6	567.5	240	344	12
333	4.5	0.5	93.6	567.5	245	342	12
333	4.5	0.5	93.6	567.5	250	338	12
333	4.5	0.5	93.6	567.5	255	335	12
333	4.5	0.5	93.6	567.5	260	332	12

333	4.5	0.5	93.6	567.5	270	324	12
333	4.5	0.5	93.6	567.5	280	315	12
333	4.5	0.5	93.6	567.5	300	297	12
333	4.5	0.5	93.6	567.5	320	266	12
333	4.5	0.5	93.6	567.5	340	250	12
333	4.5	0.5	93.6	567.5	350	241	12
333	4.5	0.5	93.6	2491	0	575	12
333	4.5	0.5	93.6	2491	10	542	12
333	4.5	0.5	93.6	2491	20	518	12
333	4.5	0.5	93.6	2491	30	493	12
333	4.5	0.5	93.6	2491	40	478	12
333	4.5	0.5	93.6	2491	50	462	12
333	4.5	0.5	93.6	2491	60	447	12
333	4.5	0.5	93.6	2491	70	433	12
333	4.5	0.5	93.6	2491	80	421	12
333	4.5	0.5	93.6	2491	90	408	12
333	4.5	0.5	93.6	2491	100	393	12
333	4.5	0.5	93.6	2491	110	376	12
333	4.5	0.5	93.6	2491	120	375	12
333	4.5	0.5	93.6	2491	130	358	12
333	4.5	0.5	93.6	2491	140	341	12
333	4.5	0.5	93.6	2491	150	332	12
333	4.5	0.5	93.6	2491	160	317	12
333	4.5	0.5	93.6	2491	170	302	12
333	4.5	0.5	93.6	2491	180	287	12

333	4.5	0.5	93.6	2491	190	273	12
333	4.5	0.5	93.6	2491	200	262	12
333	4.5	0.5	93.6	2491	220	232	12
333	4.5	0.5	93.6	2491	240	210	12
333	4.5	0.5	93.6	2491	260	182	12
333	4.5	0.5	93.6	2491	280	154	12
333	4.5	0.5	93.6	2491	300	129	12
333	5.5	1	108.7	603	0	715	13
333	5.5	1	108.7	603	10	680	13
333	5.5	1	108.7	603	40	603	13
333	5.5	1	108.7	603	60	582	13
333	5.5	1	108.7	603	80	563	13
333	5.5	1	108.7	603	100	528	13
333	5.5	1	108.7	603	120	494	13
333	5.5	1	108.7	603	140	487	13
333	5.5	1	108.7	603	160	483	13
333	5.5	1	108.7	603	180	460	13
333	5.5	1	108.7	603	200	435	13
333	5.5	1	108.7	603	210	433	13
333	5.5	1	108.7	603	220	420	13
333	5.5	1	108.7	603	230	416	13
333	5.5	1	108.7	603	240	403	13
333	5.5	1	108.7	603	250	400	13
333	5.5	1	108.7	603	260	379	13
333	5.5	1	108.7	603	270	374	13

333	5.5	1	108.7	603	280	365	13
333	5.5	1	108.7	603	300	361	13
333	5.5	1	108.7	603	320	340	13
333	5.5	1	108.7	603	340	328	13
333	5.5	1	108.7	603	400	287	13
333	5.5	1	108.7	603	450	263	13
333	5.5	1	108.7	603	500	228	13
333	5.5	1	108.7	603	550	189	13
333	4.5	1.5	125.2	641.5	0	722	14
333	4.5	1.5	125.2	641.5	10	570	14
333	4.5	1.5	125.2	641.5	40	533	14
333	4.5	1.5	125.2	641.5	60	509	14
333	4.5	1.5	125.2	641.5	80	503	14
333	4.5	1.5	125.2	641.5	100	496	14
333	4.5	1.5	125.2	641.5	120	475	14
333	4.5	1.5	125.2	641.5	140	462	14
333	4.5	1.5	125.2	641.5	160	448	14
333	4.5	1.5	125.2	641.5	180	435	14
333	4.5	1.5	125.2	641.5	200	421	14
333	4.5	1.5	125.2	641.5	220	407	14
333	4.5	1.5	125.2	641.5	230	401	14
333	4.5	1.5	125.2	641.5	240	388	14
333	4.5	1.5	125.2	641.5	250	378	14
333	4.5	1.5	125.2	641.5	260	370	14
333	4.5	1.5	125.2	641.5	270	363	14

333	4.5	1.5	125.2	641.5	280	356	14
333	4.5	1.5	125.2	641.5	300	341	14
333	4.5	1.5	125.2	641.5	320	328	14
333	4.5	1.5	125.2	641.5	340	314	14
333	4.5	1.5	125.2	641.5	400	274	14
333	4.5	1.5	125.2	641.5	450	245	14
333	4.5	1.5	125.2	641.5	500	214	14
333	4.5	1.5	125.2	641.5	550	176	14
333	5.5	1.5	140.8	681	0	581	15
333	5.5	1.5	140.8	681	10	555	15
333	5.5	1.5	140.8	681	40	518	15
333	5.5	1.5	140.8	681	60	498	15
333	5.5	1.5	140.8	681	80	483	15
333	5.5	1.5	140.8	681	100	471	15
333	5.5	1.5	140.8	681	120	456	15
333	5.5	1.5	140.8	681	140	444	15
333	5.5	1.5	140.8	681	160	430	15
333	5.5	1.5	140.8	681	180	418	15
333	5.5	1.5	140.8	681	200	406	15
333	5.5	1.5	140.8	681	220	394	15
333	5.5	1.5	140.8	681	230	389	15
333	5.5	1.5	140.8	681	240	384	15
333	5.5	1.5	140.8	681	250	377	15
333	5.5	1.5	140.8	681	260	370	15
333	5.5	1.5	140.8	681	270	364	15

333	5.5	1.5	140.8	681	280	355	15
333	5.5	1.5	140.8	681	300	342	15
333	5.5	1.5	140.8	681	350	308	15
333	5.5	1.5	140.8	681	380	284	15
333	5.5	1.5	140.8	681	400	274	15
333	5.5	1.5	140.8	681	450	230	15
333	5.5	1.5	140.8	681	500	198	15
333	5.5	1.5	140.8	1247.5	0	533	15
333	5.5	1.5	140.8	1247.5	10	514	15
333	5.5	1.5	140.8	1247.5	40	506	15
333	5.5	1.5	140.8	1247.5	60	501	15
333	5.5	1.5	140.8	1247.5	80	478	15
333	5.5	1.5	140.8	1247.5	100	465	15
333	5.5	1.5	140.8	1247.5	120	438	15
333	5.5	1.5	140.8	1247.5	140	432	15
333	5.5	1.5	140.8	1247.5	160	424	15
333	5.5	1.5	140.8	1247.5	180	412	15
333	5.5	1.5	140.8	1247.5	200	398	15
333	5.5	1.5	140.8	1247.5	220	384	15
333	5.5	1.5	140.8	1247.5	230	375	15
333	5.5	1.5	140.8	1247.5	240	372	15
333	5.5	1.5	140.8	1247.5	250	371	15
333	5.5	1.5	140.8	1247.5	260	365	15
333	5.5	1.5	140.8	1247.5	270	362	15
333	5.5	1.5	140.8	1247.5	280	358	15

333	5.5	1.5	140.8	1247.5	300	322	15
333	5.5	1.5	140.8	1247.5	350	278	15
333	5.5	1.5	140.8	1247.5	380	269	15
333	5.5	1.5	140.8	1247.5	400	258	15
333	5.5	1.5	140.8	1247.5	450	224	15
333	5.5	1.5	140.8	1247.5	500	178	15
333	5.5	1.5	140.8	1794	0	515	15
333	5.5	1.5	140.8	1794	10	508	15
333	5.5	1.5	140.8	1794	40	438	15
333	5.5	1.5	140.8	1794	60	400	15
333	5.5	1.5	140.8	1794	80	379	15
333	5.5	1.5	140.8	1794	100	335	15
333	5.5	1.5	140.8	1794	120	288	15
333	5.5	1.5	140.8	1794	140	267	15
333	5.5	1.5	140.8	1794	160	226	15
333	5.5	1.5	140.8	1794	180	196	15
333	5.5	1.5	140.8	1794	200	163	15
333	5.5	1.5	140.8	1794	220	132	15
333	5.5	1.5	140.8	1794	230	122	15
333	5.5	1.5	140.8	1794	240	106	15
333	5.5	1.5	140.8	1794	250	95	15
333	5.5	1.5	140.8	1794	260	82	15
333	5.5	1.5	140.8	1794	270	68	15
333	5.5	1.5	140.8	1794	280	55	15
333	5.5	1.5	140.8	1794	300	22	15

333	5.5	1.5	140.8	1794	306	16	15
333	3.5	2	108.7	716.5	0	363	16
333	3.5	2	108.7	716.5	10	340	16
333	3.5	2	108.7	716.5	40	333	16
333	3.5	2	108.7	716.5	60	307	16
333	3.5	2	108.7	716.5	80	285	16
333	3.5	2	108.7	716.5	100	272	16
333	3.5	2	108.7	716.5	120	233	16
333	3.5	2	108.7	716.5	130	228	16
333	3.5	2	108.7	716.5	140	218	16
333	3.5	2	108.7	716.5	150	214	16
333	3.5	2	108.7	716.5	155	212	16
333	3.5	2	108.7	716.5	160	211	16
333	3.5	2	108.7	716.5	165	208	16
333	3.5	2	108.7	716.5	170	203	16
333	3.5	2	108.7	716.5	175	202	16
333	3.5	2	108.7	716.5	180	197	16
333	3.5	2	108.7	716.5	185	183	16
333	3.5	2	108.7	716.5	190	152	16
333	3.5	2	108.7	716.5	200	123	16
333	3.5	2	108.7	716.5	220	114	16
333	3.5	2	108.7	716.5	240	104	16
333	3.5	2	108.7	1283	0	462	16
333	3.5	2	108.7	1283	10	446	16
333	3.5	2	108.7	1283	40	396	16

333	3.5	2	108.7	1283	60	365	16
333	3.5	2	108.7	1283	70	348	16
333	3.5	2	108.7	1283	80	331	16
333	3.5	2	108.7	1283	100	293	16
333	3.5	2	108.7	1283	110	275	16
333	3.5	2	108.7	1283	120	262	16
333	3.5	2	108.7	1283	140	230	16
333	3.5	2	108.7	1283	160	216	16
333	3.5	2	108.7	1283	180	184	16
333	3.5	2	108.7	1283	200	140	16
333	3.5	2	108.7	1283	220	118	16
333	3.5	2	108.7	1283	240	85	16
333	3.5	2	108.7	1283	260	50	16
333	3.5	2	108.7	1283	280	23	16
333	3.5	2	108.7	1826	0	340	16
333	3.5	2	108.7	1826	10	317	16
333	3.5	2	108.7	1826	40	247	16
333	3.5	2	108.7	1826	60	208	16
333	3.5	2	108.7	1826	80	180	16
333	3.5	2	108.7	1826	100	125	16
333	3.5	2	108.7	1826	120	121	16
333	3.5	2	108.7	1826	140	57	16
333	3.5	2	108.7	1826	150	52	16
333	3.5	2	108.7	1826	160	45	16
333	3.5	2	108.7	1826	170	20	16

333	4	0.25	140.8	1914	0	673	17
333	4	0.25	140.8	1914	10	600	17
333	4	0.25	140.8	1914	20	577	17
333	4	0.25	140.8	1914	30	538	17
333	4	0.25	140.8	1914	40	516	17
333	4	0.25	140.8	1914	50	492	17
333	4	0.25	140.8	1914	60	468	17
333	4	0.25	140.8	1914	70	452	17
333	4	0.25	140.8	1914	80	431	17
333	4	0.25	140.8	1914	90	412	17
333	4	0.25	140.8	1914	100	392	17
333	4	0.25	140.8	1914	110	379	17
333	4	0.25	140.8	1914	120	348	17
333	4	0.25	140.8	1914	130	328	17
333	4	0.25	140.8	1914	140	311	17
333	4	0.25	140.8	1914	150	296	17
333	4	0.25	140.8	1914	160	280	17
333	4	0.25	140.8	1914	170	265	17
333	4	0.25	140.8	1914	180	253	17
333	4	0.25	140.8	1914	190	235	17
333	4	0.25	140.8	1914	200	216	17
333	4	0.25	140.8	1914	220	188	17
333	4	0.25	140.8	1914	240	162	17
333	4	0.25	140.8	1914	260	133	17
333	4	0.25	140.8	1914	280	94	17

333	4	0.25	140.8	1914	300	113	17
333	4	0.25	140.8	1914	350	26	17
333	4.5	0.25	93.6	1944.5	0	701	18
333	4.5	0.25	93.6	1944.5	10	670	18
333	4.5	0.25	93.6	1944.5	20	569	18
333	4.5	0.25	93.6	1944.5	30	549	18
333	4.5	0.25	93.6	1944.5	40	514	18
333	4.5	0.25	93.6	1944.5	50	496	18
333	4.5	0.25	93.6	1944.5	60	478	18
333	4.5	0.25	93.6	1944.5	70	497	18
333	4.5	0.25	93.6	1944.5	80	468	18
333	4.5	0.25	93.6	1944.5	90	364	18
333	4.5	0.25	93.6	1944.5	100	256	18
333	4.5	0.25	93.6	1944.5	110	222	18
333	4.5	0.25	93.6	1944.5	120	151	18
333	4.5	0.25	93.6	1944.5	130	132	18
333	4.5	0.25	93.6	1944.5	140	108	18
333	4.5	0.25	93.6	1944.5	150	81	18
333	4.5	0.25	93.6	1944.5	160	58	18
333	4.5	0.25	93.6	1944.5	170	37	18
333	4.5	0.25	93.6	1944.5	180	8	18
323	5.5	0.5	93.6	748.5	0	555	19
323	5.5	0.5	93.6	748.5	10	536	19
323	5.5	0.5	93.6	748.5	40	518	19
323	5.5	0.5	93.6	748.5	60	504	19

323	5.5	0.5	93.6	748.5	80	484	19
323	5.5	0.5	93.6	748.5	100	473	19
323	5.5	0.5	93.6	748.5	120	458	19
323	5.5	0.5	93.6	748.5	140	445	19
323	5.5	0.5	93.6	748.5	160	432	19
323	5.5	0.5	93.6	748.5	180	417	19
323	5.5	0.5	93.6	748.5	200	395	19
323	5.5	0.5	93.6	748.5	220	388	19
323	5.5	0.5	93.6	748.5	230	380	19
323	5.5	0.5	93.6	748.5	240	374	19
323	5.5	0.5	93.6	748.5	250	366	19
323	5.5	0.5	93.6	748.5	260	360	19
323	5.5	0.5	93.6	748.5	270	354	19
323	5.5	0.5	93.6	748.5	280	340	19
323	5.5	0.5	93.6	748.5	300	328	19
323	5.5	0.5	93.6	748.5	320	315	19
323	5.5	0.5	93.6	748.5	340	280	19
323	5.5	0.5	93.6	748.5	400	218	19
323	5.5	0.5	93.6	1979.5	0	485	19
323	5.5	0.5	93.6	1979.5	10	451	19
323	5.5	0.5	93.6	1979.5	40	430	19
323	5.5	0.5	93.6	1979.5	60	412	19
323	5.5	0.5	93.6	1979.5	80	402	19
323	5.5	0.5	93.6	1979.5	100	388	19
323	5.5	0.5	93.6	1979.5	120	374	19

323	5.5	0.5	93.6	1979.5	140	358	19
323	5.5	0.5	93.6	1979.5	160	342	19
323	5.5	0.5	93.6	1979.5	180	335	19
323	5.5	0.5	93.6	1979.5	200	326	19
323	5.5	0.5	93.6	1979.5	220	312	19
323	5.5	0.5	93.6	1979.5	230	302	19
323	5.5	0.5	93.6	1979.5	240	288	19
323	5.5	0.5	93.6	1979.5	250	281	19
323	5.5	0.5	93.6	1979.5	260	278	19
323	5.5	0.5	93.6	1979.5	270	269	19
323	5.5	0.5	93.6	1979.5	280	262	19
323	5.5	0.5	93.6	1979.5	300	252	19
323	5.5	0.5	93.6	1979.5	320	246	19
323	5.5	0.5	93.6	1979.5	340	221	19
323	5.5	0.5	93.6	1979.5	400	188	19
323	4	1	125.2	788.5	0	554	20
323	4	1	125.2	788.5	10	534	20
323	4	1	125.2	788.5	40	508	20
323	4	1	125.2	788.5	60	482	20
323	4	1	125.2	788.5	80	480	20
323	4	1	125.2	788.5	100	453	20
323	4	1	125.2	788.5	120	446	20
323	4	1	125.2	788.5	140	428	20
323	4	1	125.2	788.5	160	421	20
323	4	1	125.2	788.5	180	397	20

323	4	1	125.2	788.5	200	389	20
323	4	1	125.2	788.5	220	377	20
323	4	1	125.2	788.5	230	369	20
323	4	1	125.2	788.5	240	353	20
323	4	1	125.2	788.5	250	350	20
323	4	1	125.2	788.5	260	344	20
323	4	1	125.2	788.5	270	339	20
323	4	1	125.2	788.5	280	330	20
323	4	1	125.2	788.5	300	318	20
323	4	1	125.2	788.5	340	286	20
323	4	1	125.2	788.5	400	247	20
323	4	1	125.2	788.5	450	220	20
323	4	1	125.2	788.5	500	187	20
323	4	1	125.2	788.5	550	140	20
323	4.5	1	125.2	836.5	0	523	21
323	4.5	1	125.2	836.5	10	515	21
323	4.5	1	125.2	836.5	40	485	21
323	4.5	1	125.2	836.5	60	465	21
323	4.5	1	125.2	836.5	80	446	21
323	4.5	1	125.2	836.5	100	428	21
323	4.5	1	125.2	836.5	120	413	21
323	4.5	1	125.2	836.5	140	406	21
323	4.5	1	125.2	836.5	160	390	21
323	4.5	1	125.2	836.5	180	374	21
323	4.5	1	125.2	836.5	200	359	21

323	4.5	1	125.2	836.5	220	345	21
323	4.5	1	125.2	836.5	230	341	21
323	4.5	1	125.2	836.5	240	334	21
323	4.5	1	125.2	836.5	250	331	21
323	4.5	1	125.2	836.5	260	325	21
323	4.5	1	125.2	836.5	270	319	21
323	4.5	1	125.2	836.5	280	312	21
323	4.5	1	125.2	836.5	300	297	21
323	4.5	1	125.2	836.5	320	284	21
323	4.5	1	125.2	836.5	340	268	21
323	4.5	1	125.2	836.5	400	207	21
323	4.5	1	125.2	836.5	450	176	21
323	5	1	108.7	881	0	501	22
323	5	1	108.7	881	10	492	22
323	5	1	108.7	881	40	450	22
323	5	1	108.7	881	60	435	22
323	5	1	108.7	881	80	418	22
323	5	1	108.7	881	100	403	22
323	5	1	108.7	881	120	392	22
323	5	1	108.7	881	140	379	22
323	5	1	108.7	881	160	370	22
323	5	1	108.7	881	180	356	22
323	5	1	108.7	881	200	344	22
323	5	1	108.7	881	220	329	22
323	5	1	108.7	881	230	327	22

323	5	1	108.7	881	240	320	22
323	5	1	108.7	881	250	315	22
323	5	1	108.7	881	260	308	22
323	5	1	108.7	881	270	301	22
323	5	1	108.7	881	280	296	22
323	5	1	108.7	881	300	281	22
323	5	1	108.7	881	320	267	22
323	5	1	108.7	881	340	255	22
323	5	1	108.7	881	400	214	22
323	5	1	108.7	881	450	182	22
323	5	1	108.7	881	500	152	22
323	4	1.5	93.6	917.5	0	425	23
323	4	1.5	93.6	917.5	10	417	23
323	4	1.5	93.6	917.5	40	388	23
323	4	1.5	93.6	917.5	60	367	23
323	4	1.5	93.6	917.5	80	342	23
323	4	1.5	93.6	917.5	100	332	23
323	4	1.5	93.6	917.5	120	322	23
323	4	1.5	93.6	917.5	140	300	23
323	4	1.5	93.6	917.5	160	288	23
323	4	1.5	93.6	917.5	180	265	23
323	4	1.5	93.6	917.5	200	242	23
323	4	1.5	93.6	917.5	220	221	23
323	4	1.5	93.6	917.5	230	212	23
323	4	1.5	93.6	917.5	240	208	23

323	4	1.5	93.6	917.5	250	201	23
323	4	1.5	93.6	917.5	260	188	23
323	4	1.5	93.6	917.5	270	180	23
323	4	1.5	93.6	917.5	280	174	23
323	4	1.5	93.6	917.5	300	142	23
323	4	1.5	93.6	917.5	320	128	23
323	4	1.5	93.6	917.5	340	108	23
323	5	2	93.6	949	0	458	24
323	5	2	93.6	949	10	435	24
323	5	2	93.6	949	40	375	24
323	5	2	93.6	949	60	332	24
323	5	2	93.6	949	80	296	24
323	5	2	93.6	949	90	285	24
323	5	2	93.6	949	100	253	24
323	5	2	93.6	949	110	223	24
323	5	2	93.6	949	120	220	24
323	5	2	93.6	949	130	213	24
323	5	2	93.6	949	140	208	24
323	5	2	93.6	949	160	172	24
323	5	2	93.6	949	170	138	24
323	5	2	93.6	949	180	135	24
323	5	2	93.6	949	190	115	24
323	5	2	93.6	949	200	94	24
323	5	2	93.6	949	210	58	24
323	5	2	93.6	949	220	31	24

323	5	2	93.6	949	230	23	24
323	5	2	93.6	949	240	13	24
323	5	2	125.2	983	0	515	25
323	5	2	125.2	983	10	502	25
323	5	2	125.2	983	40	422	25
323	5	2	125.2	983	60	380	25
323	5	2	125.2	983	80	353	25
323	5	2	125.2	983	100	318	25
323	5	2	125.2	983	120	282	25
323	5	2	125.2	983	140	248	25
323	5	2	125.2	983	160	220	25
323	5	2	125.2	983	180	181	25
323	5	2	125.2	983	190	173	25
323	5	2	125.2	983	200	153	25
323	5	2	125.2	983	210	143	25
323	5	2	125.2	983	220	125	25
323	5	2	125.2	983	230	106	25
323	5	2	125.2	983	240	95	25
323	5	2	125.2	983	250	88	25
323	5	2	125.2	983	260	70	25
323	5	2	125.2	983	270	51	25
323	5	2	125.2	983	280	38	25
323	5	2	125.2	983	300	15	25
323	3.5	2	140.8	1016.5	0	506	26
323	3.5	2	140.8	1016.5	10	499	26

323	3.5	2	140.8	1016.5	40	431	26
323	3.5	2	140.8	1016.5	60	377	26
323	3.5	2	140.8	1016.5	80	367	26
323	3.5	2	140.8	1016.5	100	321	26
323	3.5	2	140.8	1016.5	120	293	26
323	3.5	2	140.8	1016.5	140	252	26
323	3.5	2	140.8	1016.5	160	220	26
323	3.5	2	140.8	1016.5	180	192	26
323	3.5	2	140.8	1016.5	190	175	26
323	3.5	2	140.8	1016.5	200	157	26
323	3.5	2	140.8	1016.5	210	147	26
323	3.5	2	140.8	1016.5	220	118	26
323	3.5	2	140.8	1016.5	230	102	26
323	3.5	2	140.8	1016.5	240	94	26
323	3.5	2	140.8	1016.5	250	79	26
323	3.5	2	140.8	1016.5	260	61	26
323	3.5	2	140.8	1016.5	270	46	26
323	3.5	2	140.8	1016.5	280	23	26
323	3.5	2	140.8	1016.5	300	14	26
323	4	0.25	81.2	2010.5	0	625	27
323	4	0.25	81.2	2010.5	10	580	27
323	4	0.25	81.2	2010.5	20	547	27
323	4	0.25	81.2	2010.5	30	518	27
323	4	0.25	81.2	2010.5	40	492	27
323	4	0.25	81.2	2010.5	50	470	27

323	4	0.25	81.2	2010.5	60	450	27
323	4	0.25	81.2	2010.5	70	429	27
323	4	0.25	81.2	2010.5	80	408	27
323	4	0.25	81.2	2010.5	90	389	27
323	4	0.25	81.2	2010.5	100	378	27
323	4	0.25	81.2	2010.5	110	356	27
323	4	0.25	81.2	2010.5	120	339	27
323	4	0.25	81.2	2010.5	130	320	27
323	4	0.25	81.2	2010.5	140	299	27
323	4	0.25	81.2	2010.5	150	282	27
323	4	0.25	81.2	2010.5	160	264	27
323	4	0.25	81.2	2010.5	170	247	27
323	4	0.25	81.2	2010.5	180	229	27
323	4	0.25	81.2	2010.5	190	211	27
323	4	0.25	81.2	2010.5	200	194	27
323	4	0.25	81.2	2010.5	220	160	27
323	4	0.25	81.2	2010.5	240	124	27
323	4	0.25	81.2	2010.5	260	88	27
323	4	0.25	81.2	2010.5	280	60	27
298	5	0.5	81.2	1046.5	0	585	28
298	5	0.5	81.2	1046.5	10	525	28
298	5	0.5	81.2	1046.5	40	452	28
298	5	0.5	81.2	1046.5	60	408	28
298	5	0.5	81.2	1046.5	80	366	28
298	5	0.5	81.2	1046.5	100	326	28

298	5	0.5	81.2	1046.5	120	315	28
298	5	0.5	81.2	1046.5	140	275	28
298	5	0.5	81.2	1046.5	160	242	28
298	5	0.5	81.2	1046.5	180	212	28
298	5	0.5	81.2	1046.5	200	195	28
298	5	0.5	81.2	1046.5	210	187	28
298	5	0.5	81.2	1046.5	220	176	28
298	5	0.5	81.2	1046.5	230	163	28
298	5	0.5	81.2	1046.5	240	150	28
298	5	0.5	81.2	1046.5	250	134	28
298	5	0.5	81.2	1046.5	260	118	28
298	5	0.5	81.2	1046.5	270	97	28
298	5	0.5	81.2	1046.5	280	88	28
298	5	0.5	81.2	1046.5	300	75	28
298	5	0.5	81.2	1046.5	350	18	28
298	4	0.5	140.8	1081.5	0	560	29
298	4	0.5	140.8	1081.5	10	515	29
298	4	0.5	140.8	1081.5	40	440	29
298	4	0.5	140.8	1081.5	60	405	29
298	4	0.5	140.8	1081.5	80	368	29
298	4	0.5	140.8	1081.5	100	338	29
298	4	0.5	140.8	1081.5	120	315	29
298	4	0.5	140.8	1081.5	140	282	29
298	4	0.5	140.8	1081.5	160	252	29
298	4	0.5	140.8	1081.5	180	233	29

298	4	0.5	140.8	1081.5	200	207	29
298	4	0.5	140.8	1081.5	210	194	29
298	4	0.5	140.8	1081.5	220	183	29
298	4	0.5	140.8	1081.5	230	171	29
298	4	0.5	140.8	1081.5	240	158	29
298	4	0.5	140.8	1081.5	250	147	29
298	4	0.5	140.8	1081.5	260	132	29
298	4	0.5	140.8	1081.5	270	122	29
298	4	0.5	140.8	1081.5	280	115	29
298	4	0.5	140.8	1081.5	300	92	29
298	4	0.5	140.8	1081.5	350	29	29
298	4.5	1	125.2	1319.5	0	560	30
298	4.5	1	125.2	1319.5	10	515	30
298	4.5	1	125.2	1319.5	40	440	30
298	4.5	1	125.2	1319.5	60	405	30
298	4.5	1	125.2	1319.5	80	368	30
298	4.5	1	125.2	1319.5	100	338	30
298	4.5	1	125.2	1319.5	120	315	30
298	4.5	1	125.2	1319.5	140	282	30
298	4.5	1	125.2	1319.5	160	252	30
298	4.5	1	125.2	1319.5	180	233	30
298	4.5	1	125.2	1319.5	200	207	30
298	4.5	1	125.2	1319.5	210	194	30
298	4.5	1	125.2	1319.5	220	183	30
298	4.5	1	125.2	1319.5	230	171	30

298	4.5	1	125.2	1319.5	240	158	30
298	4.5	1	125.2	1319.5	250	147	30
298	4.5	1	125.2	1319.5	260	132	30
298	4.5	1	125.2	1319.5	270	122	30
298	4.5	1	125.2	1319.5	280	115	30
298	4.5	1	125.2	1319.5	300	92	30
298	4.5	1	125.2	1319.5	340	29	30
298	5	1	93.6	1360.5	0	523	31
298	5	1	93.6	1360.5	10	490	31
298	5	1	93.6	1360.5	40	421	31
298	5	1	93.6	1360.5	60	382	31
298	5	1	93.6	1360.5	80	348	31
298	5	1	93.6	1360.5	100	314	31
298	5	1	93.6	1360.5	120	288	31
298	5	1	93.6	1360.5	140	260	31
298	5	1	93.6	1360.5	160	239	31
298	5	1	93.6	1360.5	180	218	31
298	5	1	93.6	1360.5	200	190	31
298	5	1	93.6	1360.5	210	178	31
298	5	1	93.6	1360.5	220	166	31
298	5	1	93.6	1360.5	230	160	31
298	5	1	93.6	1360.5	240	147	31
298	5	1	93.6	1360.5	250	134	31
298	5	1	93.6	1360.5	260	122	31
298	5	1	93.6	1360.5	270	119	31

298	5	1	93.6	1360.5	280	105	31
298	5	1	93.6	1360.5	300	77	31
298	5	1	93.6	1360.5	350	18	31
298	5.5	1.5	93.6	1402.5	0	515	32
298	5.5	1.5	93.6	1402.5	10	571	32
298	5.5	1.5	93.6	1402.5	40	356	32
298	5.5	1.5	93.6	1402.5	60	321	32
298	5.5	1.5	93.6	1402.5	80	275	32
298	5.5	1.5	93.6	1402.5	100	241	32
298	5.5	1.5	93.6	1402.5	120	219	32
298	5.5	1.5	93.6	1402.5	140	194	32
298	5.5	1.5	93.6	1402.5	160	154	32
298	5.5	1.5	93.6	1402.5	180	144	32
298	5.5	1.5	93.6	1402.5	200	118	32
298	5.5	1.5	93.6	1402.5	210	98	32
298	5.5	1.5	93.6	1402.5	220	94	32
298	5.5	1.5	93.6	1402.5	230	84	32
298	5.5	1.5	93.6	1402.5	240	71	32
298	5.5	1.5	93.6	1402.5	250	61	32
298	5.5	1.5	93.6	1402.5	260	46	32
298	5.5	1.5	93.6	1402.5	270	37	32
298	5.5	1.5	93.6	1402.5	280	24	32
298	5.5	1.5	93.6	1402.5	300	21	32
298	5.5	1.5	93.6	1402.5	350	12	32
298	4	2	81.2	1438.5	0	491	33

298	4	2	81.2	1438.5	10	441	33
298	4	2	81.2	1438.5	40	361	33
298	4	2	81.2	1438.5	60	322	33
298	4	2	81.2	1438.5	80	286	33
298	4	2	81.2	1438.5	100	253	33
298	4	2	81.2	1438.5	120	224	33
298	4	2	81.2	1438.5	140	195	33
298	4	2	81.2	1438.5	160	168	33
298	4	2	81.2	1438.5	180	143	33
298	4	2	81.2	1438.5	200	116	33
298	4	2	81.2	1438.5	210	103	33
298	4	2	81.2	1438.5	220	95	33
298	4	2	81.2	1438.5	230	86	33
298	4	2	81.2	1438.5	240	74	33
298	4	2	81.2	1438.5	250	56	33
298	4	2	81.2	1438.5	260	49	33
298	4	2	81.2	1438.5	270	38	33
298	4	2	81.2	1438.5	280	25	33
298	4	2	81.2	1438.5	300	19	33
298	4	2	81.2	1438.5	350	15	33
298	4.5	2	140.8	1476	0	525	34
298	4.5	2	140.8	1476	10	451	34
298	4.5	2	140.8	1476	40	355	34
298	4.5	2	140.8	1476	60	318	34
298	4.5	2	140.8	1476	80	281	34

298	4.5	2	140.8	1476	100	251	34
298	4.5	2	140.8	1476	120	222	34
298	4.5	2	140.8	1476	130	193	34
298	4.5	2	140.8	1476	140	198	34
298	4.5	2	140.8	1476	160	158	34
298	4.5	2	140.8	1476	180	134	34
298	4.5	2	140.8	1476	200	108	34
298	4.5	2	140.8	1476	210	94	34
298	4.5	2	140.8	1476	220	84	34
298	4.5	2	140.8	1476	230	64	34
298	4.5	2	140.8	1476	240	58	34
298	4.5	2	140.8	1476	250	44	34
298	4.5	2	140.8	1476	260	35	34
298	4.5	2	140.8	1476	270	22	34
298	4.5	2	140.8	1476	280	15	34
298	3.5	0.25	125.2	2092	0	598	35
298	3.5	0.25	125.2	2092	10	552	35
298	3.5	0.25	125.2	2092	40	448	35
298	3.5	0.25	125.2	2092	60	383	35
298	3.5	0.25	125.2	2092	80	355	35
298	3.5	0.25	125.2	2092	90	336	35
298	3.5	0.25	125.2	2092	100	309	35
298	3.5	0.25	125.2	2092	110	268	35
298	3.5	0.25	125.2	2092	120	253	35
298	3.5	0.25	125.2	2092	130	230	35

298	3.5	0.25	125.2	2092	140	204	35
298	3.5	0.25	125.2	2092	150	188	35
298	3.5	0.25	125.2	2092	160	166	35
298	3.5	0.25	125.2	2092	170	143	35
298	3.5	0.25	125.2	2092	180	115	35
298	3.5	0.25	125.2	2092	190	89	35
298	3.5	0.25	125.2	2092	200	66	35
298	3.5	0.25	125.2	2092	210	35	35
298	3.5	0.25	125.2	2092	220	22	35
298	3.5	0.25	125.2	2092	230	12	35
298	5	0.25	108.7	2124	0	758	36
298	5	0.25	108.7	2124	10	721	36
298	5	0.25	108.7	2124	20	501	36
298	5	0.25	108.7	2124	30	466	36
298	5	0.25	108.7	2124	40	433	36
298	5	0.25	108.7	2124	50	401	36
298	5	0.25	108.7	2124	60	371	36
298	5	0.25	108.7	2124	70	341	36
298	5	0.25	108.7	2124	80	310	36
298	5	0.25	108.7	2124	90	282	36
298	5	0.25	108.7	2124	100	255	36
298	5	0.25	108.7	2124	110	232	36
298	5	0.25	108.7	2124	120	208	36
298	5	0.25	108.7	2124	130	185	36
298	5	0.25	108.7	2124	140	172	36

298	5	0.25	108.7	2124	150	145	36
298	5	0.25	108.7	2124	160	112	36
298	5	0.25	108.7	2124	170	90	36
298	5	0.25	108.7	2124	180	68	36
298	5	0.25	108.7	2124	190	46	36
298	5	0.25	108.7	2124	200	24	36
343	5	0.5	140.8	1509	0	592	37
343	5	0.5	140.8	1509	10	560	37
343	5	0.5	140.8	1509	40	493	37
343	5	0.5	140.8	1509	60	458	37
343	5	0.5	140.8	1509	80	434	37
343	5	0.5	140.8	1509	100	403	37
343	5	0.5	140.8	1509	120	376	37
343	5	0.5	140.8	1509	130	348	37
343	5	0.5	140.8	1509	140	325	37
343	5	0.5	140.8	1509	160	303	37
343	5	0.5	140.8	1509	180	281	37
343	5	0.5	140.8	1509	200	266	37
343	5	0.5	140.8	1509	220	244	37
343	5	0.5	140.8	1509	240	224	37
343	5	0.5	140.8	1509	260	205	37
343	5	0.5	140.8	1509	280	195	37
343	5	0.5	140.8	1509	300	178	37
343	5	0.5	140.8	1509	320	156	37
343	5	0.5	140.8	1509	340	98	37

343	5	0.5	140.8	1509	400	43	37
343	5	0.5	140.8	1509	485	25	37
343	4	0.5	108.7	1534.5	0	597	38
343	4	0.5	108.7	1534.5	10	570	38
343	4	0.5	108.7	1534.5	40	522	38
343	4	0.5	108.7	1534.5	60	494	38
343	4	0.5	108.7	1534.5	80	464	38
343	4	0.5	108.7	1534.5	100	437	38
343	4	0.5	108.7	1534.5	120	420	38
343	4	0.5	108.7	1534.5	130	396	38
343	4	0.5	108.7	1534.5	140	375	38
343	4	0.5	108.7	1534.5	160	357	38
343	4	0.5	108.7	1534.5	180	337	38
343	4	0.5	108.7	1534.5	200	317	38
343	4	0.5	108.7	1534.5	220	296	38
343	4	0.5	108.7	1534.5	240	272	38
343	4	0.5	108.7	1534.5	260	255	38
343	4	0.5	108.7	1534.5	280	231	38
343	4	0.5	108.7	1534.5	300	209	38
343	4	0.5	108.7	1534.5	320	186	38
343	4	0.5	108.7	1534.5	340	118	38
343	4	0.5	108.7	1534.5	400	63	38
343	4	0.5	108.7	1534.5	485	25	38
343	5.5	1	81.2	1565.5	0	349	39
343	5.5	1	81.2	1565.5	10	338	39

343	5.5	1	81.2	1565.5	40	304	39
343	5.5	1	81.2	1565.5	60	275	39
343	5.5	1	81.2	1565.5	80	245	39
343	5.5	1	81.2	1565.5	100	219	39
343	5.5	1	81.2	1565.5	120	212	39
343	5.5	1	81.2	1565.5	130	191	39
343	5.5	1	81.2	1565.5	140	141	39
343	5.5	1	81.2	1565.5	160	134	39
343	5.5	1	81.2	1565.5	180	121	39
343	5.5	1	81.2	1565.5	200	94	39
343	5.5	1	81.2	1565.5	230	62	39
343	3.5	1	140.8	1599	0	595	40
343	3.5	1	140.8	1599	10	554	40
343	3.5	1	140.8	1599	40	488	40
343	3.5	1	140.8	1599	60	456	40
343	3.5	1	140.8	1599	80	432	40
343	3.5	1	140.8	1599	100	406	40
343	3.5	1	140.8	1599	120	382	40
343	3.5	1	140.8	1599	140	359	40
343	3.5	1	140.8	1599	160	338	40
343	3.5	1	140.8	1599	180	317	40
343	3.5	1	140.8	1599	200	294	40
343	3.5	1	140.8	1599	220	272	40
343	3.5	1	140.8	1599	240	252	40
343	3.5	1	140.8	1599	260	235	40

343	3.5	1	140.8	1599	280	213	40
343	3.5	1	140.8	1599	300	192	40
343	3.5	1	140.8	1599	320	170	40
343	3.5	1	140.8	1599	340	148	40
343	3.5	1	140.8	1599	360	129	40
343	3.5	1	140.8	1599	400	86	40
343	3.5	1	140.8	1599	450	38	40
343	4	1.5	125.2	1628	0	373	41
343	4	1.5	125.2	1628	10	363	41
343	4	1.5	125.2	1628	40	331	41
343	4	1.5	125.2	1628	60	307	41
343	4	1.5	125.2	1628	80	286	41
343	4	1.5	125.2	1628	100	262	41
343	4	1.5	125.2	1628	120	246	41
343	4	1.5	125.2	1628	140	218	41
343	4	1.5	125.2	1628	160	193	41
343	4	1.5	125.2	1628	180	168	41
343	4	1.5	125.2	1628	200	138	41
343	4	1.5	125.2	1628	220	101	41
343	4	1.5	125.2	1628	240	70	41
343	4	1.5	125.2	1628	260	32	41
343	4	1.5	125.2	1628	270	14	41
343	4.5	2	81.2	1653	0	335	42
343	4.5	2	81.2	1653	10	322	42
343	4.5	2	81.2	1653	40	280	42

343	4.5	2	81.2	1653	60	249	42
343	4.5	2	81.2	1653	80	190	42
343	4.5	2	81.2	1653	100	148	42
343	4.5	2	81.2	1653	120	102	42
343	4.5	2	81.2	1653	140	56	42
343	4.5	2	81.2	1653	160	21	42
343	4.5	2	81.2	1653	163	7	42
343	5	2	108.7	1676	0	336	43
343	5	2	108.7	1676	10	313	43
343	5	2	108.7	1676	40	290	43
343	5	2	108.7	1676	60	275	43
343	5	2	108.7	1676	80	242	43
343	5	2	108.7	1676	100	180	43
343	5	2	108.7	1676	120	54	43
343	5	2	108.7	1676	140	101	43
343	5	2	108.7	1676	160	62	43
343	5	2	108.7	1676	180	22	43
343	5	2	108.7	1676	190	11	43
343	3.5	0.25	93.6	2040	0	642	44
343	3.5	0.25	93.6	2040	10	608	44
343	3.5	0.25	93.6	2040	20	582	44
343	3.5	0.25	93.6	2040	30	563	44
343	3.5	0.25	93.6	2040	40	542	44
343	3.5	0.25	93.6	2040	50	521	44
343	3.5	0.25	93.6	2040	60	503	44

343	3.5	0.25	93.6	2040	70	485	44
343	3.5	0.25	93.6	2040	80	476	44
343	3.5	0.25	93.6	2040	90	455	44
343	3.5	0.25	93.6	2040	100	447	44
343	3.5	0.25	93.6	2040	110	425	44
343	3.5	0.25	93.6	2040	120	378	44
343	3.5	0.25	93.6	2040	130	341	44
343	3.5	0.25	93.6	2040	140	319	44
343	3.5	0.25	93.6	2040	150	308	44
343	3.5	0.25	93.6	2040	160	295	44
343	3.5	0.25	93.6	2040	170	280	44
343	3.5	0.25	93.6	2040	180	352	44
343	3.5	0.25	93.6	2040	190	346	44
343	3.5	0.25	93.6	2040	200	326	44
343	3.5	0.25	93.6	2040	250	259	44
343	3.5	0.25	93.6	2040	300	185	44
343	3.5	0.25	93.6	2040	320	168	44
343	3.5	0.25	93.6	2040	340	142	44
343	5.5	0.25	125.2	2066	0	676	45
343	5.5	0.25	125.2	2066	10	628	45
343	5.5	0.25	125.2	2066	40	543	45
343	5.5	0.25	125.2	2066	60	508	45
343	5.5	0.25	125.2	2066	80	476	45
343	5.5	0.25	125.2	2066	100	442	45
343	5.5	0.25	125.2	2066	120	415	45

343	5.5	0.25	125.2	2066	140	380	45
343	5.5	0.25	125.2	2066	160	341	45
343	5.5	0.25	125.2	2066	180	350	45
343	5.5	0.25	125.2	2066	200	307	45
343	5.5	0.25	125.2	2066	220	257	45
343	5.5	0.25	125.2	2066	240	222	45
343	5.5	0.25	125.2	2066	260	216	45
343	5.5	0.25	125.2	2066	280	199	45
343	5.5	0.25	125.2	2066	300	199	45
343	5.5	0.25	125.2	2066	320	179	45
343	5.5	0.25	125.2	2066	340	155	45
343	5.5	0.25	125.2	2066	360	130	45
343	5.5	0.25	125.2	2066	380	105	45
343	5.5	0.25	125.2	2066	400	83	45